DISSERTATION

Titel der Dissertation

Organosilica Monoliths with Multiscale Porosity: Detailed Investigation of their Formation and their Potential as Ceramic Precursors

angestrebter akademischer Grad

Doktor der Naturwissenschaften (Dr. rer. nat.)

Verfasser:	Manuel Weinberger
Matrikel-Nummer:	0603202
Dissertationsgebiet (lt. Studienblatt):	411 Physik
Betreuer:	Univ.-Prof. Dr. Herwig Peterlik

Wien, am 09. November 2009

Kurzfassung

Monolithische Materialien mit einer hierarchischen Porenstruktur sind vielversprechende Kandidaten für Anwendungen wie Chromatographie und Katalyse. Mikrometer-große und interpenetrierende Poren sorgen für einen sehr guten Massentransport durch das Material. Nanoporen, welche sich in dem Grundgerüst des Materials befinden, schaffen eine hohe Oberfläche und damit viel Platz für etwaige Funktionalisierungen. Jedoch ist die Synthese solcher Materialien immer noch eine große Herausforderung. Üblicherweise werden diese Materialien über einen Sol-Gel-Prozess hergestellt, welcher im Rahmen der Dissertation durch die Zugabe eines Amphiphils wie Pluronic P123 modifiziert wurde. Die Wechselwirkung zwischen P123 und der Sol-Gel-Precursorspezies führt durch die fortschreitende Kondensation zu einer Phasenseparation, die zur Ausbildung des makroporösen Gerüsts und der Nanoporen führt. Jedoch lassen sich diese Vorgänge vor allem mit komplexen und funktionellen molekularen Precursoren nicht immer ohne weiteres reproduzieren.

Ziel dieser Arbeit ist es daher ein besseres Verständnis für die vielen Faktoren zu bekommen, die letztlich im Zusammenspiel zur Erzeugung von monolithischen Organosilika-Materialen mit einer hierarchischen Porenstruktur führen. Ethylenglykol-modifizierte Carbosilane wurden hergestellt, da Ethylenglykol aufgrund seiner Polarität eine bessere Kompatibilität mit Flüssigkristallbildnern wie Pluronic P123 bietet und somit die Erzeugung von hochgeordneten Nanoporen vereinfachen sollte. Hierfür wurden einfache und kommerziell erhältliche Alkoxysilane wie 1,2-Bis(triethoxysilyl)ethan und nicht kommerziell erhältliche, komplexe ethan-verbrückte und dendrimerartige Silane wie Tetrakis[(triethoxysilyl)ethyl]silan mit Ethylenglykol transesterifiziert. Die modifizierten Silane wurden dann im Anschluss über den Sol-Gel-Prozess in einer Lösung bestehend aus dem Blockcopolymer Pluronic P123 und wässriger Salzsäure umgesetzt. Nach Entfernen des Amphiphils und überkritischer Trocknung der nassen Gele wurden hochporöse Organosilika-Monolithen erhalten. Diese zeigen hinsichtlich der verwendeten Silane und unterschiedlicher Syntheseparameter verschiedenste Morphologien auf Mikrometer- und Nanometerebene. Die Materialien wurden mit Standardmethoden der Materialwissenschaften analysiert und die Unterschiede diskutiert. Es konnte gezeigt werden, dass mit einfachen molekularen Precursoren wie dem bis-silylierten Ethan makroporöse Materialien mit hochgeordnete Nanostrukturen im Gerüst leich zugänglich sind, was auf die molekulare Beschaffenheit der Precursoren hinsichtlich eines geringeren Anteils hydrophober Organik und damit einer wesentlich besseren Kompatibilität mit dem Amphiphil und/oder einer unterschiedlichen

Reaktivität im Sol-Gel-Prozess hinsichtlich der Erhöhung der funktionellen Alkoxid/Glykolat-Gruppen zurückzuführen ist.

Röntgenkleinwinkelstreuung (SAXS) ist eine hervorragend geeignete Technik, um sowohl hochgeordnete wie auch amorphe Nanostrukturen zu analysieren. In dieser Arbeit wurde SAXS ausgiebig verwendet, um verschiedenste Gel-Nanostrukturen zu charakterisieren. Vor allem aber eignet sich die Kleinwinkelstreuung auch, um das Fortschreiten des Sol-Gel-Prozesses *in-situ* zu verfolgen. Mechanismus- und Kinetikstudien wurden daher im Falle des bis-silylierten Ethans unternommen. Es konnte gezeigt werden, dass die polymerisationsinduzierte Phasenseparation offensichtlich zu einem metastabilen Zustand führt, aus welchem die Mesokristalle durch einen Keimbildungs- und Wachstumsprozess hervorgehen. Durch Anwendung der Avrami-Theorie konnte die Kinetik dieses Prozesses erfolgreich beschrieben werden.

Organosilika-Materialien haben sich in der Vergangenheit als ausgezeichnete Keramik-Precursoren herausgestellt. Die Organosilika-Monolithen, die in dieser Arbeit hergestellt wurden, konnten ebenfalls für diesen Zweck verwendet werden. Ein ethylenglykol-modifiziertes 1,3,5-Trisilacyclohexan-Carbosilan wurde synthetisiert und analog zu dem ethanverbrückten Silan in einem Sol-Gel Prozess umgesetzt. Um die Agglomeration des polymerisierenden Organosilikas zu erleichtern, wurde der Sol-Gel-Prozess jedoch um die Zugabe von Kaliumchlorid erweitert. Auf diese Weise war es möglich Monolithe mit hierarchisch-strukturiertem Porensystem zu erzeugen. Diese wurden bei Temperaturen um die 1000 °C in Schutzgasatmosphäre erfolgreich zu Siliziumoxycarbid-Monolithen unter Erhalt aller strukturellen Besonderheiten umgesetzt. Diese Materialien sind interessante Kandidaten für katalytische Anwendungen unter extremen Umgebungsbedingungen.

Abstract

Monolithic materials with a hierarchical pore structure are promising candidates for applications, such as chromatography or catalysis. Micrometer-sized and interconnected pores provide very good mass transport through the material. Nanopores, which are contained within the framework, give the material a high specific surface area and therewith a lot of room for possible functionalizations. However, the synthesis of such materials is still a challenging task. Generally such materials are prepared by sol-gel processing, which was modified by the addition of the amphiphile Pluronic P123 in the course of this work. The interaction between P123 and the sol-gel precursor species is leading to a phase separation with ongoing condensation, by which the macroporous framework and the nanopores are formed. However, such processes may not be initiated so easily with more complex and functional molecular precursors.

The aim of this work is thus to get a better understanding of the many factors finally working together to create monolithic organosilica materials with a hierarchically organized pore structure. Ethylene glycol-modified carbosilanes were prepared, since ethylene glycol exhibits – due to its polarity – a better compatibility with liquid crystalline phases, which are, for example, obtained from Pluronic P123. Thus, the formation of highly ordered nanopores should be facilitated. This was the starting point to use commercially available alkoxysilanes, such as 1,2-bis(triethoxysilyl)ethane, as well as non-commercially available more complex ethane-bridged and dendrimeric silanes, such as tetrakis[(triethoxysilyl)ethyl]silane. Via transesterification reaction with ethylene glycol, the modified silanes were obtained, which were then condensed via sol-gel processing within an aqueous solution of the block copolymer Pluronic P123 and hydrochloric acid. After removal of the amphiphile and supercritical drying of the wet gels, highly porous organosilica monoliths were obtained. These gels show various morphologies in the micrometer as well as in the nanometer range, depending on the applied silanes and the different synthesis conditions. These structural differences in the newly developed materials were characterized with SAXS (small-angle X-ray scattering), electron microscopy and nitrogen sorption. It could be shown that with simple molecular precursors, such as the bis-silylated ethane macroporous materials with highly ordered nanostructures within the framework are accessible easily. This may be explained by the molecular composition of the precursor comprising a relatively low hydrophobic organic content and therewith a better compatibility with the amphiphile and/or the relatively low content of functional alkoxide/glycoxide groups.

Small angle X-ray scattering (SAXS) is an excellent technique to characterize both highly ordered, and amorphous nanostructures. Within this work we applied SAXS extensively to fully analyze various gel nanostructures. But above all, SAXS is suitable to follow the evolution of the sol-gel process *in-situ*. Mechanistic and kinetic studies were thus conducted in the case of the bis-silylated ethane. We could show that the polymerization-induced phase separation apparently is leading to a metastable state, from which the mesocrystallites evolve by nucleation and growth. The kinetics of this process could successfully be described by application of the Avrami theory.

In the past organosilica materials have proven to be excellent ceramic precursors. It could be shown that this is also the case for the organosilica monoliths developed within the frame of this thesis. An ethylene glycol-modified 1,3,5-trisilacyclohexane carbosilane was synthesized and converted to a monolithic hybrid material analogously to the ethane-bridged silane by sol-gel processing. To facilitate the agglomeration of the polymerizing organosilica, potassium chloride was added. That way it was possible to generate monoliths with hierarchically organized pores. These were successfully converted into silicon oxycarbide monoliths at temperatures of 1000 °C in inert gas atmosphere with simultaneously maintaining the structural features. The high porosity of these materials opens the opportunity to use them in catalytic applications in a harsh environment.

Table of Contents

1. Introduction

Finding new concepts and methods for the preparation and design of novel materials is one of the most important goals in modern inorganic chemistry and materials science. Recently, scientists took a close look at the creations of one of the best inventors for highly specialized materials: Within a period of several millions of years nature created truly complex materials, such as bone or wood by biological evolution. Both these biomaterials exhibit a complex hierarchical build-up, which apparently leads to a combination of contradictory properties like high elasticity together with high rigidity and low weight[1]. An impressive example for a natural structure with hierarchy on at least seven levels is given by the biosilica sponge skeleton of Euplectella, a deep-sea dwelling sponge (figure.1.1)[2]. This material is based mainly on the brittle material silica, but overcomes the brittleness by the addition of a small amount of an organic polymer phase. The cellular structure is important for structural stability together with the high porosity, which allows for the circulation of cellular fluids.
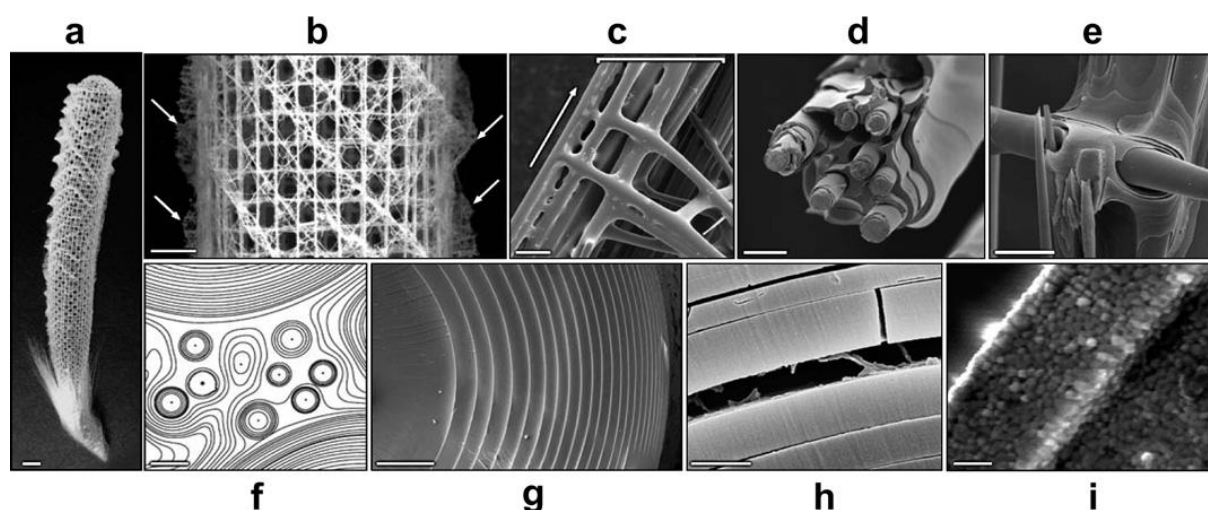

Fig. 1.1. a) Entire skeleton of Euplectella (scale bar 1 cm); b – h) several levels of hierarchy with decreasing size dimensions; i) silica nanoparticles as basic structural units (scale bar 500 nm); image taken from [2]

The combination of hierarchical porosity and stability within a material are highly desirable features. Not until the discovery of electron microscopy, scientist realized finally the complexity of natures' architectures and with ongoing progress in the field of nanotechnology they discovered methods with which it was possible to mimick these examples. Soft chemistry methods, such as the sol-gel process in combination with self-organizing systems, such as surfactants are indeed powerful tools to prepare (hierarchically) organized materials[3-6]. However, the interplay of simultaneously occurring processes, in particular chemical reactions and physical forces, which are influenced by many factors such as kind

and concentration of reaction components, temperature or pH, is rather complex. Still many efforts have to be taken to gain the ability to deliberately direct and control these processes.

This work is thus focused on the preparation and characterization of novel organosilica monoliths with multiscale porosity together with mechanistic studies to get a better understanding of the formation of these truly sophisticated materials. Such monoliths can be understood as cm-sized gel pieces, comprising μm-sized interconnected pores and frameworks as well as nm-sized (periodically arranged) mesopores. Mesopores (mesos; greek for in the middle) are in-between micropores (pore diameters of < 2 nm) and macropores (pore diameters > 50 nm)[7]. In the following figure 1.2 the hierarchical build-up of such a monolithic material is shown to visualize the structure at the respective size level.
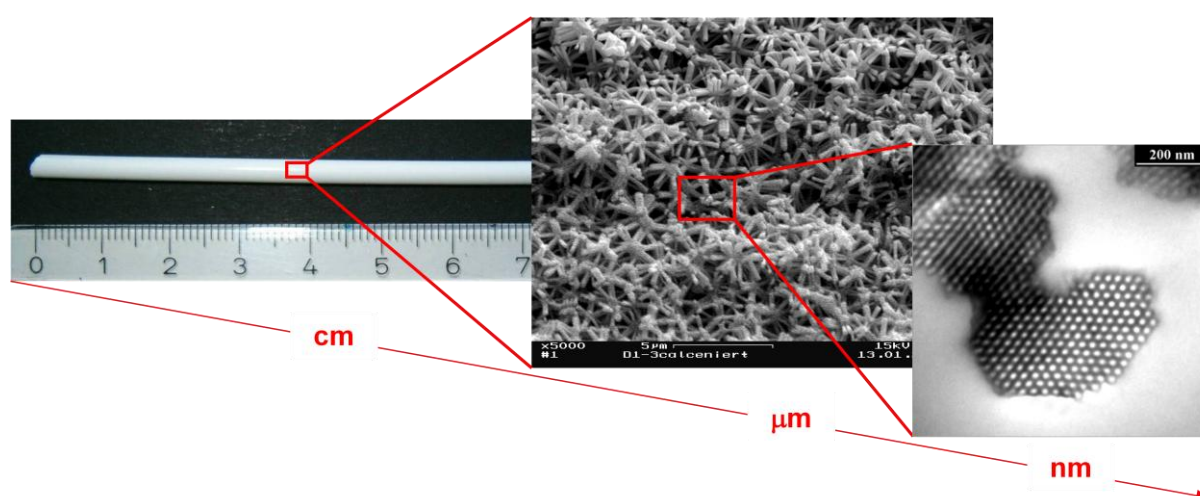

Fig. 1.2. Hierarchical build-up of a silica monolith; left: rod-like porous monolith; middle: cellular macroporous structure; right: periodically arranged mesopores within the rods of the framework domains; image taken and modified from **[8]**

These rather uniform sol-gel materials exhibit a unique interconnected pore structure and thus an excellent mass transfer through the whole material. This has the advantage that within a very short time every region of the materials is accessible by solvents. In addition, the mesopores give the material a huge surface area, which could be functionalized by post-synthetic treatments, making these monoliths promising candidates in the fields of chromatography or catalysis.

The main results of this dissertation were published in three peer-reviewed journals. However, since the preparation and characterization of such complex monoliths is a difficult task, we restrict ourselves to an extensive overview about the most important topics related to these publications in the introduction. Precise details can be found in the sections of the three publications.

1.1 Porous silica monoliths obtained from phase separation processes

The preparation of (organo)silica monoliths with multiscale porosity is a delicate task. A detailed understanding of the occurring processes requires an advanced knowledge of sol-gel chemistry as well as of phase separation phenomena in polymeric systems. Thus, in the next two subsections the reader may find the respective theoretical background.
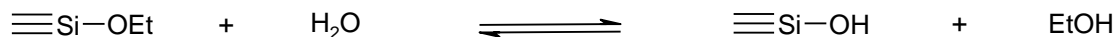
1.1.1 The sol-gel process

Nowadays, sol-gel chemistry is a quickly expanding field and covers lots of routes for the preparation of a huge number of various kinds of materials. Based on the processing technique it is possible to prepare powders, films, monoliths or fibers[9-11]. There are a lot of reaction parameters which allow a careful control of the materials' structural features on several length scales. The basic requirement for every sol-gel processing is the preparation of a more or less stable sol. This is a colloidal solution of stabilized nanometer-sized particles. The most common routes to prepare such sols are mainly the conversion of alkoxysilanes, such as tetramethoxysilane (TMOS) in water or alcohol based media yielding a silica material, in fact a material that consists of covalently linked SiO_4 tetrahedra. But it is likewise possible to introduce organic groups into the precursor, which is useful for the preparation of inorganic-organic hybrid materials, so-called organosilicas. (Organo)silica based sol-gel chemistry is well understood since the reactivity of these systems is easy to control by adjusting the synthesis parameters[12]. Of course it is also possible to use sol-gel-processing for the preparation of materials composed of titanium dioxide[13-15] or other transition and main-group metal oxides[16]. The difficulty is that the corresponding precursor compounds, such as alkoxides, are far more reactive, especially under aqueous conditions and a control of the materials structure is thus difficult to achieve. Consequently, recent efforts apply the promising sol-gel chemistry in non-aqueous medium[17-19]. However, in the course of this contribution we will concentrate on the sol-gel-processing of alkoxy(organo)silanes under aqueous conditions.

This short introduction is based on the well known textbook from Iler[20] as well as the one from Brinker and Scherer[9]. An excellent review article from Hüsing and Schubert covers almost every aspect of aerogels[12]. The reader may find further information in these citations.

Sol-gel chemistry can be understood as a subgroup of polymer science since the formation of the sol particles as well as the gel is based on the polymerization of hydrolyzed precursor species. The chemical processes occurring after the addition of an alkoxysilane such as

TMOS into water are illustrated in figure 1.3, where the fundamental hydrolysis and condensation reactions are shown.

1.) Hydrolysis

$\equiv$Si$-$OEt   + H_2O $\rightleftharpoons$ $\equiv$Si$-$OH   +   EtOH

2.) Condensation

$\equiv$Si$-$OEt   +   HO$-$Si$\equiv$ $\rightleftharpoons$ $\equiv$Si$-$O$-$Si$\equiv$ +   EtOH

$\equiv$Si$-$OH   +   HO$-$Si$\equiv$ $\rightleftharpoons$ $\equiv$Si$-$O$-$Si$\equiv$ + H_2O
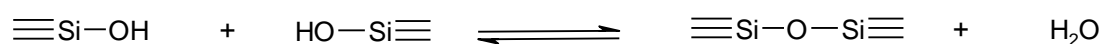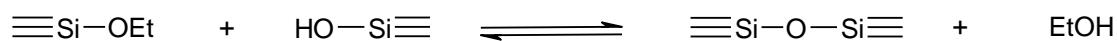
Fig. 1.3. Hydrolysis and condensation reactions

In the course of the hydrolysis the alkoxygroups of the precursor react to form silanol groups, which are able to form the siloxane bonds by the elimination of water or alcohol (a condensation reaction) in a second step. The addition of an acid or base will catalyze both the hydrolysis and condensation reactions (Fig. 1.4)**[21].**
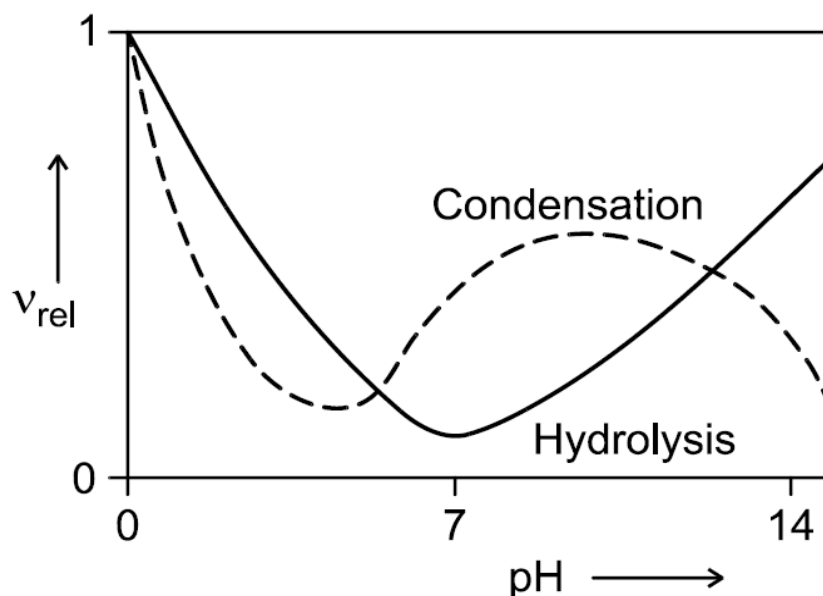
Fig. 1.4. Relative rates of hydrolysis (continuous line) and condensation (dotted line) in dependence of the pH in the silica system; image taken from **[9]**

For a minimum rate of hydrolysis, the number of catalyzing OH^- -and H_3O^+ has to be minimal. This is achieved for pH = 7. The decrease of the pH will lead to protonated oxygen atoms of the alkoxygroups and therewith a good leaving group is formed. In the case of a higher pH, the OH^- ions will undergo a nucleophilic attack directly at the silicon atom to displace the alkoxygroup.

For silicic acid the pH value where all silanol groups are neither protonated nor deprotonated is at about pH = 2. This point is also called the "Point of Zero Charge" (PZC). At this point, the condensation reaction exhibits a minimum. If the pH is decreased to a lower pH, the silanol groups get protonated and good leaving groups are formed. In the other case, when the pH is increased above the PZC, deprotonated silanol species are formed, which will substitute OH^- or alkoxide ions of neutral silicate species. In addition, a further increase of the pH will also favor the dissolution of silica and thus counteract to the condensation.

We have already defined the term sol, but for further discussions we also need to know what exactly is meant by a gel. A gel can be understood as a three-dimensional agglomeration of the sol particles. This is the basis for the formation of a solid, that shows a porous framework and which comprises the solvent within pores between interconnected particles. In an aqueous acid- or base-catalyzed sol-gel process of alkoxysilanes, the maximum size of the sol particles depends strongly on the pH. Since under acidic conditions the protonation of a silanol group is leading to a good leaving group, a new siloxane bond is rapidly formed by the reaction of a neutral silanol and the protonated species. Under acidic conditions the hydrolysis is the rate controlling step. A vast number of monomers are quickly formed and the most basic silanol groups, which are found in monomers and weakly branched oligomers will preferentially be protonated. Thus, instead of further growth, the primary particles will form so-called polymeric gels. This mechanism is denoted as the Reaction-Limited Cluster Aggregation (RLCA)[22]. In the other case, under basic conditions, the most acidic silanol group is found in highly branched species. Since the hydrolysis is slow compared to the condensation reaction, the hydrolyzed monomers will quickly be consumed by the large clusters, which will thus grow in size rather than react with other clusters. This is the so-called Reaction-Limited Monomer Cluster growth (RLMC) or Eden growth[23, 24]. The reaction between clusters is hindered due to electrostatic repulsion as well as the fact, that a condensation under basic conditions necessitates an inversion at the respective silicon atom where the substitution should occur[9]. The result of the base-catalyzed sol-gel-process is a so-called colloidal gel, consisting of three dimensionally agglomerated large clusters. The drawing from Iler[20] in figure 1.5 gives an excellent idea of the formation of the different morphologies in dependence of the pH.
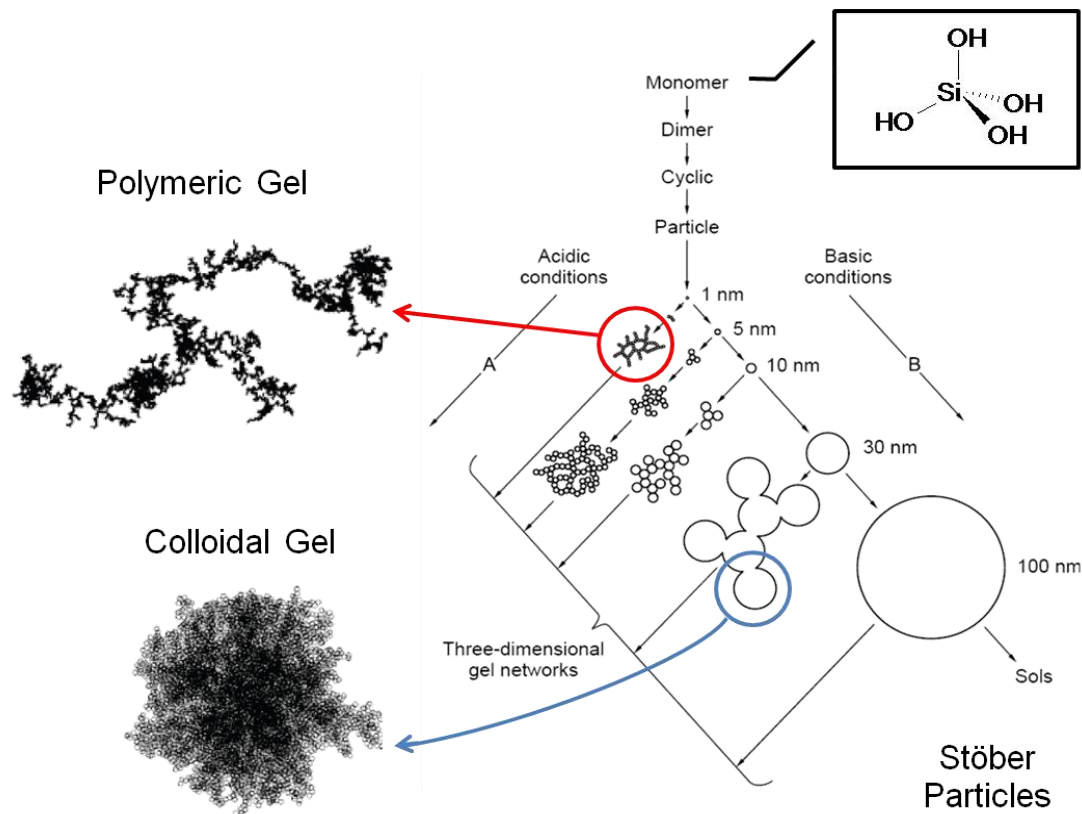
Fig. 1.5. Morphology control for sol-gel processing of alkoxysilanes in dependence of the pH; taken and modified from **[20, 21]**

A colloidal particle within a sol is stabilized by electrostatic repulsion due to the charged groups on the surface. It is clearly understood that if the electrostatic repulsion between silica colloids is low, gelation should be facilitated. In the case of silica the isoelectric point (net neutral surface charge) is in the pH range of 2-3. Among and above this value the positive or negative surface charge will lead to a different agglomeration behaviour. At basic conditions, the growth of the clusters is supported and thus even the so-called Stöber particles[25] may be synthesized, which show a monodisperse size distribution. However, it is possible to influence the electric double layer of the silica particles by the addition of salt. This will enhance the shielding of the surface charge. Consequently, the particles do not reject each other and agglomeration will be facilitated. This is a prominent way to selectively destabilize a colloidal solution at a certain time.

The pH is a powerful tool to tune the materials morphology. However, there are lots of other parameters which affect the sol-gel transition, such as kind and concentration of the precursor, solvent (for example, the water/alcohol – ratio), temperature or additives, such as surfactants. In addition, one has to keep in mind the various processing techniques, which demand different requirements to the sol concerning all these parameters. It is obvious that

sol-gel chemistry has a great potential for the preparation of materials. Its advantage is that it is a gentle and cheap method, its disadvantage that it is also a rather complex one.

The processing of really sophisticated materials, such as aerogels, i.e. monolithic materials, which contain air within their pores and which do not shrink significantly upon drying, involves several additional steps after the gelation. Solvent containing gels are usually called wet gels, in particular "hydrogels" if water was used as a gelation medium, or "alcogels" in the case of alcohols. After gel formation, which is obtained by a three-dimensional connection of the sol particles, the hydrolysis and condensation reactions are not completed. The sol is usually still inside the pores of the newly formed framework. Thus, further reactions will occur. Since the condensation reactions are reversible and the solubility on convex surfaces is higher than on concave ones, a material transport will occur due to Ostwald ripening. This leads in summary to a further stiffening of the network and therewith an increase in the stability. Further crosslinking of the network will likewise lead to shrinkage and the expulsion of solvent from the wet gel, which is called syneresis. Removing the solvent from the gel without destroying the gel body is a delicate task and indeed the most critical step for the preparation of aerogels. However, if successful, highly porous and transparent monoliths with outstanding properties may be obtained (see figure 1.6).
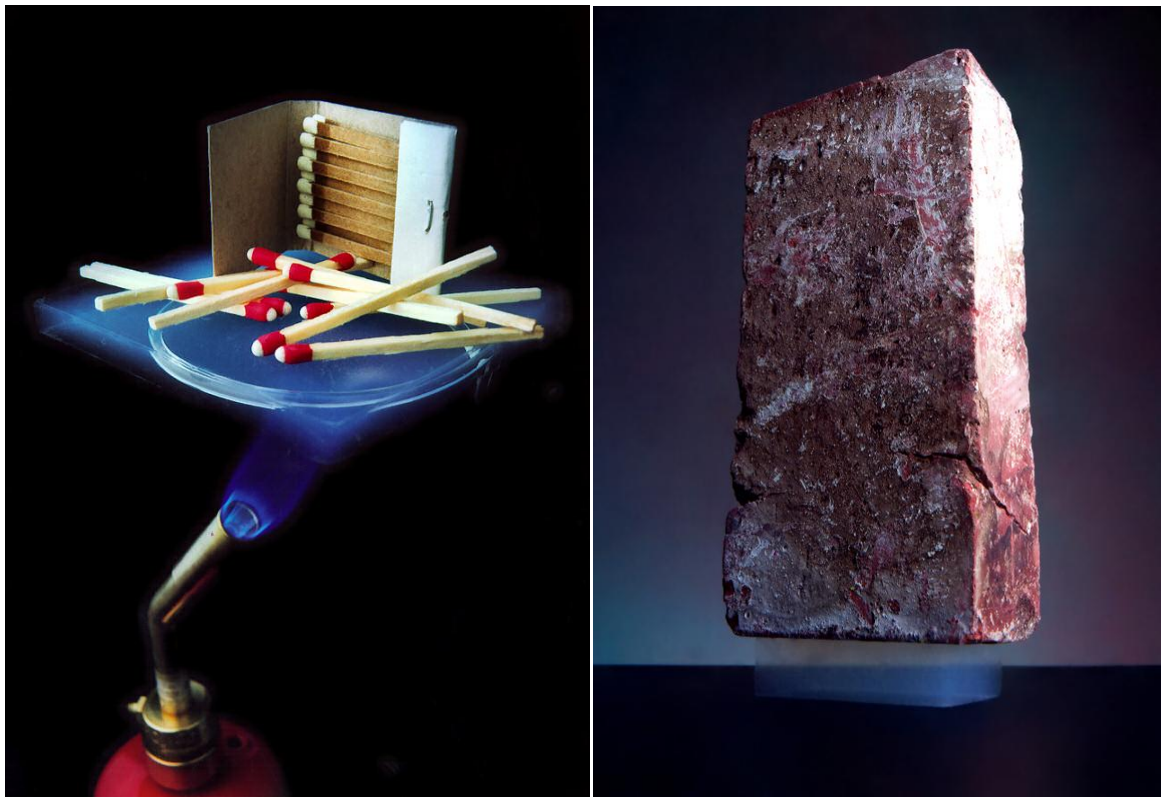

Fig. 1.6. Aerogels and their outstanding properties, such as excellent thermal insulation behaviour (left) and mechanical stability (right); 2 g aerogel carries a 2.5 kg brick; images taken from **[36]**

It has to be mentioned that the preparation of aerogels is not restricted to silica[26-28] or organosilica materials[29-31]: Many efforts were also made for the preparation of aerogels consisting of other metal oxides[32-34] and even for purely organic ones[35], for example from resorcinol/formaldehyde precursor mixtures.

If a wet gel is subjected to conditions, where the solvent is able to evaporate, the gel body will shrink by the same amount of volume the evaporated solvent had in the liquid state. This may be attributed to capillary forces, which occur due to surface tension. The shrinkage will proceed as long as the network is flexible enough. Such a behavior is primarily found in silicon alkoxide systems. Due to this process, the pores will shrink and hydroxyl groups on the surface may come together and form new siloxane bonds, leading to a further stiffening of the network. An ongoing crosslinking will lead to a state, where the capillary forces are no longer able to force the gel to further shrinkage. This is the most "critical point" since the tension inside the gel reaches a maximum. Evaporation of the solvent no longer occurs solely from the exterior surface of the gel body, which leads to a pressure gradient being responsible for cracks. In addition, solvent within larger pores will evaporate faster from the gel, which is leading to inhomogeneities concerning the tension on different sides of the pores, and thus to further cracking. Huge efforts were taken to develop strategies, which counteract the crack formation by capillary forces. Large pores, for example, are advantageous due to weaker tension[37, 38]. Other ways are ageing to increase the rigidity or the addition of surfactants to reduce the surface tension in the pores, both being valuable tools to produce crack-free but strongly shrunken gels, so-called xerogels[39]. Nevertheless, this is not sufficient for the preparation of aerogels and more effective procedures have to be applied. One chemical approach is an appropriate solvent exchange and hydrophobizing of the surface, for example with trimethylchlorosilane, which enables a strong reduction of the capillary forces. In addition, the blocked silanol groups are no longer able to form new siloxane bonds. The gel remains flexible and shrinks as long as solvent is still located inside the pores. If evaporation is finally completed, the gel may "spring-back" to its initial size. This was first reported by Brinker and coworkers[40]. Another drying approach is the so-called supercritical drying. Using this method, the solvent inside the gel body will be put into the supercritical state, in which liquid/gas – interfaces no longer exist. This is simply achieved by replacing, for example, alcohol from a wet gel with liquid carbon dioxide within an autoclave and subsequent heating above the critical point (31 °C, 7,375 MPa). Above this temperature and pressure the supercritical state of carbon dioxide enables drying of the gel by a direct transition of the supercritical fluid (SCF) into the gaseous phase (see grey curve in figure 1.7).
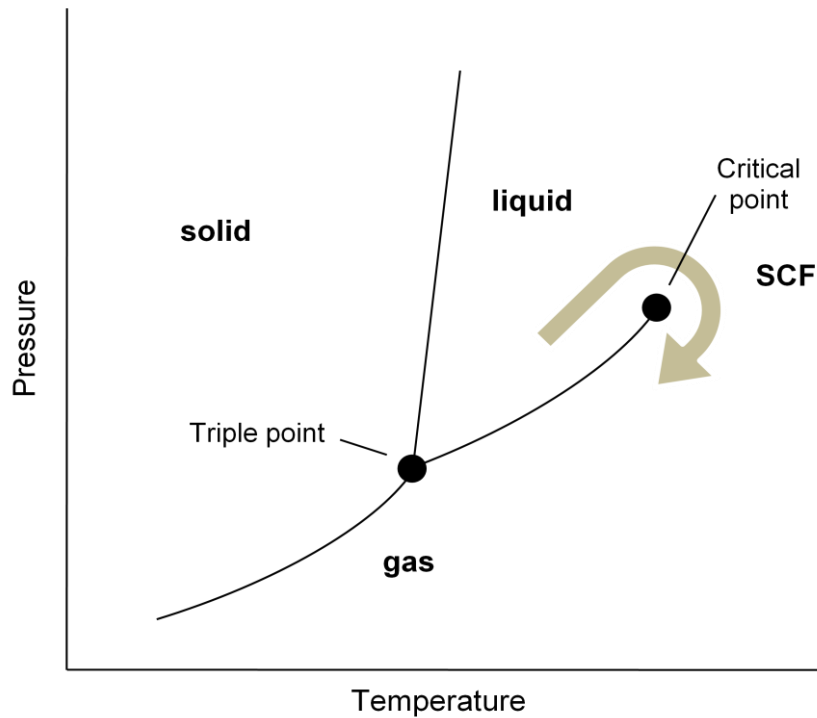
Fig. 1.7. Phase transitions during supercritical drying; the grey curve represents the phase transitions

1.1.2 Polymerisation-induced phase separation

Aerogels consist of large and disordered nanopores with broad size distributions. However, for many applications, monolithic materials would be desirable, combining huge and interconnected micrometer-sized macropores and nanopores within the framework domains. In the 70's Shoup presented the preparation of materials with large micrometer-sized continuous pores from colloidal silica dispersion and alkali silicate solution**[41]**. However, the preparation of a monolithic double pore material by this method would be rather complex. In the early 90's, Nakanishi and Soga introduced a completely new and innovative procedure for the preparation of monolithic sol-gel materials with multiscale porosity**[42]**. From conventional polymer chemistry it is well known that polymer solutions exhibit rather complex phase behaviours. The molecular weight as well as interactions between different kinds of polymers or the solvent have a significant influence on the stability of the system. First attempts to describe these phenomena were conducted quantitatively within the Flory-Huggins theory**[43, 44]**. Flory and Huggins developed a model which describes the enthalpic and entropic contributions of mixing polymer(s) and solvent to Gibbs' free enthalpy of mixing. Whereas the entropic contribution arises from the whole number of possible arrangements within a certain volume, the enthalpic contribution takes interactions (dipole-dipole or hydrogen bonds etc.) between the components into account. Polymerizing silica will as well underlie such phase relations under certain conditions. For example, the addition of poly(sodium styrenesulfonate) (PSS) to polymerizing silica will indeed lead to an entropy

driven phase separation with ongoing polymerization of silica. In figure 1.8 a typical phase diagram for a polymer/solvent or a quasi binary polymer mixture (if the phase relation is essentially determined by the affinity between two polymers) with an upper critical solution temperature for certain polymerization degrees is shown. The continuous line represents the binodal barrier between the one phase and the metastable region. The area within the dotted spinodal line is the unstable two phase region. If the system is pushed either into the metastable or unstable region, phase separation will be observed. At the beginning of the polymerization, the system will be in the one phase region. A destabilization could be obtained by a physical (left graph) or chemical cooling (right graph) of the system. Physical cooling means a temperature decrease of the system, but chemical cooling means an extension of the two-phase region due to an increase of chemical bonds (increase of polymerization degree). Thus, in the case of a silica sol, which contains a polymeric additive, the initial composition may be eventually thrust into the two phase region by ongoing condensation of silica.
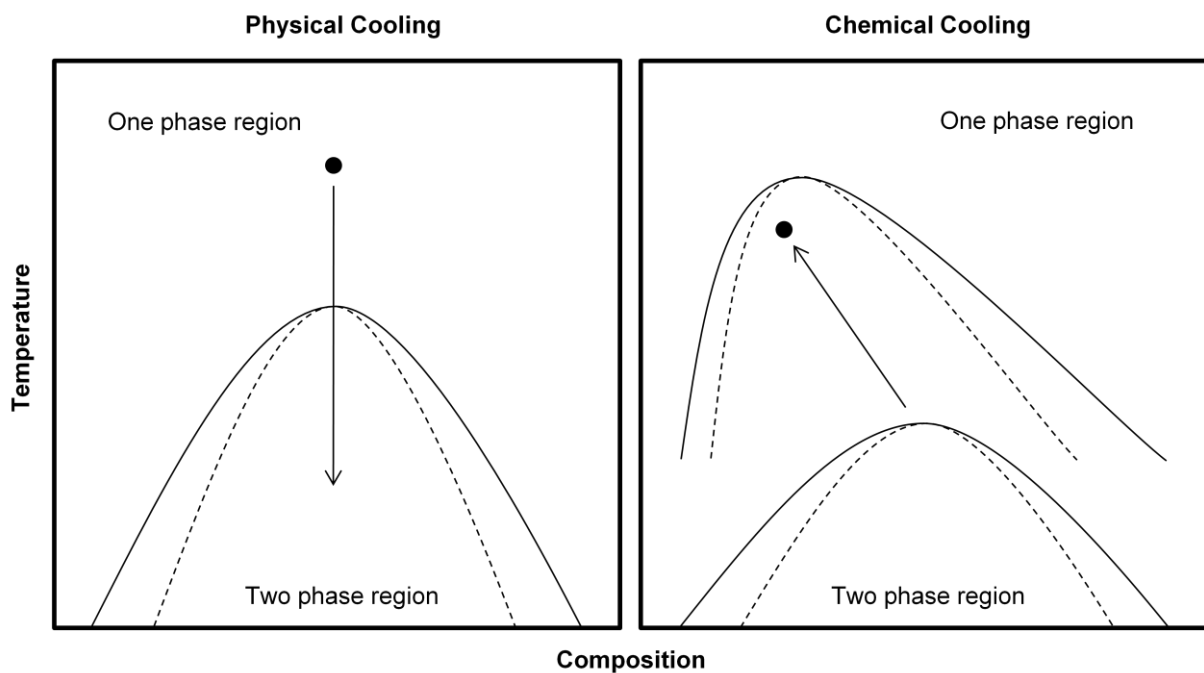

Fig. 1.8. Physical or chemical cooling of a polymer mixture with an upper critical solution temperature; taken and modified from **[45]**

In the metastable region the phase separation will follow a nucleation and growth mechanism induced by impurities or by small nuclei formed due to concentration fluctuations, leading to particulate morphologies, as is shown in the left scheme of figure 1.9. A completely different phase separation mechanism is observed if the system is thrust into the spinodal region. Then the system spontaneously will collapse, since it is unstable even against smallest concentration fluctuations. In the case of the spinodal decomposition there is no clear

interface between the phase domains at the initial stages, however contrast will increase with time. The result of this is usually a bicontinuous morphology.
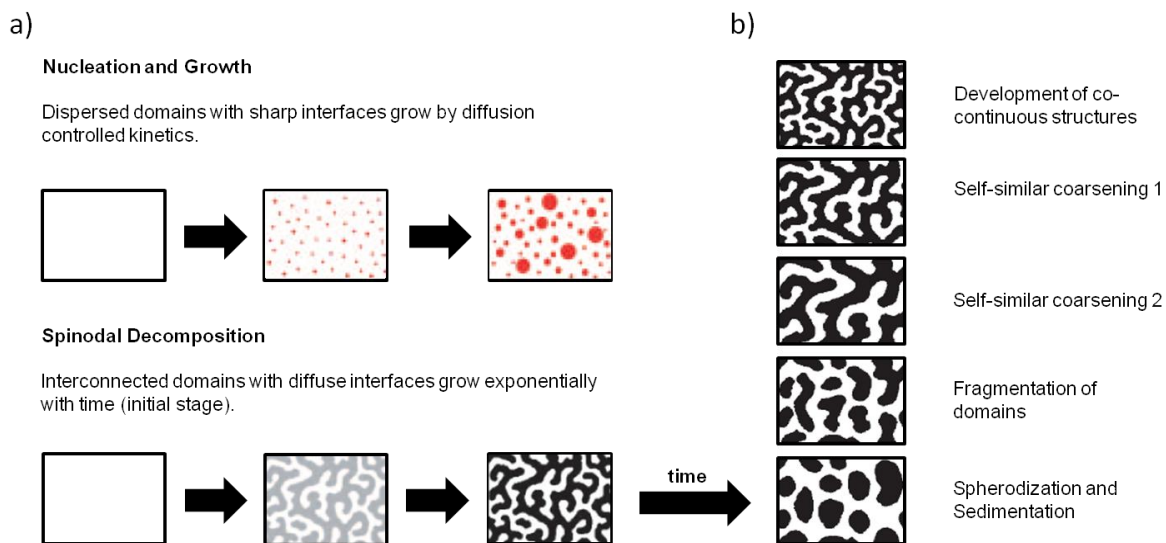

Fig. 1.9. a) Nucleation and growth and spinodal decomposition mechanism; b) Coarsening during spinodal decomposition; taken and modified from **[45]**

In the silica/PSS system two continuous phases of silica/solvent and PSS/solvent will be formed. The sol-gel-transition will freeze the silica at a certain time. By removing the organic polymer, a silica gel with huge interconnected macropores could be obtained. However, the spinodal decomposition is accompanied by a self-similar coarsening of the bicontinuous structure due to interface instabilities (see right scheme in figure 1.9). If the sol-gel transition freezing occurs late also particulate morphologies or gels with micrometer-sized isolated pores are accessible.

If the interactions between polymerizing silica and polymeric additive are strong, the phase separation is mainly driven due to the enthalpic contribution. If poly(ethylene oxide) is added to polymerizing silica, the affinity of the poly(ethylene oxide) (PEO) to the solvent may be decreased due to the hydrogen bonds between the silanol groups and the ether oxygens of the PEO. Thus, the silica/PEO complex becomes unstable and will phase separate into one phase rich in silica and PEO and one rich in solvent**[46, 47]**. Although the interactions in the silica/PEO and silica/PSS systems are different, the resulting gel morphologies are similar. If one is able to remove the phase separation inducing agent, for example by washing procedures followed by careful drying and/or calcination, gels may be obtained. In contrast to aerogels, these gels are not transparent, since the macroscopic pore structures are larger than the wavelength of visible light. A welcome by-product of the interconnected macropores is usually the formation of nanopores inside the framework domains. Their size distribution and number can moreover be influenced by treatment of the gel with alkaline

solution.**[45, 48]** However, these pores are irregularly shaped and show relatively broad size distributions. Thus, the next sub-chapter deals with the use of poly(ethylene oxide)-block-poly(propylene oxide)-block-poly(ethylene oxide) copolymers (PEO-PPO-PEO copolymers) as structure-directing agents to encourage the formation of highly ordered mesostructures.

The polymerization-induced phase separation process is not restricted to (organo)silica. Recently the preparation of titanium and zirconium dioxide**[49-51]** as well as aluminum oxide**[52]** monoliths with multiscale porosity were presented. It was furthermore possible to use the concept of polymerization induced phase separation in living radical polymerization systems to generate purely organic monoliths with interconnected macropores**[53, 54]**.

1.2 Periodic mesoporous (organo)silicas

Almost 20 years ago, scientists of the Mobil Research and Development Corporation have discovered a new class of porous materials by the hydrothermal processing of aluminosilicate gels in the presence of quaternary ammonium surfactants[55, 56]. Transmission electron microscopy images revealed that a material with a highly ordered nanopore structure, in particular two-dimensionally arranged cylindrical pores, with rather large pore diameters in the range of 4 nm were formed. Figure 1.10 shows a transmission electron microscopy (TEM) image of such a material.
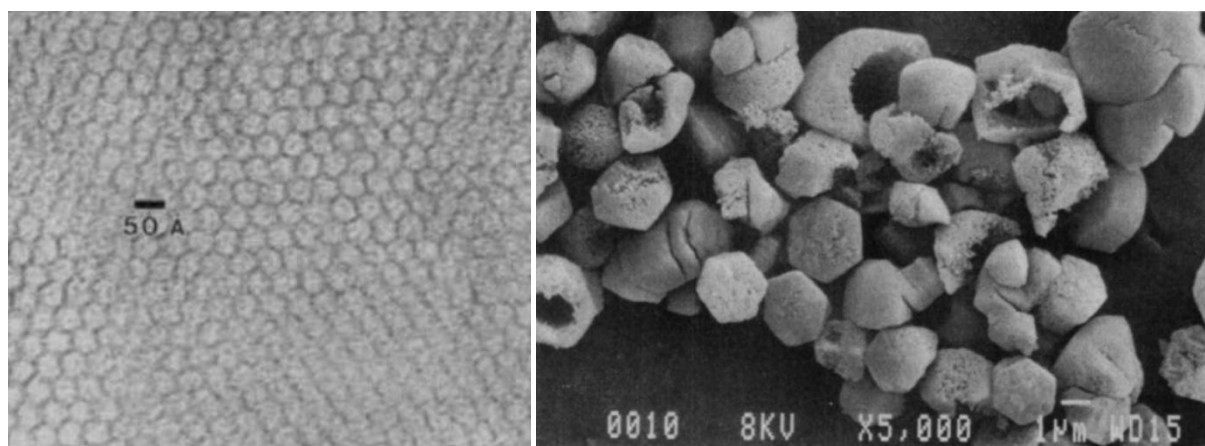

Fig. 1.10. Electron microscopy images of MCM 41; left: TEM shows the two-dimensionally arranged entries of the cylindricaly pores; right: SEM shows the mesocrystals; images taken from **[55]**

Porous materials with pores in the range of 2 – 50 nm are usually called mesoporous materials, in particular mesostructured, if the pores show certain crystalline ordering. Up to the discovery of the Mobil Composition of Matter (MCM) class mainly microporous and crystalline zeolites (aluminosilicate minerals) with diameters smaller than 2 nm were known. The discovery gave rise to a completely new and promising research area with lots of possible applications in the fields of adsorption, chromatography, catalysis, gas storage and sensor technology for new porous materials. Most routes use sol-gel-processing of alkoxysilanes in the presence of ionic or non-ionic surfactants. These are molecules which comprise, for example, a hydrophilic headgroup and a hydrophobic chain, such as the ionic cetyltrimethylammonium bromide (CTAB). These amphiphiles are able to form micelles in solution and at higher concentrations even lyotropic liquid crystals by an agglomeration of the micelles. Cylindrical micelles, for example, may form two-dimensionally arranged aggregates, whereas spherical micelles lead to cubic ones. Shape of the surfactant, concentration and temperature are factors which strongly influence the phase diagrams of surfactant/solvent mixtures and thus the resulting mesophases[57-60]. In the following figure

a ternary phase diagram for a CTAB/water/hexanol mixture is shown to demonstrate the complex phase behavior of surfactants (see figure 1.11).
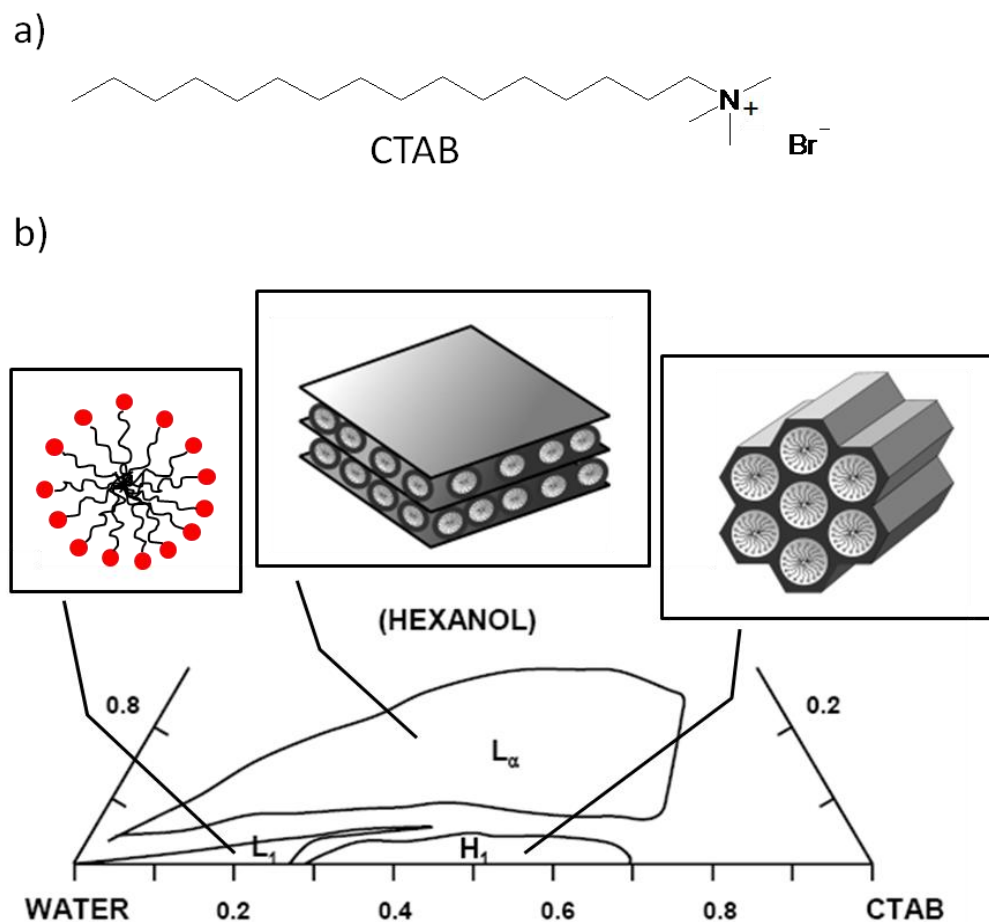

Fig. 1.11. a) CTAB surfactant; b) Ternary phase diagram for a CTAB/water/hexanol mixture (L_α represents a lamellar phase, H_1 the hexagonal one and L_1 the normal micellar phase); taken and modified from **[57, 61, 62]**

The charged precursor species will undergo interactions with the (charged) surfactant molecules and form eventually larger aggregates, the mesoscopic crystallites (see the right image in figure 1.10 for an example). There are two mechanistic suggestions for the formation of mesostructured materials: On the one hand it is believed that the structure directing agent will form liquid crystalline aggregates and the precursor will polycondense around them. This rather simple suggestion is generally known as the "true liquid crystal templating (TLCT)" mechanism**[55]**. However, such a mechanism will only work if a true liquid crystalline phase is already present. Further mechanistic studies have shown that even at very low concentrations of the surfactant, mesostructured powders were formed**[63, 64]**. This suggested a cooperative arrangement of the inorganic precursor species together with the surfactant, which is now known as the "cooperative mechanism". Most synthesis conditions are probably best described by this model. *In-situ* infrared spectroscopy**[65],** and a large number of detailed *in-situ* small angle X-ray scattering studies**[66, 67]** were performed

to get a better insight into the mechanism of the mesostructure formation. Indeed, these investigations support the cooperative mechanism and it was also found that the mesostructure formation may be treated similar to a conventional crystallization process, following a nucleation and growth mechanism of the precursor/surfactant hybrid micelles[65-67].

Whereas ionic surfactants lead to materials with small pores and relatively thin walls, the use of non-ionic surfactants produces larger pores and thicker walls[68]. A typical non-ionic surfactant would be a poly(ethylene oxide)-block-poly(propylene oxide)-block-poly(ethylene oxide) copolymer such as Pluronic P123. In that case there is no sharp boundary between the solvent and the shell (the hydrophilic poly(ethylene oxide) moieties) of the micelle. It is also well known that non-ionic surfactants produce microporosity within the pore walls, since the poly(ethylene oxide) chains are homogeneously distributed within the inorganic matrix[69]. The removal of the surfactant from the material is easily obtained by washing or calcination giving access to the corresponding porous silicas.

The sol-gel-process is the most valuable method for the preparation of mesostructured materials even in non-siliceous systems, such as titania[70], zirconia[71] or alumina[72]. In the meanwhile, other routes to produce mesostructured materials have been published in the literature: A recent example is given by the co-assembly of ligand stabilized platinum nanoparticles with block copolymers to form hybrids, from which even mesostructured platinum is accessible[73]. Other research groups use mesostructured silica as hard template. The impregnation of these mesostructured silicas with, for example, sucrose (a so-called nanocasting approach) and subsequent carbonization followed by HF etching to remove the silica matrix may yield mesostructured carbons[74]. Recently, there is an increasing interest in nanocasting for the preparation of various kinds of mesostructured materials[75, 76]

Today many routes for the preparation of mesostructured silicas are known[6]. Chemists have learned to tailor the materials structural features, such as pore diameter and structure by a variation of the synthetic conditions[77, 78] However, it took quite a long time until three groups almost simultaneously reported the preparation of periodic mesoporous organosilicas (PMOs) from bis-silylated organosilane alkoxides[79-81]. The incorporation of organic groups into the inorganic mesostructured framework produced novel organic-inorganic hybrid materials with promising properties. This is in particular interesting in the case of sol-gel-coatings for electronics devices, such as computer chips[82]. The high porosity and the organic content of the coating is leading to a lesser polarizability and thus to less charge transfer and signal losses. Compared to silica, organosilicas are more stable under basic conditions, which is in particular interesting in the case of monolithic materials for

applications in chromatography[83]. In figure 1.12 several carbosilanes like the ethane-[79] and ethene-bridged[81], the thiophene-[84] and phenylene-bridged[85] as well as more complex cyclic[82] and dendrimeric[86] ones, which have been already successfully applied for the synthesis of mesostructured materials are shown.
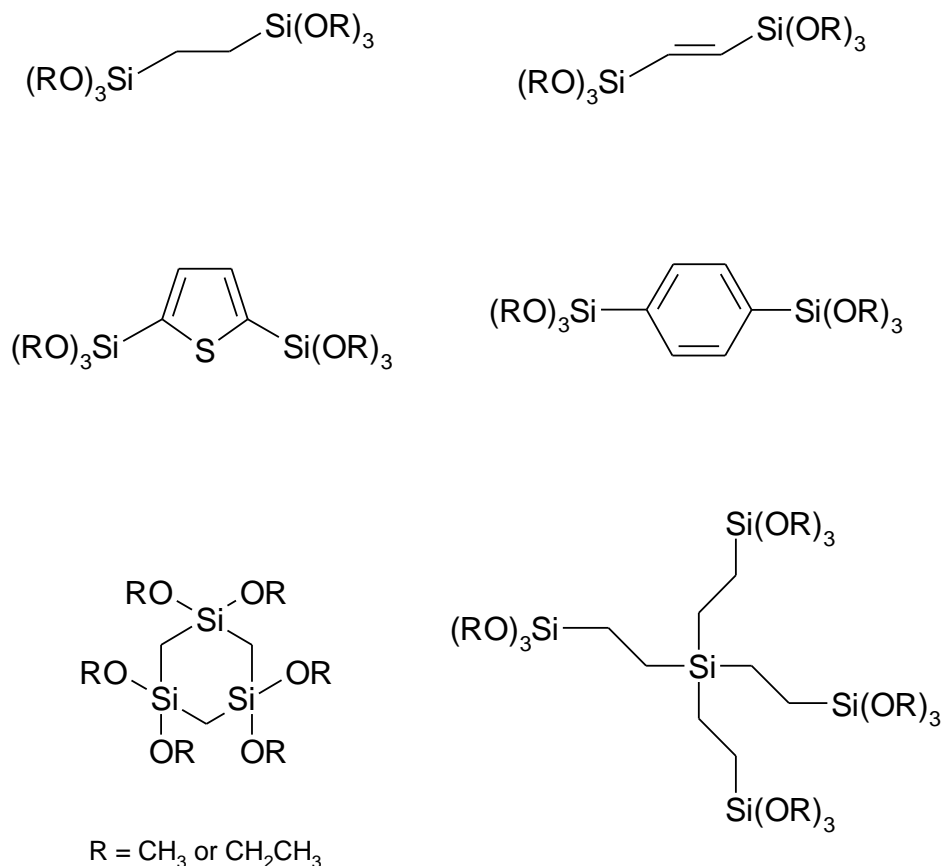

Fig. 1.12. Several organosilane precursors for the preparation of PMO materials

As in the case of silica it is possible to functionalize the surface of these materials with post-synthetic treatments[62], but this will not necessarily lead to a large surface density of functional groups. Recently two interesting approaches were presented for the preparation of highly functionalized PMOs: The first is the so-called "all in one approach"[87-89]. The ethene-bridged alkoxysilane was hydroborated with a boron hydride substituted by a long alkyl chain. The resulting precursor not only possessed the sol-gel reactivity but was at the same time a surfactant by itself. The precursor was wet chemically converted into an organosilica material and treated with hydroxylamine-*O*-sulfonic acid to quantitatively remove the alkyl chain and to form an aminogroup, which extends directly into the newly formed pore (on the left in figure 1.13). This is an elegant one pot approach, but it was not possible to generate ordered pore structures. Those could only be obtained when another surfactant like the non-ionic Pluronic P123 was added to the sol. By an asymmetric hydroboration it was even possible to generate a chiral organosilane precursor. After the already described

processing, an organosilica with true chiral amino groups in the pores was obtained. This makes these materials in particular interesting candidates in the field of chiral chromatography. In a different approach Polarz and coworkers first prepared 3,5-bis(triisopropoxysilyl)bromobenzene by lithiation with butyllithium (BuLi) and subsequent reaction with tetraisopropoxysilane. Now it is possible to do further synthetic work and to substitute the resulting bromo atoms to yield a functionalized sol-gel precursor[90, 91]. For example, lithiation and reaction with CO_2 will lead to a carboxy-substituted precursor, The reaction with thionyl chloride will then form the respective benzoyl chloride, which is reacted with a protected alanine by forming a peptide bond. The resulting precursor was successfully converted into a highly ordered, functionalized as well as chiral PMO material (on the right in figure 1.13).
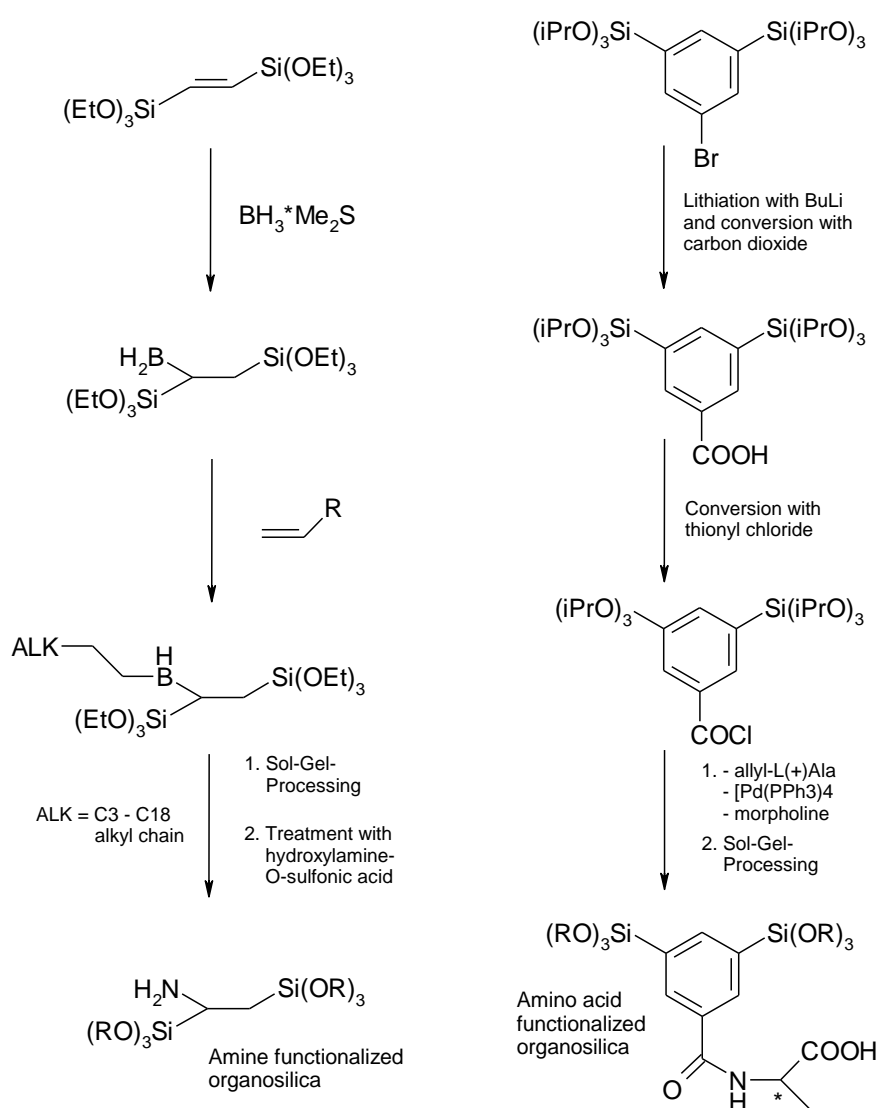

Fig. 1.13. "All in one approach" from Thomas et al. on the left and advanced precursor design by Polarz et al. on the right

Without a doubt these materials are at the forefront of functionalized (organo)silicas, but until now it was not possible to prepare hierarchically structured monoliths from the respective precursors. Monoliths, however, would be advantageous for several applications, for example in chromatography.

1.2.1 Monoliths with multiscale porosity prepared from glycol-modified silanes

Although silica monoliths with multiscale porosity (macro- and disordered mesopores) are accessible for almost twenty years, the synthesis of silica gels with mesostructured frameworks was first reported in 2003 by Hüsing and coworkers[92]. The development of such materials is driven by a phase separation induced by an increasing incompatibility in the silica/polymeric additive/solvent system during silica condensation. It is therefore necessary that the surfactant itself is not only able to lead to the formation of a mesostructure, but in addition to a polymerization-induced phase separation. Non-ionic surfactants, such as poly(ethylene oxide)-block-poly(propylene oxide)-block-poly(ethylene oxide) copolymers (for example Pluronic P123) have an ability for inducing a phase separation that is comparable to poly(ethylene oxide). In addition, they are even capable to induce mesostructure formation. Indeed, the conversion of the ethylene glycol-modified silane (tetrakis(2-hydroxyethyl)orthosilicate; EGMS) in aqueous hydrochloric acid solution in the presence of the non-ionic surfactant P123 led to the formation of a cellular mesoscopically organized silica gel. In this material, thin rods are three-dimensionally connected to form a macroporous framework comprising two-dimensionally arranged cylindrical mesopores inside the rods (see figure 1.14 for an example).
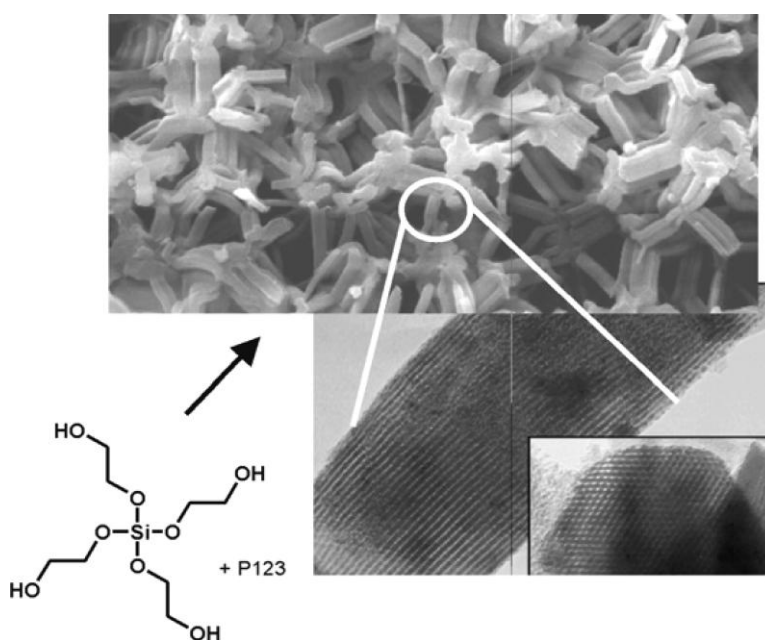

Fig. 1.14. Hierarchically structured silica[93]

Diol- or polyol-modified silanes are usually obtained by a transalkoxylation reaction of conventional alkoxides with diols or polyols[94] and offer several advantages to the alkoxides: First, the free hydroxy groups give the precursor an excellent solubility under aqueous conditions. Thus, a homogeneous sol is quickly prepared under ambient conditions. Based on the choice of the diol or polyol, the sol-gel precursor could be modified to be more biocompatible. For example, glycerine- or sugar-modified silanes could be used for entrapment of enzymes into (organo)silica matrices[95]. It was also shown, that the use of such silanes will lead to a reduced shrinkage of monolithic materials during sol-gel processing[96]. Second, the most interesting aspect for the preparation of (organo)silica monoliths with multiscale porosity is a better compatibility with surfactant mesophases. This was investigated intensively by Alexandridis and coworkers for poly(alkylene oxide)-based block copolymer mixtures. They varied the composition of mixtures containing a PEO-PPO-PEO triblock copolymer (Pluronic P105), water and organic additives like glycerol or ethanol[59]. The latter possesses different polarities and thus has a significant influence on the phase diagrams shown in figure 1.15. L1 denotes the ternary composition region of liquid clear isotropic micellar solution and the others (I_1, H_1, L_α and V_1) are lyotropic liquid crystalline phases. The more polar additives like glycerol suppress the isotropic region and favor the liquid crystalline phases, whereas the phase diagram is dominated by the isotropic region in the case of ethanol. Only at very small concentrations of ethanol, LC phases are observed.
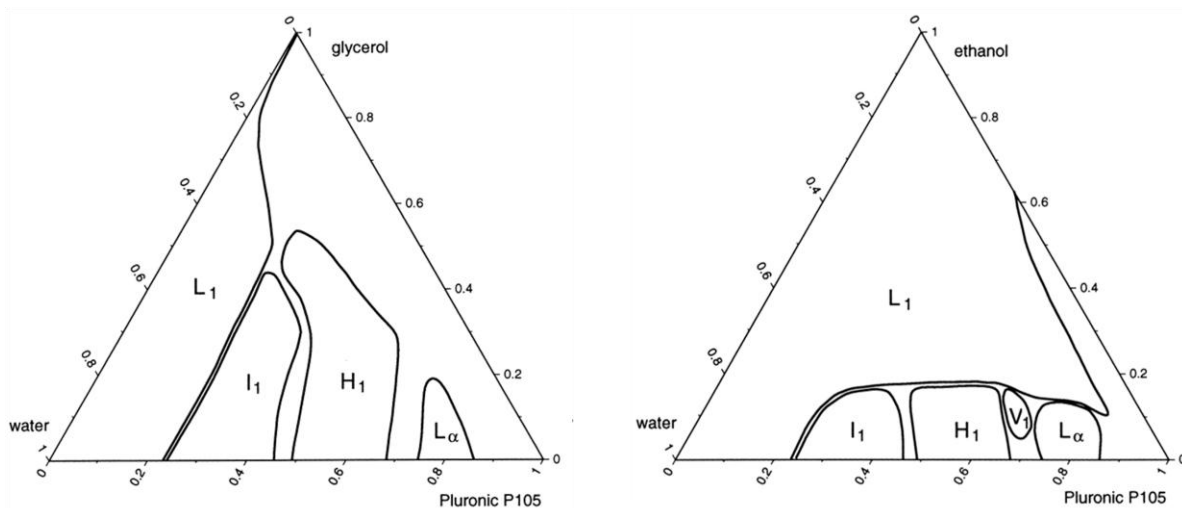

Fig. 1.15. Ternary phase diagrams for Pluronic P105/water/organic solvent-systems[59]

Ethanol is a good solvent for both the PEO and PPO block of the copolymer and has thus a strong influence on the micellar aggregates[58]. It increases the critical micelle temperature and concentration at which micelles are formed. In addition the aggregation number of the copolymer micelles is decreased. This has two consequences for the preparation of

hierarchically structured monoliths via sol-gel processing. If conventional alkoxides are used as precursors, the ethanol produced upon hydrolysis will disturb the formation of the surfactant/silica complex and thus suppress the phase separation. Although, it was possible to prepare macroporous monoliths with disordered mesopores from conventional alkoxides, the preparation of such monoliths with ordered mesopores was rather difficult. In 2004 Nakanishi reported the preparation of the first inorganic-organic hybrid monoliths with interconnected macropores and highly ordered 2D-hexagonally arranged mesopores from sol-gel processing of 1,2-bis(trimethoxysilyl)ethane and Pluronic P123[97]. However, they had to add a certain amount of mesitylene to the sol, most probably to stabilize the micelles. But even with organosilanes, which possess large organic groups, such as the benzene ring, the modification with ethylene glycol is leading to a precursor from which the desired materials are easily obtained without the addition of other additives. This was presented in 2006, by the successful conversion of the glycol-modified phenylene-bridged silane (PGMS) into porous monoliths with even four levels of hierarchy (see figure 1.16)[98]. Wide angle X-ray scattering measurements and high resolution TEM observations have shown an additional order within the pore walls due to a staggering of the phenylene rings.
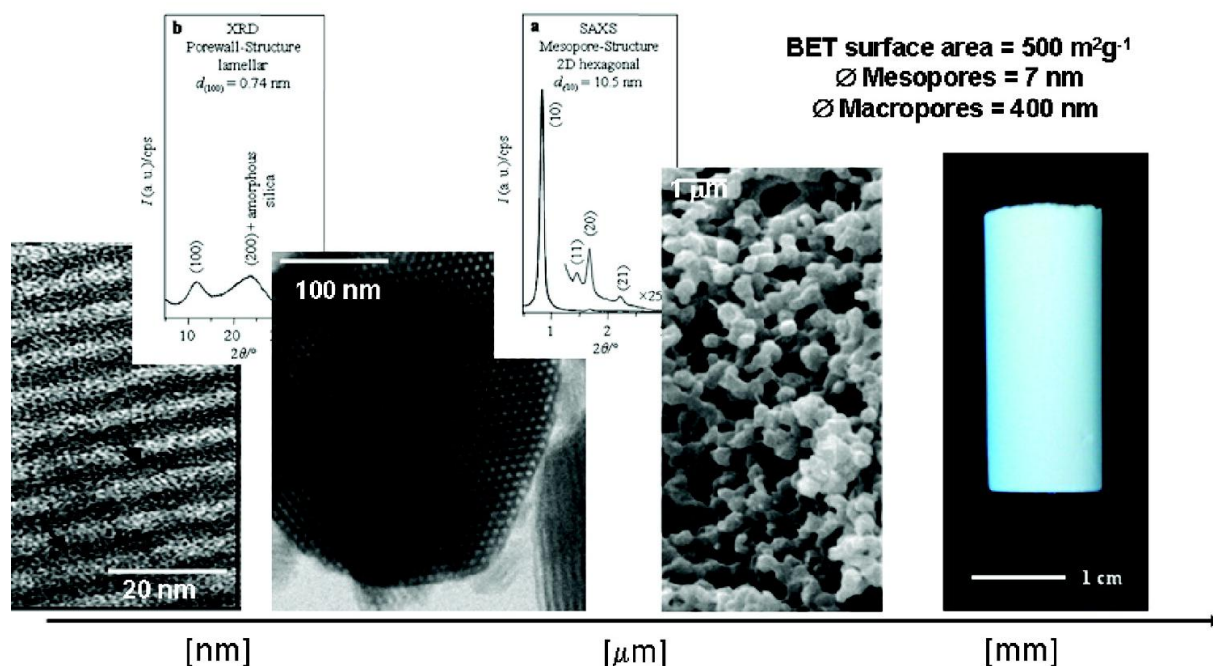

Fig. 1.16. Monolith obtained from the glycol-modified phenylene-bridged silane with four levels of hierarchy; images taken from **[98]**

Since these materials have a huge potential as columns in chromatography**[99]** or as microreactors in catalysis**[100]**, a detailed understanding of the formation is essential in order to prepare more complex and functional monoliths. *In-situ* SAXS measurements were conducted to get a deeper insight into the formation of these silica and organosilica

materials: Fritscher and coworkers investigated both, the EGMS and the PGMS systems[61]. They found that before gelation occurred, only weakly oriented hybrid micelles were visible and the mesostructure growth started not until a certain time passed after the gelation, indicating a certain flexibility of the system. However, from these studies it was not possible to evaluate whether or not the phase separation follows a nucleation and growth or a spindodal decomposition mechanism. To clarify this question, further studies have to be performed to gain a deeper insight into the growth mechanism of the mesostructure. In addition, investigations of the temperature dependence of the mesostructure growth would be helpful to describe and quantify the kinetics of the whole process.

1.2.2 Organosilicas as ceramic precursors

Modern ceramic materials, such as silicon carbides or nitrides offer a variety of beneficial properties such as high temperature stability, excellent heat conductivity together with hardness. These materials are usually synthesized at high temperatures, which makes the control of the final morphology a challenging task. The preparation of silicon carbide (SiC), for example, demands the carbothermal reduction of silicon dioxide with carbon at elevated temperatures of 1500°C or higher (Acheson process). Since SiC is an important catalyst support for highly exothermic reactions, people applied extensive efforts for the preparation of porous SiC with high surface areas in recent years[101-103]. A versatile approach is the nanocasting technique[75, 76]. Scientists infiltrated mesostructured silicas with respective SiC precursor components, such as polycarbosilanes, and subsequent thermal treatment and removal of excess silicon dioxide with, for example, HF solution will yield the desired product. That way it is indeed possible to prepare mesostructured ceramics with high surface areas. This technique could even be applied for the preparation of hierarchically structured SiC monoliths by using the respective silica monoliths as a hard template[104].

However, the nanocasting procedure is rather complex and involves several steps. The direct conversion of an organosilca into a material with comparable properties, as a so-called silicon oxycarbide (SiCO), would be much more cost-effective and less time-consuming. SiCO could be interpreted as a silica matrix, where divalent oxygen is partly substituted by tetravalent carbon. Many publications have investigated extensively the synthesis and properties of these promising materials (see introduction in chapter 5). The transformation of an organosilica or a polycarbosilane into SiCO takes already place at temperatures of 800 °C, thus lower temperatures are needed as in the case of SiC. The carbon definitely improves the thermal and mechanical stability, making these materials a valuable alternative to SiCs. However, few publications report the direct transformation of mesostructured organosilica powders into the respective SiCOs[105, 106]. It was proposed that only cubic

mesostructres could be successfully transformed into SiCO[107, 108]. Thus, much research effort has still to be devoted to get a better understanding of the various synthesis parameters affecting the carbidic carbon content and thus the properties of the mesostructured SiCO materials. In addition, for some applications it would be also attractive to prepare these materials in form of films or monoliths.
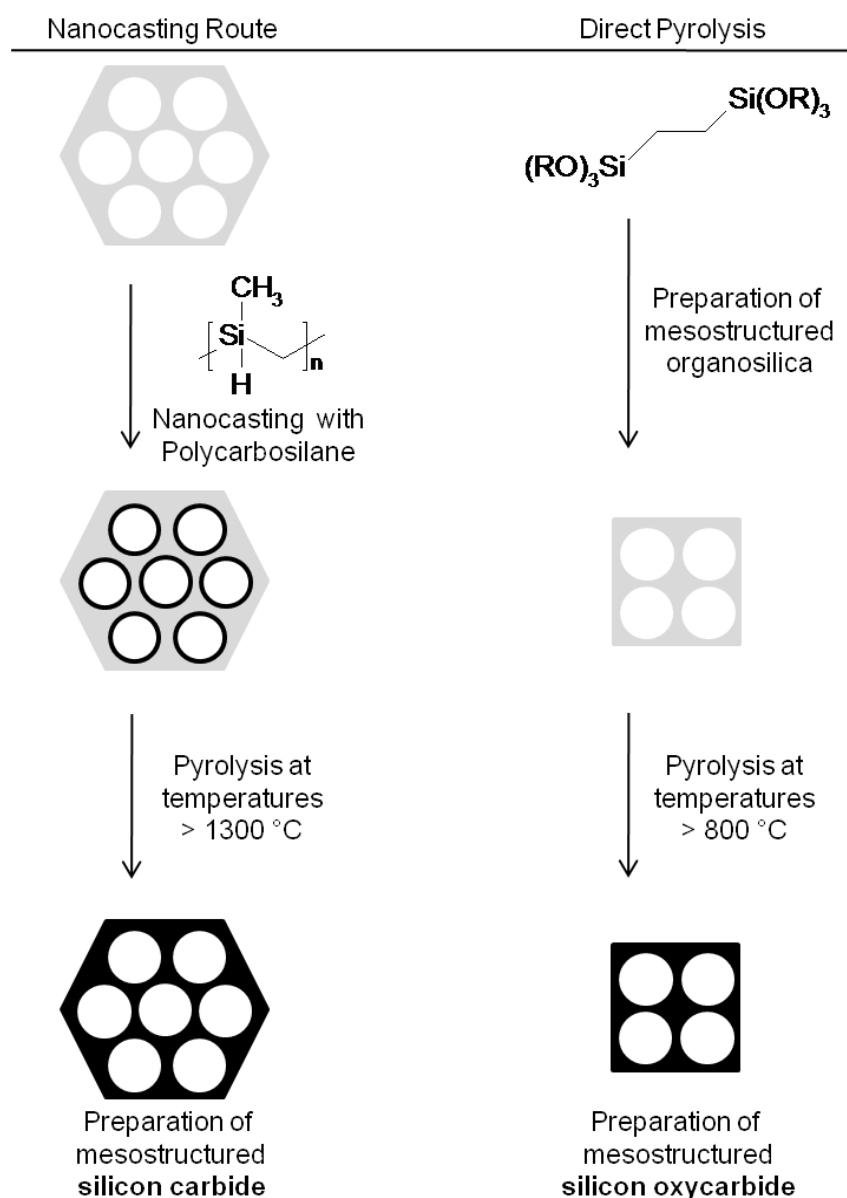

Fig. 1.17. Nanocasting approach for the preparation of SiC and the direct conversion of mesostructured organosilica to SiCO (SiCO with 2D-hexagonal mesopores are not known yet)

1.3 Characterization methods

In this subsection, a short theoretical background on the most important characterization techniques, which were used during this work, will be given.

1.3.1 Small-angle X-ray scattering (SAXS)

X-ray scattering is a valuable technique to get structural information of a material on several length scales. Conventional wide-angle X-ray scattering thereby covers the atomic level. The scattering of larger structures, in particular with a size of 1 – 100 nm, will be observed in the small angle region. For modern nanoscience SAXS has proven to be an irreplaceable tool for the characterization of nanoscopic systems such as "amorphous" aerogels or highly ordered gels such as mesostructured systems, for example periodic mesoporous materials or lyotropic liquid crystals[109]. Since very powerful X-ray sources are accessible (ranging from rotating anode devices to synchrotron radiation sources), X-ray scattering methods are as well applicable for *in-situ* investigations of colloidal systems like gelling silica[110] or the time and temperature dependent transformation of mesostructured silica/surfactant composites[111]. Within this work SAXS was extensively used as an analytical method, thus the theoretical background will be given on the next pages. The reader may also find extensive general theory on SAXS in textbooks **[112-114]**.

If X-rays hit matter, the electric field of the waves will interact with the electrons. Since the energy of an X-ray photon is very high compared to the binding energy of an atom, all these electrons will behave as if they were free. Thus, the energy of the emitted X-ray is identical to the energy of the X-ray of the primary beam, which is called elastic scattering. In figure 1.18 a) a geometrical visualization for the scattering of an incident wave by an object is shown.
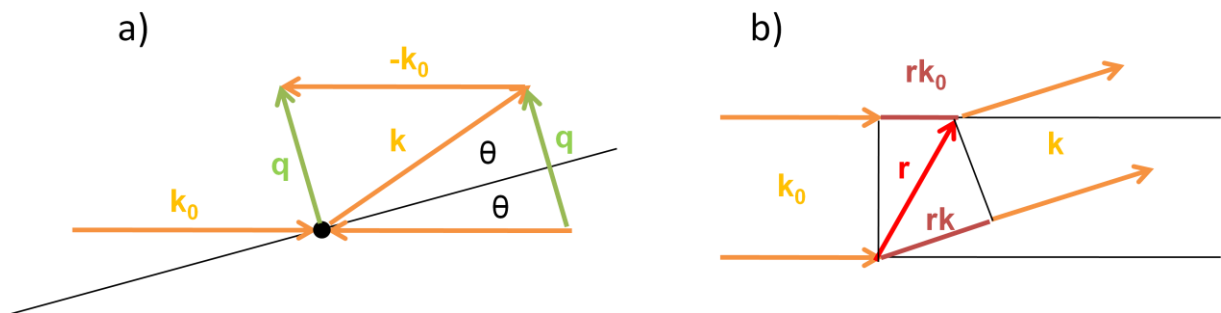

Fig. 1.18. a) Geometrical derivation of the scattering vector q; b) Scattering by two point centers

The incident beam with a wave vector k_0 hits a point center and as a result a scattered wave with the wave vector k is formed with a scattering angle of 2θ. Here θ means the glancing

angle, which is the widely used denomination in crystallography. The difference of $k - k_0$ represents the so-called scattering vector $q = (4\pi/\lambda)\sin\theta$, which is perpendicular to the reflection plane. The reciprocal value of $d = 2\pi/q$ directly gives access to the corresponding d-spacings. It should be noted that the latter relation holds only for large crystalline systems, for nanocrystalline systems deviations from this relation are possible[109].

If a second point center is added in a distance specified by the vector r, which is shown in figure 1.18 b), we may derive the phase difference between the two scattered waves, which is directly given by $\varphi = -r(k - k_0) = -rq$. The total amplitude is then obtained by a summation of all secondary waves, each represented by a term e^{-iqr}. As usually an enormous number of electrons exists within a body, which are not exactly localized, their distribution is described by an electron density $\rho(r)$. By integration over the whole volume, the amplitude $F(q)$ is obtained (equation 1.1). This is mathematically equivalent to a Fourier transform of the electron density of the investigated object[114].

$$F(q) = \iiint dV \cdot \rho(r)\, e^{-iqr} \tag{1.1}$$

However, from scattering experiments only the intensity distribution is accessible, which is given by the square of the complex amplitude:

$$I(q) = |F(q)|^2 \tag{1.2}$$

A very useful equation, which is based on formulas (1.1) and (1.2) is obtained, if further assumptions are made. In the case of a system, which is statistically isotropic and no long range order exists, one obtains the intensity of the scattered beam from a particle with maximum diameter D from the auto-correlation function $\gamma(r)$:

$$I(q) = 4\mu \int_0^D \gamma(r) \frac{\sin(qr)}{qr} r^2 dr \tag{1.3}$$

The function $\gamma(r) = \langle \rho(r)\rho(-r) \rangle$ is interpreted as the averaged self-convolution of the electron density distribution.

There are general relations for the scattering intensity from particles. A widely used parameter to evaluate scattering data is the invariant, which is proportional to the volume of the scattering structure:

$$Q = \int_0^\infty q^2 I(q) dq \tag{1.4}$$

In a typical SAXS experiment, the scattered intensity from a sample is measured in transmission (see figure 1.19). It is essential to use X-rays with a very sharp energy distribution (which is equivalent to a monochromatic beam), since the scattering depends on the wave length. This is achieved by specific absorbers or X-ray mirrors (Göbel mirrors). For a good resolution in the small angle regime it is as well important to use a highly collimated beam, since significant divergence would smear out the scattering signal at low angles. One widely used possibility to avoid this is the use of a pinhole system between the X-ray source and sample.
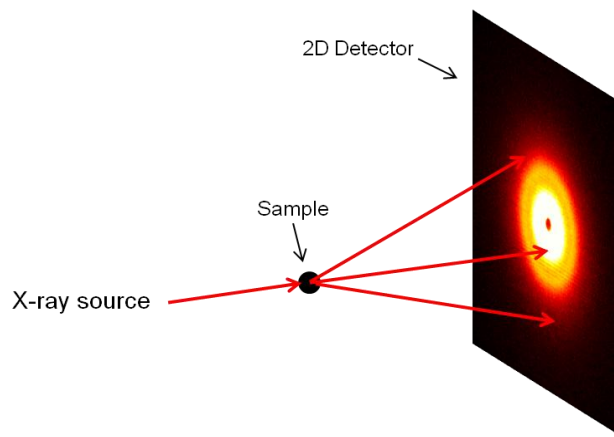

Fig. 1.19. Typical scattering experiment

In modern laboratories the intensity of the scattered waves is measured with area detectors. The detector to sample distance thereby determines the accessible q-range. By radial integration of the two-dimensional data, the scattering intensity is obtained in dependence of the scattering vector. A first idea of the structural features of a sample is gained from a logarithmic plot of the acquired data. In figure 1.20, a typical SAXS pattern is shown. The main features visible in this pattern are inserted into the figure.
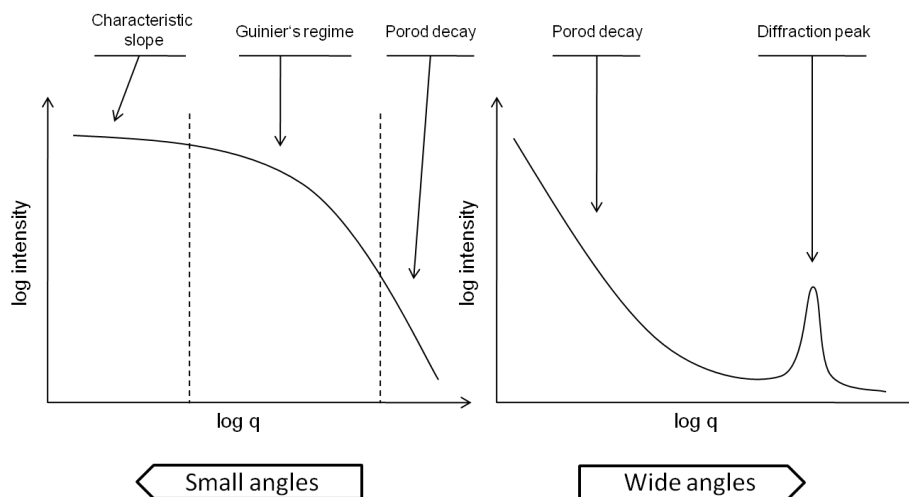

Fig. 1.20. Schematic presentation of scattering features in the small and wide angle regions

Small angle scattering from particulate systems usually shows a power law decay of the scattering intensity in dependence on the scattering vector, which is visible in figure 1.20, left part. The knee in the intermediate region (the low q region) can be correlated to a characteristic size in real space. For low q there exists a universal approximation being valid for all particulate systems. This was first given by Guinier and a derivation of it can be found in **[115]**:

$$I(q) = Ce^{\frac{-q^2 R^2}{3}} \tag{1.5}$$

R thereby denotes the "radius of gyration" of the electron density of the particles and may be derived from the linear slope of a plot of $log(I(q))$ against q^2 . The Guinier's law is only valid for dilute and isolated particles. For spherical particles, the true particle radius r is connected to the radius of gyration by $R^2 = \frac{3}{5}r^2$. At very low q, the intensity for spherical particles approaches a constant value, whereas for particles with asymmetric shape the decay follows a certain power law. This depends on the dimensionality of the particles, cylinders or rods will show an intensity decay with q^{-1} and discs with q^{-2}.

If the interface between the particle and its environment is sharp, i.e. a two-phase system of two phases with different electron densities, the intensity towards large values of q in the limit q towards infinity will follow a power law decay (equation. 1.6):

$$I(q) = Pq^{-4} \tag{1.6}$$

This is generally known as the Porod's law with P the Porod constant, which is proportional to the surface S of the scattering electron density. A derivation of this law may be found in **[114]**. The determination of the Porod constant may yield unique information about the surface area and the pore size of the investigated porous materials (see **[116]** for an example). The division of the invariant (related to the volume) and Porod's constant (related to the surface) results in the specific surface area per volume:

$$\frac{S}{V} = \frac{\pi P}{Q} \tag{1.7}$$

The inverse of the specific surface area per volume is a length, which is related to the Porod length (also denoted by chord length or persistence length) by the following equation, where ϕ the amount of one phase (in the case of material/no material this is the porosity):

$$l_P = 4\phi(1 - \phi)\frac{V}{S} \tag{1.8}$$

l_P on her part is related to the average chord-lengths of the bulk l_b and the pores/voids l_v

$$\frac{1}{l_P} = \frac{1}{l_b} + \frac{1}{l_v}$$ (1.9)

For non-dilute particulate systems the scattering is usually described by $I(q) = AP(q)S(q)$, where A denotes a parameter which depends on the total volume of the particles and experimental parameters such as the beam intensity, $P(q)$ denotes the form factor for the individual particles and $S(q)$ represents a structure factor, which describes the structural arrangement of the particles. The analytical expression of the form factor of a sphere was originally derived by Lord Rayleigh and is given by [112, 113]:

$$I(q) = (\Delta\rho)^2 V^2 P(q) = (\Delta\rho)^2 V^2 \left[3\frac{sinqR_0 - qR_0 cosqR_0}{(qR_0)^3} \right]^2$$ (1.10)

$\Delta\rho$ is the difference of the electron density of the particle and its environment, V means the Volume of a sphere and R_0 the radius. If the particles are separated widely enough from each other and if the radius of the spheres is monodisperse, one will obtain a scattering pattern, showing the characteristic minima and maxima as is seen from the following figure 1.21.
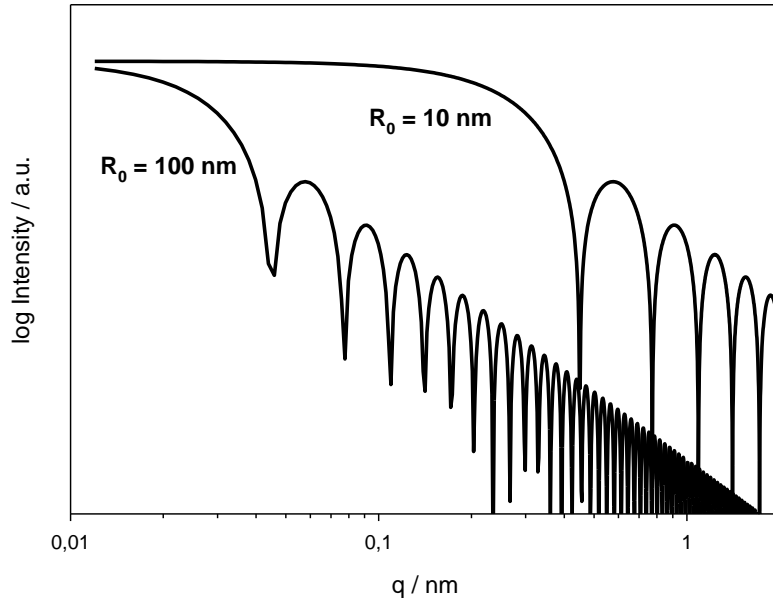

Fig. 1.21. Form factors for spheres of radii 10 nm and 100 nm

If the system exhibits a polydispersity of R_0 then the patterns will smear out very rapidly. It is then necessary to introduce a size distribution for the form factor. For a system consisting of

dilute and disordered spherical particles with a broad size distribution, the so-called Debye function (equation 1.11)[112, 113] fits the data in the low and large q region relatively well, however in the intermediate region the values of the Debye-function and the true one deviate.

$$P(q) = \left[1 + \frac{\sqrt{2}}{3}q^2R^2\right]^{-2} \tag{1.11}$$

Mesoscopically structured systems such as periodic mesoporous materials or liquid crystals from certain block copolymers will show sharp reflections in the small angle region due to the long range orders. The scattering is then described by the reflection at certain lattice planes of the mesoscopic "crystallites" and thus the position of the reflections follows the Bragg equation:

$$\lambda = 2 \cdot d_{hkl} \cdot sin\theta_{hkl} \tag{1.12}$$

Here λ denotes the wavelength of the X-ray beam, $d_{hkl} = \frac{2\pi}{q_{hkl}}$ represents a specific lattice plane distance and θ_{hkl} the respective diffraction angle for which the reflected waves are in phase. The Miller indices h, k and l define a plane that cuts the basic vectors of a certain crystal system at $\frac{1}{h}\overrightarrow{a_1}, \frac{1}{k}\overrightarrow{a_2}$ and $\frac{1}{l}\overrightarrow{a_3}$. A certain set of (hkl) thus clearly determines the respective planes. A schematic drawing of the diffraction at two-dimensionally hexagonally arranged cylindrical mesopores is shown in figure 1.22.
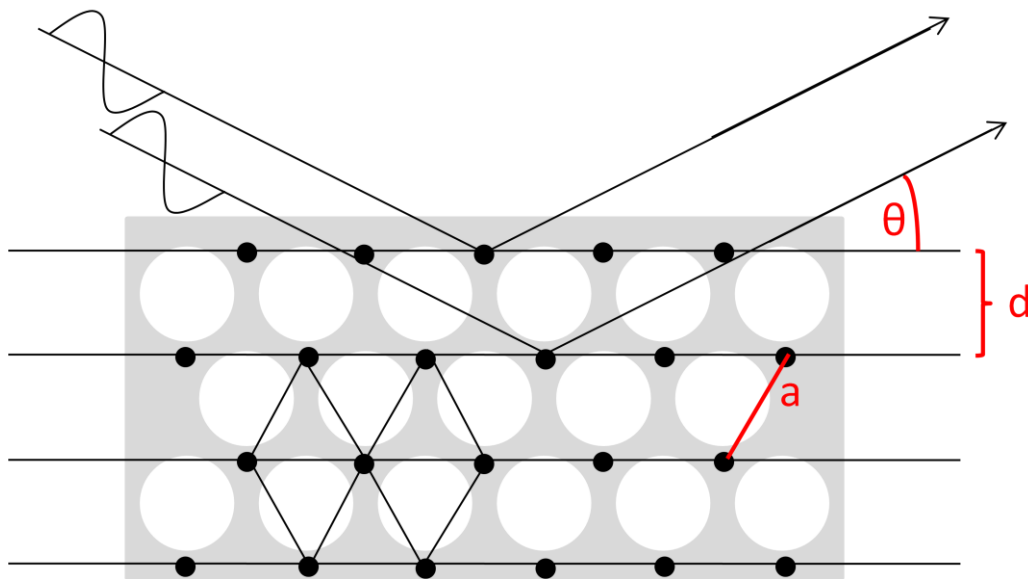

Fig. 1.22. Diffraction at lattice planes

The lattice constant a is directly connected to the lattice plane distances d_{hkl}. Table 1.1 shows the dependencies of a and d_{hkl} for 2D hexagonal, lamellar and face centered cubic (FCC) crystallographic systems.

Table 1.1 Diffraction parameters for some lattices[58]

Lattice	Position of reflections	Sequence of Bragg reflections
2D hexagonal	$q_{hk} = \dfrac{4\pi\sqrt{(h^2 + k^2 + hk)}}{a\sqrt{3}}$	$1: \sqrt{3}: 2: \sqrt{7}: 3: \sqrt{12}: \sqrt{13}....$
FCC	$q_{hkl} = \dfrac{2\pi\sqrt{(h^2 + k^2 + l^2)}}{a}$	$\sqrt{3}: 2: \sqrt{8}: \sqrt{11}: \sqrt{12}: 4: \sqrt{19}....$
Lamellar	$q_h = \dfrac{2\pi h}{a}$	1:2:3:4:5:6....

1.3.2 Electron microscopy

Optical microscopes use a certain system of lenses for the magnification of small structures. However, the resolution of such a system is restricted to the wavelength of the used electromagnetic radiation. The diffraction limited resolution of an optical microscope, which means the smallest diameter between two distinguishable objects d_{min}, was first given by Ernst Abbe:

$$d_{min} = \frac{\lambda}{2 \cdot NA} \tag{1.13}$$

Here λ denotes the respective wavelength of the radiation and $NA = n sin\alpha$, with n the refractive index and α the angle between the center axis and edge rays of the lense, is the so-called numerical arperture. An optical microscope which has an objective lens with a numerical aperture of $NA = 1$ will have a maximum resolution of $d_{min} = 200$ nm for $\lambda = 400$ nm.

In the field of fluorescence microscopy, there was a significant advance to overcome Abbe's resolution limit in 1995 with the two-photon technique[117]. However, in general it is still valid that a reduction of the wavelength would automatically lead to an increased resolution. This may be achieved by using X-rays. The resolution of modern X-ray microscopes with d_{min} of about 30 nm is indeed far better, but the access to suitable X-ray sources like synchrotron radiation is restricted. Another possibility is given by the use of electrons. Already within his thesis in 1924 De Broglie assumed that the wave-particle dualism is applicable to every kind of matter. Due to his research in this field he was honored with the Nobel prize in 1929 since

he was able to prove electrons behave also like waves. The De Broglie equation thereby gives the relation between the wavelength of the particle and its impulse $p = m \cdot v$ by

$$\lambda = \frac{h}{m \cdot v} \tag{1.14}$$

with h being the Planck constant. It is clearly seen that the wavelength not only will decrease with increasing mass but also with increasing velocity. Following this equation, an electron which is accelerated by a voltage of 100 kV will then show a wavelength of 0.0037 nm, what is 10^5 times smaller than the wavelength of visible light. Thus, it is possible to achieve a far better resolution than with optical microscopy.

Transmission electron microscopy is an excellent tool to investigate structures in the nanometer regime and is thus a valuable extension to SAXS. Scanning electron microscopy in contrast is the most useful technique to investigate structures in the micrometer down to the higher nanometer regime. Both microscopy methods were extensively used in this work and shall be discussed in the following two sub-sections in detail.

1.3.2.1 Transmission electron microscopy (TEM)

As the name of this method implies, the electrons will be transmitted through the specimen. This specimen has to be thin enough to be transparent for electrons and a part of them is scattered. This requires an extremely careful sample preparation. A common sample preparation is thus mostly the embedment of the sample into an epoxy resin, from which thin cuts are prepared with a diamond knife. These cuts, which have often to be further thinned e.g. by ion milling, are then usually put on copper grids, which are placed inside the microscope. Electron microscopes are operating under high vacuum conditions, since air molecules would lead to unwanted scattering of the electrons.

There are two possible electron beam sources: a thermal source or a field emission gun. The first-mentioned uses, for example, either a tungsten tip or a LaB_6 crystal. By heating electrons are emitted, which will be accelerated by a certain voltage (for example 100 kV) into the direction of an anode, where the sample is located. In the case of the field emission gun a tungsten filament with an atomic tip with a radius of about 50 nm is used. Due to this tip very strong electric fields are formed on the surface. With an extractor electrode free electrons are generated which will be accelerated towards the optical system by another anode. The thermal source may be understood as a filament lamp which produces lots of undirected light, whereas the field emission gun in contrast behaves like a laser, producing a very intense beam. It has to be said that for electron microscopy it is essential to use a

monochromatic beam of electrons since the resolution would suffer from a chromatic error. The following figure 1.23 shall demonstrate the schematic built-up of an electron microscope.
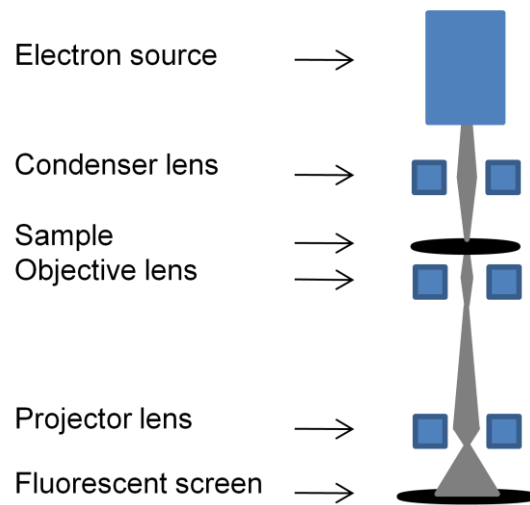

Fig. 1.23. Schematic built-up of a TEM

When the beam leaves the source it will first be focused to a coherent beam by the so-called condenser lenses. These are coils, producing magnetic fields, from which the path of the electrons is controlled due to the Lorentz force. The beam will hit the sample and the transmitted electrons will then be focused and magnified by the magnetic objective and projective lenses to finally hit the detector. In former times, photographic plates were used, whereas nowadays, a scintillator-coated fluorescent screen together with a charge-coupled device (CCD) camera is used to finally yield the desired sample image. The scattering of the electrons depends strongly on the atomic number of the elements inside the sample, thus heavier elements will produce more scattering. This is important for the interpretation of the resulting images with respect to the contrast between different phases.

1.3.2.2 Scanning electron microscopy (SEM)

A sample is scanned by a focused electron beam just like the screen of a television. Due to the interactions of the electrons with the sample, different kinds of signals may be detected. The most commonly used imaging method uses the detection of secondary electrons. They are formed due to the collision of an electron of the primary beam with an electron of the atomic shell of surface atoms. The emitted electrons will then be detected with a so-called Everhart-Thornley-detector (a scintillation counter). From the number of secondary electrons which are formed in a certain point during the scanning, it is possible to construct an image of the sample surface. The topological details of the surface are resolved with an extremely high depth of field and resolution due to the small wavelength of the electrons. The

magnification of this method depends on the ratio of the scanned area to the monitor size and the resolution may be adjusted by the spot size of the electron beam. Samples for SEM have to be electrically conductive, else the sample will be charged, which disturbs the measurement considerably. Metals may be used directly without further treatments; whereas non-conductive samples such as silica or organic substances have to be covered with a thin layer (some nanometers) of carbon or noble metals.

The buildup of a SEM (see figure 1.24) is very similar to that of a TEM. However, since it is a scanning method, the focus of the beam has to be adjusted. This can be done with specially designed coils. As electron source typically a tungsten filament or a LaB_6 crystal are used. Operating voltages are usually between 8 and 30 kV.
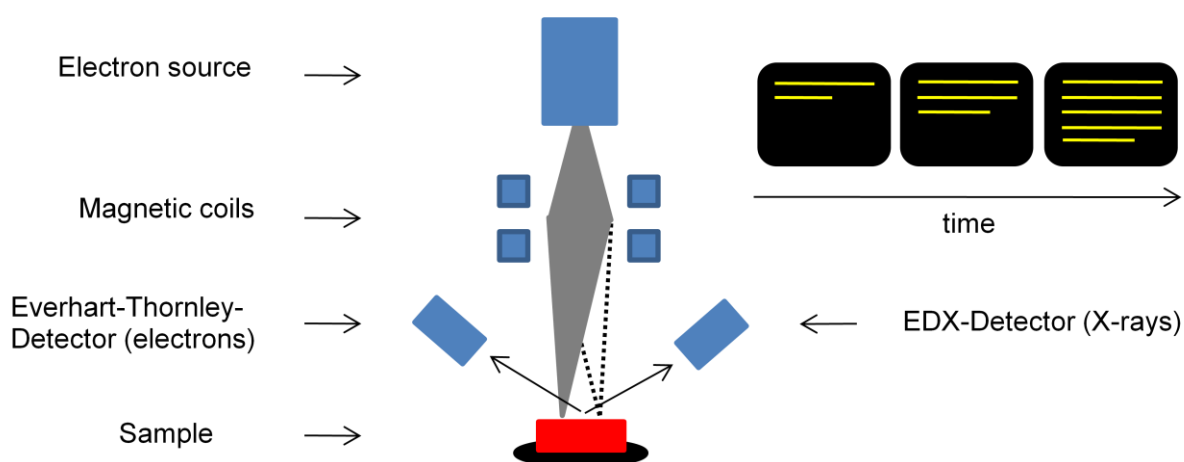

Fig. 1.24. Schematic built-up of a SEM

The vacancy in the inner shell, which is produced upon secondary electron emission, is filled by electrons from the outer shells of the atom. The energy difference is released by the emission of photons. Due to the high energy difference between inner and outer shells, X-ray photons are emitted, which are characteristic for the respective element. From this information it is possible to determine the elemental composition on the surface of the material in dependence on the local position of the electron beam. This method is called energy-dispersive X-ray spectroscopy (EDX). A more elaborate way to obtain a quantitative and local information of the elemental composition of a sample – though more time consuming – is the use of crystals to increase the resolution in reciprocal space, which is called wavelength-dispersive X-ray spectroscopy (WDX).

1.3.3 Sorption and porosimetry measurements

There are two common methods for the characterization of the porosity and the surface area of porous materials. Sorption measurements allow the determination of the surface area and

the pore size distributions in nanometer dimensions even without the destruction of the sample. Mercury porosimetry in contrast allows access to the pore size distribution in macroscopic dimensions. However, the invasive treatment of the sample with liquid mercury makes the sample useless for further investigations. Both methods will be explained in detail on the following pages.

1.3.3.1 Nitrogen sorption measurements

Nitrogen sorption measurements are the most common methods for the determination of porosity related parameters such as specific surface area or pore radii. Nitrogen is cheap, it is not very reactive and the main interaction with the surface is given by physisorption. For a typical measurement, the sample is evacuated at elevated temperatures to remove adsorbed water. For the measurement the sample is cooled down to the temperature of liquid nitrogen of 77 K. Gaseous nitrogen is then added step by step in small portions. Keeping the system in equilibrium between the adsorbed gas and the free gas, the pressure in the respective volume will change. A plot of the adsorbed volume in dependence of the relative pressure p/p_0, where p denotes the equilibrium pressure and p_0 the saturation vapor pressure, gives the so-called adsorption isotherm, which slope strongly depends on the nature of the sample. In figure 1.25 typical adsorption isotherms are shown:
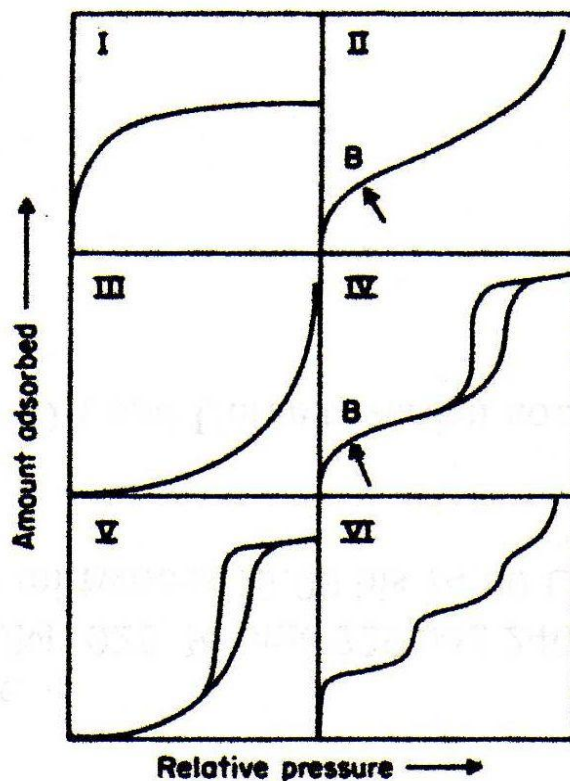

Fig. 1.25. IUPAC classification of sorption isotherms[7]

Following the IUPAC classification of sorption data[7], the Type I thus identifies a microporous material due to the steep increase of the adsorbed volume at low relative pressures. A Type II isotherm is observed for non- or macroporous materials. The point B (marked with an arrow in fig. 1.25) denotes the onset of multilayer adsorption. Type III is obtained for a weak interaction of the gas with the surface. Type V isotherms are very uncommon, but observed for certain systems like graphite, which shows a weak interaction with water molecules together with some porosity. At higher relative pressures, capillary condensation may be observed, which means that inside the pores liquid gas is formed even before the saturation pressure is reached. The capillary condensation strongly depends on the pore diameter and for small diameters condensation is observed earlier. Type VI is observed for layer by layer adsorption on a uniform non-porous surface. Finally, Type IV is the typical isotherm one would observe for a mesostructured (organo)silica material. Here, first a monolayer is formed, followed by multilayer adsorption, and in the higher relative pressure range (the mesopore regime) capillary condensation is observed. Capillary condensation is usually accompanied by a hysteresis in the pressure/adsorbed/desorbed volume plot. This means that adsorption is shifted to higher relative pressures relative to desorption and vice versa. There are two different hysteresis phenomena: On the one hand the condensation of a gas inside a nanopore is delayed due to reasons of metastability (see, for example, **[118-121]**). On the other hand the pore network itself plays an important role. If large pores are only accessible by thin necks, pore blocking or cavitation phenomena could be observed, which both lead to a delayed desorption**[122]**. In addition, from the slope of the hysteresis loop it is possible to make first conclusions concerning the pore structure and the degree of order.

In 1938 Brunauer, Emmett and Teller (BET) introduced a model into surface science which not only describes the adsorption of one but also the formation of multi layers**[123]**. With n the amount of adsorbed nitrogen, n_m the amount of nitrogen molecules needed to form a monolayer and C an empirical constant, the linearized BET equation is written as follows:

$$\frac{\frac{p}{p_0}}{n(1-\frac{p}{p_0})} = \frac{1}{n_m \cdot C} + \frac{C-1}{n_m \cdot C}\frac{p}{p_0}$$

(1.15)

Evaluating the sorption isotherm in the relative pressure range $0.05 - 0.35$, where the isotherm should behave in a linear fashion, it is possible to determine the amount n_m. Thus, it is possible with the knowledge of the cross section of a nitrogen molecule, to estimate the specific surface area. Micropores are not covered by this model and the BET equation thus

overestimates the surface area of microporous materials. Micropores may be analyzed by other means, for example by the t-plot method[124].

A common procedure to determine the mesopore size distribution of a porous material was first presented by Barrett, Joyner and Halenda (BJH)[125]. This model is based on the Kelvin equation, which describes the curvature of a spherical meniscus at a liquid/vapor interface.

$$\ln(\frac{p}{p_0}) = \frac{2 \cdot \gamma \cdot V_m}{r \cdot R \cdot T} \tag{1.16}$$

γ is the surface tension, r the radius, R denotes the universal gas constant, T means the temperature and V_m is the molar volume of the liquid. This equation can be further modified to describe the meniscus inside of cylindrical pores:

$$\ln\left(\frac{p}{p_0}\right) = -\frac{2 \cdot \gamma \cdot cos\theta}{R \cdot T \cdot \Delta\rho \cdot (r_p - t_c)} \tag{1.17}$$

r_p denotes the pore radius, $(\Delta\rho = \rho^l - \rho^g)$ the difference of the density of the bulk fluid ρ^l and the gas ρ^g, θ the contact angle of the liquid meniscus against the pore wall and t_c the thickness of an adsorbed multilayer film. Combining this equation with a multilayer thickness equation[126, 127], which is usually obtained for a non-porous solid, the computation of the mesopore distribution is possible. For this, the desorption branch should be used, since the Kelvin equation describes an equilibrium state. However, it is not considered that the curvature of the pores has a significant influence on the multilayer thickness and its interfacial tension. In addition, from a thermodynamic point of view, the Kelvin model of a smooth liquid-vapor interface and a bulk-like liquid core is not a realistic model for condensation phenomena in narrow nanoscopic pores. This model is as well not suitable to predict the pore radii in the micropore region. Other methods were thus developed, such as the nonlocal density functional theory (NLDFT), which describes the configuration of adsorbed molecules on a molecular level[128]. The NLDFT theory is able to describe both the micro- and the mesopore region quite precisely.

1.3.3.2 Mercury porosimetry

A common method for the determination of the pore size distribution of macropores as well as mesopores is the mercury intrusion method. Because of its high surface energy mercury is a non-wetting liquid for most surfaces. Thus, high pressures are required to force it into the pores of a porous material. The pressure thereby depends on the pore radii. Smaller pores will need a higher pressure to be filled. From the determination of the pressure dependence

of the intrusion process it is possible to obtain several values such as the total pore volume, the pore size distribution, the density of solids and powders and the specific surface areas.

The basis for the calculation of the pore size distribution is the Washburn equation which describes the applied pressure p needed for mercury to intrude a cylindrical pore with a pore diameter R:

$$p = -\frac{2 \cdot \gamma \cdot cos\theta}{R} \qquad (1.18)$$

γ is the surface tension of the liquid and θ denotes the contact angle of the intrusion liquid. For mercury the contact angle on silica at room temperature is 130°. Measurements are performed in two steps. First for the low pressure region, where larger micrometer-sized pores (diameters of 17 – 100 microns) are investigated, mercury will be added in vacuum and the pressure is then slowly increased until atmospheric pressure is reached. In the next step high pressure is generated by hydraulic pressurized instruments. With modern equipment it is possible to generate pressures as high as 400 MPa from which a minimum diameter of about 2 nm is accessible. However, micropores are too small to be able for mercury to penetrate and isolated pores are also not accessible. Thus, this method tends to underestimate the total pore volume. Additionally, the extrusion process may be measured, in which usually a hysteresis is observed. This can be explained by pore blocking phenomena at, for example, ink-bottle pores or due to contact angle hysteresis. The contact angles for intrusion and extrusion are different, which might be the case due to contamination of the surface with mercury.

1.3.4 Solid state magic angle spinning (MAS) nuclear magnetic resonance (NMR) spectroscopy

This method is one of the most powerful ones for the determination of the chemical composition and the molecular structure of a solid sample. In the case of organosilicas ^{13}C and ^{29}Si NMR measurements will clearly show whether decomposition in form of Si-C bond cleavage occurred or not and if certain impurities are contained within the sample. For silicon oxycarbides it is even possible to determine quantitatively different silicon species bound to a varying number of carbidic carbon. Since this method was important in the course of this work, its underlying theory is described briefly in this section.

The general basis of NMR is that the spin of certain nuclei is subjected to an extremely high magnetic field, which leads to a rotation of the spin axes around the magnetic field axis with the Larmor frequency. This spins are then perturbated by an electromagnetic pulse from a

coil (usually in the radio-frequency range). The resonance frequency is shifted as a consequence of the molecular orbital coupling of the electrons. This is called chemical shift. In solution the molecules will reorientate very rapidly, thus anisotropic nuclear interactions will be averaged out, since these interactions strongly depend on their orientation relative to the external magnetic field. In the case of a solid sample, this phenomenon will lead to line broadening for a signal in the NMR spectrum. This is attributed to different orientation dependent interactions, for example the "chemical shift anisotropy". The resonance frequency for a nucleus significantly depends on the chemical surrounding. If the molecular motion is suppressed, as in a solid, then for a certain nucleus various orientations of the chemical surroundings with respect to the external magnetic field are obtained. Due to this, the shielding of the nuclei from the external magnetic field differs in dependence of the orientation. Thus, for every orientation, a different resonance frequency will be observed, what in summary is leading to the aforementioned line broadening. In addition broadening effects due to anisotropy are also observed for dipolar and quadrupolar interactions as well as indirect spin-spin interactions. A possibility to overcome this problem is to mimick the orientation averaging from solution. This can be done by spinning the sample at the magic angle θ_m (~ 54.74°) with respect to the direction of the external magnetic field (see a) in figure 1.26). It can be shown that for an adequate rotational speed the chemical shift anisotropy is significantly reduced and that the dipole-dipole interaction between magnetic moments averages to zero at the magic angle.
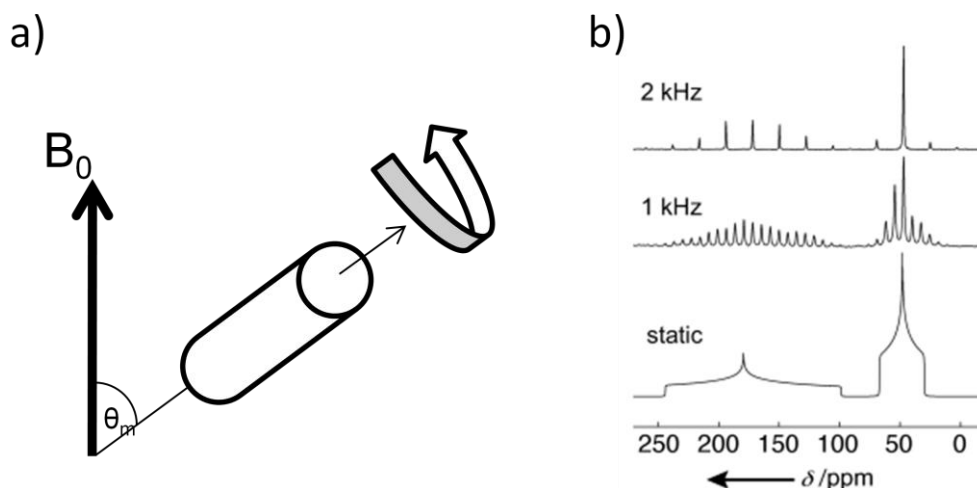

Fig. 1.26. a) Spinning of a cylindrical sample in the magic angle relative to the external magnetic field B_0; b) ^{13}C MAS solid state NMR spectra of a glycine powder sample in dependence of the spinning frequency (spectra taken from **[129]**)

In figure 1.26 b) the representative ^{13}C MAS solid state NMR spectra of a glycine powder sample are shown. The static spectrum shows very broad preaks due to the chemical shift anisotropy. However, with increasing spinning speed the resolution improves considerably,

but in addition to the true signal, numerous peaks appear which are known as spinning sidebands. These signals result from incomplete averaging and they appear at frequency distances of integer multiples of the spinning speed. They may be minimized by spinning at frequencies greater than the width of the chemical shift anisotropy pattern.

Nuclei like ^{13}C or ^{29}Si show low relative frequencies. In addition, their gyromagnetic ratios are rather low compared to ^{1}H or ^{19}F, which has a direct influence on the Boltzmann distribution of the spins and thus on the longitudinal relaxation times. The results are low intensities and long recycle delays, which lead to time-consuming measurements. To overcome this problem it is possible to use the cross polarization (CP) technique. In simple words, via a special pulse sequence, the magnetization from an abundant nucleus with a large relative frequency and large gyromagnetic ratio, such as ^{1}H, is transferred on the observed nucleus, for example ^{13}C. Thus, the intensities for ^{13}C signals are improved and the recycle delay then depends only from the longitudinal relaxation of ^{1}H, improving the measurement time in addition.

In modern spectrometers the samples are spun at frequencies of 1 to 70 kHz. The rotation is thereby induced by an air stream, to avoid disturbances by other electromagnetic fields. For (organo)silicas usually zirconia rotors are used.

1.4 References

[1]   P. Fratzl, R. Weinkamer, *Prog. Mater. Sci.*, **2007**, 52, 1263

[2]   J. Aizenberg, J.C. Weaver, M.S. Thanawala, V.C. Sundar, D.E. Morse, P. Fratzl, *Science*, **2005**, 309, 275

[3]   S. Mann, S.L. Burkett, S.A. Davis, C.E. Fowler, N.H. Mendelson, S.D. Sims, D. Walsh, N.T. Whilton, *Chem. Mate*r., **1997**, 9, 2300

[4]   C. Sanchez, H. Arribart, M.M. Giraud Guille, *Nature Materials*, **2005**, 4, 277

[5]   R. Backov, *Soft Matter*, **2006**, 2, 452

[6]   Y. Wan, D. Zhao, *Chem. Rev.*, **2007**, 107, 2821

[7]   K.S.W. Sing, D.H. Everett, R.A.W. Haul, L. Moscou, R.A. Rouquerol, T. Siemieniewska, *Pure and Appl. Chem.*, **1985**, 57, 603

[8]   S.Geist, Pseudomorphic transformation of mesostructured silica gels to other metal oxides, PhD thesis, Ulm University, Germany, **2008**

[9]   C.J. Brinker, G.W. Scherer, Sol-Gel Science, Academic Press, New York, **1990**

[10]   A.C. Pierre, Introduction to Sol-Gel Processing, Springer, Berlin, **1998**

[11]   J.D. Wright, N.A.J.M. Sommerdijk, Sol-Gel Materials: Chemistry and Applications, Taylor & Francis Books Ltd, London, **2001**

[12]   N. Hüsing, U. Schubert, *Angew. Chem.* **1998**, 110, 22

[13]   J.E.G.J. Wijnhoven, L. Bechger, W.L. Vos, *Chem. Mater.*, **2001**, 13, 4486

[14]   H. Zhang, J.F. Banfield, *Chem. Mater.*, **2002**, 14, 4145

[15]   P. Liu, J. Bandara, Y. Lin, D. Elgin, L.F. Allard, Y-P. Sun, *Langmuir*, **2002**, 18, 10398

[16]   J. Livage, M. Henry, C. Sanchez, *Prog. Solid State Chem.*, **1988**, 18, 259

[17]   M. Niederberger, *Acc. Chem. Res.*, **2007**, 40, 793

[18]   N. Pinna, M. Niederberger, *Angew. Chem. Int. Ed.*, **2008**, 47, 5292

[19]   M. Niederberger, G. Garnweitner, N. Pinna, G. Neri, Prog. *Sol. State Chem.*, **2005**, 33, 59

[20]   R. Aelion, A. Loebel, F. Eirich, *J. Am. Chem. Soc.*, **1950**, 72, 5705

[21]   D. Schäfer, *Science*, **1989**, 243, 1023

[22]   K.D. Keefer, D.W. Schaefer, *Phys. Rev. Lett.*, **1986**, 56, 2376

[23]   K.D. Keefer, D.W. Schaefer, *Phys. Rev. Lett.*, **1986**, 56, 2199

[24]   R. K. Iler, The Chemistry of Silica, Wiley, New York, **1979**

[25]   W. Stöber, A. Fink, E. Bohn, *J. Colloid. Interf. Sci.*, **1968**, 26, 62

[26]   S.S. Kistler, *Nature*, **1931**, 127, 741

[27]   G.A. Nicolaon, S.J. Teichner, *Bull. Soc. Chim. F.*, **1968**, 1906

[28]   M. Cantin, M. Casse, M. Koch, L. Jouan, R. Mestrau, P. Roussel, F. Bormin, J. Montel, S.J. Teichner, *Nucl. Instr. Methods*, **1974**, 118, 177

[29]   K. Kanamori, M. Aizawa, K. Nakanishi, T. Hanada, *Adv. Mater.*, **2007**, 19, 1589

[30]   F. Schwertfeger, W. Glaubitt, U. Schubert, *J. Non-Cryst. Solids*, **1992**, 145, 85

[31]   F. Schwertfeger, N. Hüsing, U. Schubert, *J. Sol-Gel Sci. Technol.*, **1994**, 2, 103

[32]   Y. Mizushima, M. Hori*, J. Non-Cryst. Solids*, **1994**, 167, 1

[33]   Z. Zhu, Y. Tsung, M. Tomkiewicz, *J. Phys. Chem.*, **1995**, 99, 15945

[34] A. Benedetti, G. Fagherazzi, P. Riello, Y.W. Zeng, F. Pinna, M. Signoretto, *J. Appl. Crystallogr.*, **1993**, 26, 717

[35] R.W. Pekala, *J. Mater. Sci.*, **1989**, 24, 3221

[36] http://de.wikipedia.org/wiki/Aerogel; http://stardust.jpl.nasa.gov/photo/aerogel.html

[37] P.J. Davis, C.J. Brinker, D.M. Smith, *J. Non-Cryst. Solids*, **1992**, 142, 189

[38] T. Mizuno, H. Nagata, S. Manabe, *J. Non-Cryst. Solids*, **1988**, 100, 236

[39] J. Zarzycki, M. Prassas, J. Phalippou, *J. Mater. Sci.*, **1982**, 17, 3371

[40] C.J. Brinker, *Mater. Res. Soc. Symp. Proc.*, **1992**, 567

[41] R.D. Shoup, *J. Colloid Interf. Sci.*, **1976**, 3, 63

[42] K. Nakanishi, N. Soga, *J. Am. Ceram. Soc.*, **1991**, 74, 2518

[43] P.J. Flory, *J. Chem. Phys.*, **1942**, 10, 51

[44] M.L. Huggins, *J. Chem. Phys.*, **1941**, 9, 440

[45] K. Nakanishi, *Bull. Chem. Soc. Jpn.*, **2006**, 79, 673

[46] K. Nakanishi, H. Komura, R. Takahashi, N. Soga, *Bull. Chem. Soc. Jpn.*, **1994**, 67, 1327

[47] K. Nakanishi, N. Soga, *Bull. Chem. Soc. Jpn.*, **1997**, 70, 587

[48] K. Nakanishi, *J. Porous Mat.*, **1997**, 4, 67

[49] J. Konishi, K. Fujita, K. Nakanishi, K. Hirao, *Chem. Mater.*, **2006**, 18, 864

[50] J. Konishi, K. Fujita, K. Nakanishi, K. Hirao, *Chem. Mater.*, **2006**, 18, 6069

[51] J. Konishi, K. Fujita, S. Oiwa, K. Nakanishi, K. Hirao, *Chem. Mater.*, **2008**, 20, 2165

[52] Y. Tokudome, K. Fujita, K. Nakanishi, K. Miura, K. Hirao, *Chem. Mater.*, **2007**, 19, 3393

[53] K. Kanamori, J. Hasegawa, K. Nakanishi, T. Hanada, *Macromolecules*, **2008**, 41, 7186

[54] J. Hasegawa, K. Kanamori, K. Nakanishi, T. Hanada, S. Yamago, *Macromolecules*, **2009**, 42, 1270

[55] C.T. Kresge, M. E. Leonowicz, W.J. Roth, J. C. Vartuli, J. S. Beck, *Nature*, **1992**, 359, 710-712

[56] J. S. Beck, J. C. Vartuli, W. J. Roth, M. E. Leonowicz, C. T. Kresge, K. D. Schmitt, C. T-W. Chu, D. H. Olson, E. W. Sheppard, S. B. McCullen, J. B. Higgins, J. L. Schlenker, *J. Am. Chem. Soc.*, **1992**, 114, 10834

[57] K.C. Singh, P.H. Khani, R. Yadav, P.C. Jain, *J. Colloid. Interf. Sci.*, **2005**, 282, 176

[58] S.S. Soni, G. Brotons, M. Bellour, T. Narayanan, A. Gibaud, *J. Phys. Chem. B*, **2006**, 110, 15157

[59] R. Ivanova, B. Lindman, P. Alexandridis, *Langmuir,* **2000**, 16, 3660

[60] D. Varade, K. Aramaki, C. Stubenrauch, *Colloids Surf. A*, **2008**, 315, 205

[61] C. Fritscher, Self-Assembly, Hierarchical Structure and Mechanical Properties of (Organo) Silica Monoliths, PhD thesis, Vienna University of Technology, Austria, **2008**

[62] F. Hoffmann, M. Cornelius, J. Morell, M. Fröba, *Angew. Chem.* **2006**, 118, 3290

[63] Q. S. Huo, D. T. Margolese, D. G. Demuth, P. Y. Feug, T. E. Gier, P. Sieger, A. Firouzi, B.F. Chmelka, F. Schuth, G. D. Stucky, *Chem. Mater.*, **1994**, 6, 1176

[64] 64Q. S. Huo, D. I. Margolese, U. Ciesla, P. Y. Feng, T. E. Gier, P. Sieger, R. Leon, P. M. Petroff, F. Schüth, G. D. Stucky, *Nature*, **1994**, 368, 317

[65] S. M. Holmes, V. L. Zholobenko, A. Thursfield, R. J. Plaisted, C. S. Cundy, J. Dwyer, *J. Chem. Soc., Faraday Trans.*, **1998**, 94, 2025

[66]   J. Morell, C.V. Teixeira, M. Cornelius, V. Rebbin, M. Tiemann, H. Amenitsch, M. Fröba, M. Lindén, *Chem. Mater.*, **2004**, 16, 5564

[67]   I. Beurroies, P. Ågren, G. Büchel, J. B. Rosenholm, H. Amenitsch, R. Denoyel, M. Lindén, *J. Phys. Chem. B*, **2006**, 110, 16254

[68]   O. Muth, C. Schellbach, M. Fröba, *Chem. Commun.*, **2001**, 2032

[69]   C. Göltner-Spieckermann, *Curr. Opin. Colloid Interface Sci.*, **2002**, 7, 173

[70]   B. Smarsly, D. Grosso, T. Brezesinski, N. Pinna, C. Boissière, M. Antonietti, C. Sanchez, *Chem. Mater.*, **2004**, 16, 2948

[71]   M.S. Wong, J.Y. Ying, *Chem. Mater.*, **1998**, 10, 2067

[72]   Z. Zhang, T.J. Pinnavaia, *J. Am. Chem. Soc.*, **2002**, 124, 12294

[73]   S. Warren, L. Messina, L. Slaughter, M. Kamperman, Q. Zhou, S. Gruner, F. DiSalvo, U. Wiesner, *Science*, **2008**, 320, 1748

[74]   S.H. Joo, S. Jun, R. Ryoo, *Microporous Mesoporous Mater.*, **2001**, 44-45, 153

[75]   A-H. Lu, F. Schüth, *Adv. Mater.*, **2006**, 18, 1793

[76]   H. Yang, D. Zhao, *J. Mater. Chem.*, **2005**, 15, 1217

[77]   C. Yu, J. Fan, B. Tian, G.D. Stucky, D. Zhao, *J. Phys. Chem. B*, **2003**, 107, 13368

[78]   S.K. Jana, A. Mochizuki, S. Namba, *S. Catal. Surv. Asia*, **2004**, 8, 1

[79]   S. Inagaki, S. Guan, Y. Fukushima, T. Ohsuna, O. Terasaki, *J. Am. Chem. Soc.*, **1999**, 121, 9611

[80]   B.J.Melde, B.T. Holland, C.F. Blanford, A. Stein, *Chem. Mater.* **1999**, 11, 3302

[81]   T. Asefa, M. J. McLachlan, N. Coombs, G. A. Ozin, *Nature*, **1999**, 402, 867

[82]   K. Landskron, B. Hatton, D.D. Perovic, G.A. Ozin, *Science*, **2003**, 302, 266

[83]   K. Nakanishi, T. Amatani, S. Yano, T. Kodaira, *Chem. Mater.*, **2008**, 20, 1108

[84]   J. Morell, G. Wolter, M. Fröba, *Chem. Mater.*, **2005**, 17, 804

[85]   S. Inagaki, S. Guan, T. Ohsuna, O. Terasaki, *Nature*, **2002**, 416, 304

[86]   K. Landskron, G.A. Ozin, *Science*, **2004**, 306, 1529

[87]   R. Voss, A. Thomas, M. Antonietti, G.A. Ozin, *J. Mater. Chem.*, **2005**, 15, 4010

[88]   A. Ide, R. Voss, G. Scholz, G.A. Ozin, M. Antonietti, A. Thomas, *Chem. Mater.*, **2007**, 19, 2649

[89]   A. Ide, G. Scholz, A. Thomas, *Langmuir*, **2008**, 24, 12539

[90]   A. Kuschel, S. Polarz, *Adv. Funct. Mat.*, **2008**, 18, 1272

[91]   A. Kuschel, H. Sievers, S. Polarz, *Angew. Chem. Int. Ed.*, **2008**, 47, 9513

[92]   N. Hüsing, C. Raab, V. Torma, A. Roig, H. Peterlik, *Chem. Mater.* **2003**, 15, 2690

[93]   D. Brandhuber, V. Torma, C. Raab, H. Peterlik, A. Kulak, N. Hüsing, *Chem. Mater.*, **2005**, 17, 4262

[94]   R.C. Mehrotra, R.P. Narain, *Indian J. Chem.*, **1966**, 5, 444

[95]   I. Gill, A. Ballesteros, *J. Am. Chem. Soc.*, **1998**, 120, 8587

[96]   M.A. Brook, Y. Chen, K. Guo, Z. Zhang, J.D. Brennan, *J. Mater. Chem.*, **2004**, 14, 1469

[97]   K. Nakanishi, Y. Kobayashi, T. Amatami, K. Hirao, T. Kodaira, *Chem. Mater.*, **2004**, 16, 3652

[98]   D. Brandhuber, H. Peterlik, N. Hüsing, *Small*, **2006**, 2, 503

[99]   B. Chankvetadze, C. Yamamoto, M. Kamigaito, N. Tanaka, K. Nakanishi, Y. Okamoto, *J. Chromatogr. A*, **2006**, 1110, 46

[100] A. El Kadib, R. Chimenton, A. Sachse, F. Fajula, A. Galarneau, B. Coq, *Angew. Chem. Int. Ed.*, **2009**, 48, 4969

[101] A-H. Lu, W. Schmidt, W. Kiefer, F. Schüth, *J. Mater. Sci.*, **2005**, 40, 5091

[102] Y. Shi, Y. Meng, D. Chen, S. Cheng, P. Chen, H. Yang, Y. Wan, D. Zhao, *Adv. Funct. Mater.*, **2006**, 16, 561

[103] P. Krawiec, D. Geiger, S. Kaskel, *Chem. Commun.*, **2006**, 2469

[104] K. Sonnenburg, P. Adelhelm, M. Antonietti, B. Smarsly, R. Nöske, P. Strauch, *PCCP*, **2006**, 8, 3561

[105] A. Pauletti, S. Handjani, C. Fernandez-Martin, C. Gervais, F. Babonneau, *J. Ceram. Soc. Jpn.*, **2008**, 116, 449

[106] B. Toury, R. Blum, V. Goletto, F. Babonneau, *J. Sol-Gel Sci. Techn.*, **2005**, 33, 99

[107] B. Toury, F. Babonneau, *J. Eur. Ceram. Soc.*, **2005**, 25, 265

[108] S. Masse, G. Laurent, F. Babonneau, *J. Non-Cryst. Sol.*, **2007**, 353, 1109

[109] H. Peterlik and P. Fratzl, *Monatsh. Chem.*, **2006**, 137, 529

[110] V. Torma, H. Peterlik, U. Bauer, W. Rupp, N. Hüsing, S. Bernstorff, M. Steinhart, G. Goerigk, U. Schubert, *Chem. Mater.*, **2005**, 17, 3146

[111] C.C. Landry, S.H. Tolbert, K.W. Gallis, A. Monnier, G.D. Stucky, P. Norby, J.C. Hanson, *Chem. Mater.*, **2001**, 13, 1600

[112] L.A. Feigin, D.I. Svergun, Structure analysis by small angle X-ray and neutron scattering, Plenum Press, New York, **1987**

[113] A. Guinier, G. Fournet, Small angle scattering of X-rays, Wiley, London, New York, **1955**

[114] O. Glatter, O. Kratky, Small angle X-ray scattering, Academic press, London, **1982**

[115] G. Beaucage, *J. Appl. Cryst.*, **1995**, 28, 717

[116] B. Smarsly, M. Antonietti, T. Wolff, *J. Chem. Phys.*, **2002**, 116, 2618

[117] P. E. Hänninen, S. W. Hell, J. Salo, E. Soini, C. Cremer, *Appl. Phys. Lett.*, **1995**, 68, 1698

[118] A.G. Foster, *Trans. Faraday Soc.* **1932**, 28, 645

[119] L.H. Cohan, *J. Am. Chem. Soc.*, **1938**, 60, 433

[120] L.H. Cohan, *J. Am. Chem. Soc.*, **1944**, 66, 98

[121] P.C. Ball, R. Evans, *Langmuir*, **1989**, 5, 714

[122] P.I. Ravikovitch, A.V. Neimark, *Langmuir*, **2002**, 18, 9830

[123] S. Brunauer, P.H. Emmett, E. Teller, *J. Am. Chem. Soc.*, **1938**, 60, 309

[124] B.C. Lippens, J.H. de Boer, *J. Catal.*, **1965**, 4, 319

[125] E.P. Barrett, L.G. Joyner, P.P. Halenda, *J. Am. Chem. Soc.*, **1951**, 73, 373

[126] M. Kruk, V. Antochshuk, M. Jaroniec, A. Sayari, *J. Phys. Chem. B.*, **1999**, 103, 10670

[127] M. Jaroniec, M. Kruk, J.P. Olivier, *Langmuir*, **1999**, 15, 5410

[128] P.I. Ravikovitch, S.C. Ò Domhnaill, A.V. Neimark, F. Schüth, K.K. Unger, *Langmuir*, **1995**, 11, 4765

[129] D.D. Laws, H-M. L. Bitter, A. Jerschow, *Angew. Chem. Int. Ed.*, **2002**, 41, 3096

2. Outline of this thesis

There is a great potential for highly functionalized and hierarchically structured organosilica materials on the one hand as catalytic materials and on the other hand as column materials for chromatography. Although great efforts have already been invested in the preparation of highly functionalized mesostructured organosilica materials as particles or nanoporous aerogels, until now the preparation as monoliths with multiscale porosity was not achieved. This is truly a challenging task and this work is dedicated to the preparation and characterization of novel organosilica materials as well as structural studies with *in-situ* small angle X-ray scattering to get a detailed understanding of most of the influencing factors on the materials formation. All work which will be presented was conducted within a cooperation of the Dynamics of Condensed Systems group of the Faculty of Physics at the University of Vienna and the Institute of Inorganic Chemistry I at Ulm University. The group in Vienna is specialized on X-ray scattering techniques and the group in Ulm on the synthesis of inorganic materials especially via sol-gel-processing. This has been proven to be a fruitful combination, from which 3 publications have evolved, which shall be presented in the following chapters.

Within the first peer-reviewed paper (Chapter 3) presented in this thesis, the sol-gel processing of the glycol-modified bis-silylated ethane-bridged silane was intensively investigated concerning the influence of the concentration of the surfactant Pluronic P123 on the gel formation. *In-situ* SAXS measurements at different temperatures were performed with our laboratory equipment to get a detailed understanding of the mechanism and the overall kinetics. The Avrami theory was applied to get quantitative values for the reaction rates of the mesostructure growth.

In the second publication (Chapter 4), the experience gained from the former system was transferred to a more complex glycol-modified carbosilane dendrimer. In contrast to the former silane, no hierarchically organized monoliths with macropores and periodically arranged mesopores were obtained, but nanoporous monolithic aerogels. The structures were investigated in detail with SAXS. Analytical and numerical approaches were used to fit the SAXS data and to get detailed structural information. The absence of phase separation and mesostructure formation phenomena is discussed with respect to the reactivity of the precursor during sol-gel-processing as well as a weaker compatibility with the surfactant mesophase. This paper was chosen as the title page of the Journal of Materials Chemistry.

The present approach was further extended to a cyclic carbosilane precursor, comprising a six-membered ring with three Si-methylene units. This precursor exhibited after transalkoxylation with glycols a similar sol-gel behavior as the dendrimeric silane and resulted in nanoporous, but non-organized and non-phase separated structures. In chapter 5 it is shown, that the addition of inorganic salts, such as potassium chloride, will influence the precursor/surfactant solution considerably concerning the phase separation and the mesostructure formation. Organosilica monoliths with multiscale porosity from this more complex carbosilane were successfully designed and generated. The effect of different salt concentrations on the onset of the phase separation together with the domain/macropore size as well as the quality of the mesostructures was investigated intensively with different methods such as SAXS, SEM, TEM and nitrogen sorption. Finally, in this chapter, it is demonstrated that the pyrolytic conversion of these macroporous organosilicas into true silicon oxycarbide monoliths is possible by simultaneously maintaining all structural features. This material is of particular interest for catalytic applications at harsh environmental conditions.

An in-depth summary of all these results will be given in chapter 6.

3. Organosilica monoliths with multiscale porosity: detailed investigation of the influence of the surfactant on structure formation

Manuel Weinberger [ab], **Thomas Fröschl** [b], **Stephan Puchegger** [a], **Herwig Peterlik** [a] **and Nicola Hüsing** [b]

[a]*Faculty of Physics, University of Vienna, Strudlhofgasse 4, A-1090, Vienna, Austria.*
[b]*Inorganic Chemistry I, Ulm University, Albert-Einstein Allee 11, D-89081, Ulm, Germany.*

Abstract. Monolithic inorganic-organic hybrid materials have been synthesized via sol-gel processing of an ethylene glycol-modified ethane-bridged silane precursor in aqueous solution of the non-ionic block copolymer Pluronic™ P123. The resulting materials consist of macroporous networks comprising periodically arranged mesopores, where the macropore size as well as the morphology of the material can be deliberately tailored by reducing the amount of the block copolymer template. The structure for sols prepared from different compositions was investigated by small-angle X-ray scattering as well as scanning and transmission electron microscopy. Information on the porosity, surface area and pore size distribution were obtained from BET/BJH analysis and mercury intrusion measurements. For a more detailed insight into mechanism and kinetics of the mesostructure formation, in-situ SAXS experiments were carried out.

3.1 Introduction

Since the discovery of mesostructured materials by the Mobil Oil Company in 1992, a large variety of these materials have been synthesized by sol-gel methods in combination with supramolecular templating approaches[1,2]. The pore walls may, for example, consist of silica [3], organosilica [4] and metal oxides [5,6], sulfides [7] or phosphates [8]. Because of their well-defined porous structures a wide range of possible applications exists, such as in the field of separation chemistry, drug delivery or as catalyst supports. In 1999, three different groups were almost simultaneously successful in the synthesis of periodic mesoporous organosilica (PMO) materials using bridged organo-bissilylated precursors [9-11]. The obtained materials contain hydrocarbons as an integral part of the pore walls, leading to dramatic changes in the surface/bulk properties and thus, expanding the variety of possible applications compared to silica-based mesostructured materials. A recent review of Fröba et al. gives a very good overview of the progress in PMO chemistry [12].

Today mesostructured materials are available in the form of powders, films or even monoliths. However, very few authors report the synthesis of large, truly mesoscopically ordered monoliths [13,14]. The situation gets even more problematic when materials with pore sizes on different length scales are desired, for example materials that combine small (micro- and meso-) and large (macro-)pores. For these materials multiple benefits arise from each of the pore size regimes, for example micro/mesopores for size- or shape-selective applications and macropores for a reduction of diffusion limitations to the active sites. Thus, the advantages of producing hierarchical pore structures within one material are evident.

However, the synthesis of monolithic periodic mesoporous materials still remains a challenge. One has to transfer a complex mixture of precursor, solvent, catalyst, template and maybe other additives into a "true" gel that consists of a continuous or particulate mesostructured network. This is a difficult task, in which the components and the final sol composition have to be chosen very carefully to generate a homogeneous starting solution. One approach—relying on polymerization-induced phase-separation—was presented by Nakanishi et al., using alkoxides, such as tetramethoxysilane or bis(trimethoxysilyl)ethane in the presence of amphiphilic polyoxyalkylene-based block copolymers and other polymers as templates [15, 16]. The preformed, phase separated bicontinuous network is frozen in by gelation. In addition to this macroscopic phase separation, micelles formed by the block copolymer, together with the oligomeric and polymeric silica species form a hybrid mesostructure. This mesostructure formation and especially the degree of periodicity in the final material strongly depends on the sol composition [17].

Hüsing et al. are using ethylene glycol-modified silanes for the generation of hierarchically meso/macro organized silica networks [18-20]. Substituting the alkoxy groups with the diol leads to precursors that show a superior solubility in water. Thus, hydrolysis occurs very rapidly and a homogeneous sol is quickly prepared even in the presence of other components such as surfactants. The first of theseprecursors was obtained by a transesterification reaction of tetraethoxysilane with ethylene glycol [21]. Short chain alcohols, such as methanol or ethanol, which are released through hydrolysis of conventional sol-gel precursors, are well known to strongly influence the phase diagram of poly (ethylene oxide)-poly(propylene oxide)-poly(ethylene oxide) copolymer/water mixtures because of the different polarity compared to water and better compatibility to the poly (propylene oxide)-block [22]. Ethylene glycol which is formed during hydrolysis and condensation when using a glycol-modified silane is also changing the phase behavior of non-ionic block copolymers, but allows for the formation of lyotropic liquid crystalline phases (LC phases) in a larger range of concentrations. In addition, it induces a macroscopic phase separation resulting in well-defined macroscopic morphologies. Therewith it was possible to generate macroand

periodically organized mesoporous monoliths with the block copolymer Pluronic™ P123 in a purely aqueous medium **[23]**. The precursor diolates also cooperatively arrange with the template block copolymer leading to the formation of well-defined mesostructures **[24]**. It was even possible to extend this approach to a modified phenylenebridged silane that yields silsesquioxane materials containing semicrystalline pore walls due to staggered phenylene rings **[25]**. Until now, only cylindrically arranged mesopores were obtained by using nonionic surfactants for the preparation of macroporous monolithic silica and organosilica **[15, 16, 23, 25]**. Although the synthesis of cubic mesostructured materials is often reported in literature **[26, 27]**, it was not yet possible to generate macroporous monoliths with a cubic mesostructured pore system inside the framework. Even the use of Pluronic F127 as a structure directing agent, which is known to produce preferentially spherical pore geometries led to 2D hexagonally arranged mesopores **[17]**.

In this work the number of possible ethylene glycolmodified precursors for the preparation of hierarchically porous and monolithic materials is extended to the bissilylated ethane. Meso-/macroporous materials with different pore sizes and degree of order were obtained by varying the ratio of the block copolymer P123 to the hydrochloric acid solution. Additionally, in-situ SAXS was performed to monitor the progress of the reaction and the kinetics of building up the mesoporous structure. The experiments were carried out at different temperatures **[28]**, from which numerical values for the activation energy and the growth mechanism were obtained.

3.2 Materials and Experimental

The organosilane 1,2-bis(triethoxysilyl)ethane and the block copolymer poly(ethylene oxide)-block-poly(propylene oxide)- block-poly(ethylene oxide) with M_n=5,800 g mol^{-1} were both purchased from Aldrich and used without further purification. Ethylene glycol was purchased from Merck and dried first with anhydrous sodium sulfate and then by distillation from magnesium.

The modification of the organosilane with ethylene glycol was performed according to a transesterification reaction earlier described by Mehrotra and Narain **[21]**. However, some changes in the synthesis of the modified ethane-bridged silane were necessary.

Precursor synthesis

Modification of Bis(triethoxysilyl)ethane with Ethylene Glycol. The synthesis was carried out in argon atmosphere. 38.28 g (0.11 mol) of 1,2-bis(triethoxysilyl)ethane were mixed with 133.95 g (2.16 mol) ethylene glycol. The mixture was heated to 140°C under vigorous

stirring. Most of the generated ethanol was removed by distillation. The remaining ethanol and excess ethylene glycol were removed by vacuum distillation and 44.38 g of a glassy solid were obtained. The reaction yields almost quantitatively the glycolated product. Thermogravimetric analysis showed a silicon content of 14.23% indicating a deficiency in glycol compared to the theoretically expected value for a 1:3 ratio of silicon to glycol of 12.47%. This can be explained by the presence of bridging and chelating species.

Gel synthesis

First, the block copolymer was dissolved in 0.1 M hydrochloric acid in the mass fractions of 15:85 to 30:70. Then a given amount of a polymer solution was mixed with the glycol-modified silane under vigorous stirring. The composition of the final sol was chosen to be in the ratio of 5.2:100 (mass fractions) with respect to the silicon content to the polymer/water/acid mixture. After homogenization, the sols were kept at 40°C for gelation and aging for 6 days. The gelation time at 40°C was determined to be approximately 2 to 3 h on average. After several hours all gels turned opaque. After 6 days the wet gels were washed five times with ethanol for solvent extraction in a period of 48 h. Then the gels were dried via supercritical extraction with CO_2 **[29]**. ^{13}C and ^{29}Si-CP/MAS-NMR measurements showed that no Si- C-bond cleavage occurred.

Characterisation

Small angle X-ray scattering (SAXS) measurements of the dried gels were collected in vacuum with X-rays generated by an X-ray tube (Nanostar, Bruker AXS), collimated and monochromatized from crossed Goebel mirrors and equipped with a 2D position sensitive detector (Bruker HiStar). The samples were prepared as powders and pasted between two strips of Scotch™ tape. The SAXS patterns were radially averaged to obtain the scattering intensity dependence on the scattering vector $q = (4\pi/\lambda)sin(\theta)$, where 2θ is the scattering angle and λ = 0.1542 nm the X-ray wavelength. Measurements were carried out at the sample to detector distance of 105.7 cm giving access to a q range of 0.07–2 nm^{-1}.

For the *in-situ* measurements, a rotating anode generator (Bruker Nanostar, superspeed solution) together with a 2D detector (Vantec 2000, gas detector with microgap technology) was used. The sol was filled into 1 mm quartz capillaries with 10 microns wall thickness from Hilgenberg GmbH. The experiments were performed at a constant temperature in a specially designed capillary heating device.

The morphology of the gels was investigated by scanning electron microscopy (SEM) with a Zeiss DSM 692 operating at 15 kV on gel pieces sputtered with AuPd. Transmission electron

microscopy (TEM) was performed to investigate the lower nanometer regime. Photos were taken on a Philips 400 T operating at 80 kV.

Surface areas and pore size distributions were determined by N_2-sorption measurements, which were performed at 77 K on a NOVA 4000 e (Quantachrome). The specific surface areas were determined from the lower relative pressure range (p/p_0 = 0.05-0.15), where the Brunauer/Emmett/Teller (BET) isotherm behaves in a linear fashion. The pore size distribution was calculated from Barett/Joyner/Halenda (BJH) analysis of the adsorption branch of the isotherm. The pore wall thickness (twall) was calculated by $2d_{10}(SAXS)/3^{0.5} - D^{BJH}$, where $2d_{10}(SAXS)/3^{0.5}$ equals to the centre to centre distance of the pore walls in a hexagonally arranged pore system. The subtraction of the pore diameter D^{BJH} obtained from BJH analysis then results in the pore wall thickness [29].

Some selected samples were investigated by mercury intrusion measurements on a Macropores Unit 120 and a Porosimeter 2000 both from Fisons Instruments (contact angle of 140°).

The MAS-NMR spectra were recorded on a Bruker AVANCE DRX 400 spectrometer using a 4 mm MAS broadband probe head. The rotor spinning speed for all performed experiments was 8 kHz. The ^{13}C spectra were measured with CP/MAS experiments at a resonance frequency of 100.63 MHz. The [29]Si spectra were measured with CP/MAS experiments at a resonance frequency of 79.5 MHz and a contact time of 10 ms.

The silicon content of the precursor was determined in air by thermogravimetric analysis on a Netzsch STA 449 C Jupiter.

3.3 Results and Discussion

Monolithic white hybrid silsesquioxane gels were producedby sol-gel processing of the ethylene glycol-substituted ethane-bridged silane under aqueous conditions in the presence of a polyoxyalkylene-based structure-directing agent to give hierarchically structured organosilica monoliths (see Fig. 3.1). To exclude Si-C-bond cleavage during the synthesis of the materials, ^{29}Si-MAS-NMR (solid state NMR) measurements were performed, showing no evidence of Q-units (SiO_4-units) in the material. A broad signal at about -60 to -80 ppm can be assigned to T-units (R-SiO_3).
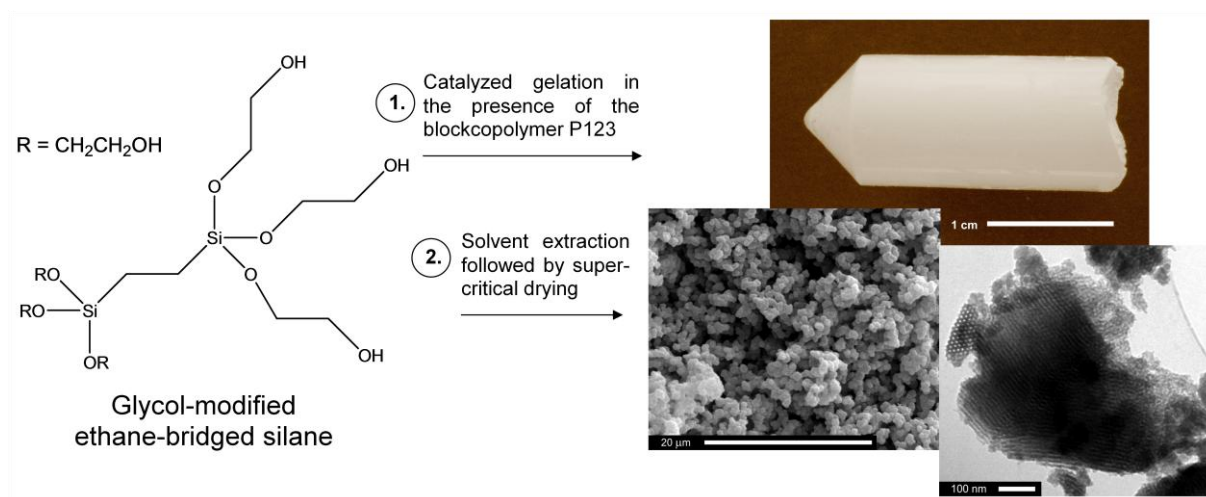
Fig. 3.1. Sol-gel processing of the ethylene glycol-modified ethane-bridged silane

It is well known that polyethylene oxide adsorbs on the surface of polymerizing silica and thus, can strongly influence the growth of the silica network **[30, 31]**. The reason for these interactions lies in strongly pH-dependent hydrogen bonding between free silanol groups of silica and the ether oxygens of the poly(ethylene oxide). For the system described in this work, it is assumed that similar interactions play a significant role in framework formation due to the hydrophilic polyethylene oxide head group of the structure-directing agent. Depending on the sol composition, the temperature, the amount and kind of alcohol, which is released upon hydrolysis of the silane, and the molecular weight of the polymeric additive, the solid framework can be constructed from interconnected particles, isolated pores, bicontinuous or nanoporous networks. For a silica/ pure poly(ethylene oxide) system it was suggested that the decreasing affinity of poly(ethylene oxide) molecules adsorbed on polymerizing silica to the solvent is leading to phase separation **[31]**. If this phase separation occurs prior to gelation, the thus formed network can be frozen by gelation. It is also known that the phase separated domains underlie a coarsening process due to interface instabilities. Thus, the slower the condensation reactions and the longer the gelation time, the coarser the solid framework. Detailed studies on the influence of ethylene oxide moieties on the structure formation have already been performed in pure silica systems **[32–34]**. For monolithic silsesquioxane materials starting from bridged organosilane precursors, significant differences in the final structure are expected due to the completely changed polarity of the precursor.

In this work, the silicon content in the precursor mixture was kept constant with respect to the amount of polymer/water/acid and only the ratio (in mass fractions) of P123/acid was varied in steps of 5% from 30:70 to 15:85. It should be noted that changing only the ratio of polymer to acid, two different parameters are affected. With a decrease of the P123 concentration,

there is greater dilution of the precursor in the acid solution and therefore, the hydrolysis and condensation kinetics will differ slightly.

Figure 3.2 shows scanning electron microscopy images for representative gel samples as a function of the P123/solvent ratio. The samples 5.2:30:70, 5.2:25:75 and 5.2:20:80 seem to be gels with a particulate gel network, whereas a co-continuous framework for the sample 5.2:15:85 is obtained. The diameter of the particles forming the macroscopic framework can be given as approximately 200 nm (30:70), 450 nm (25:75), 750 nm (20:80) and 6 µm (15:85). A comparison of all gel samples showed an increase of particle and domain sizes with decreasing P123/solvent ratio as well as a transition from particulate networks to a co-continuous morphology between 5.2:19:81 and 5.2:18:82.
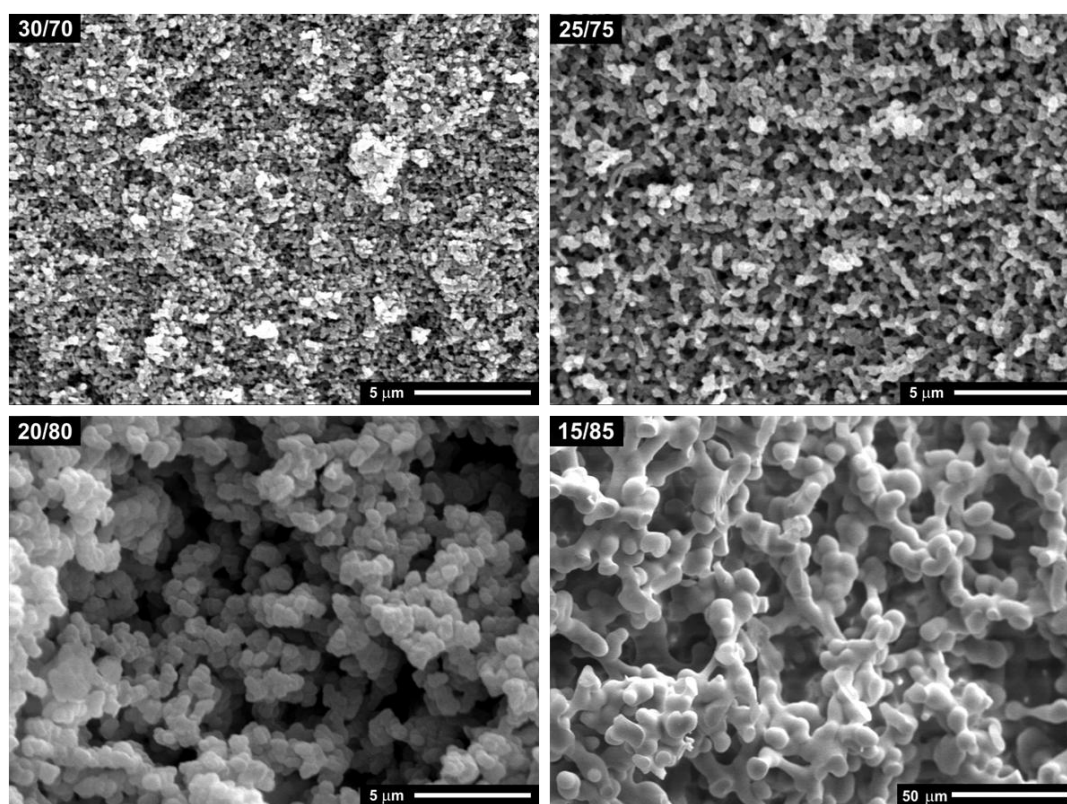
Fig. 3.2. Scanning electron microscopy images of the 5.2:30:70, 5.2:25:75, 5.2:20:80 and 5.2:15:85 gels (note the different scale bar of 50 µm for the 5.2:15:85 gel)

As expected the built-up networks strongly differ from those of pure silica gels prepared under similar experimental conditions **[23]**. The P123/solvent ratio has a significant influence on the framework formation, as seen in the domain size, which strongly depends on the amount of P123 in the precursor sol. Assuming a polymerization-induced phase separation mechanism for the gels that show a co-continuous framework, these results agree well with observations reported earlier. In silica sol-gel systems containing poly(ethylene oxide) an increase of the size of the framework was obtained when decreasing the amount of the

polymeric additive **[31]**. This is explained by a destabilization of the silica/poly(ethylene oxide) complex with a decrease of the silica/poly(ethylene oxide) ratio. The more stable this complex is, the faster phase separation occurs. Thus, for lower concentrations of the surfactant phase separation occurs faster, thereby leading to larger framework domains due to a later freezing of the network by gelation. Additionally, because of the amphiphilic nature of P123, a micellar templating has to be considered as well. Detailed studies on the increasing particle size are in progress.
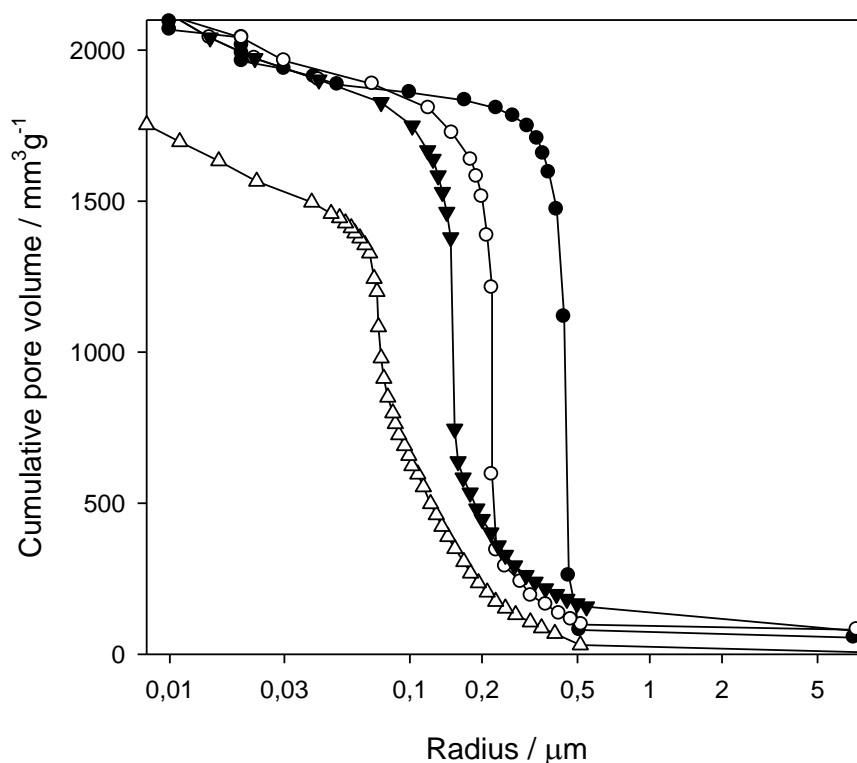
Fig. 3.3. Mercury intrusion measurements for representative gels: filled circles, 5.2:19:81; open circles, 5.2:21:79; filled triangles, 5.2:23:77; open triangles, 5.2:26:74

Figure 3.3 shows mercury intrusion measurements for the gels with compositions of 5.2:19:81, 5.2:21:79, 5.2:23:77 and 5.2:26:74. The curves give information about the macropore sizes and it is cleary seen that a quite monomodal distribution of macropores is obtained. The size of the macropores increases with decreasing P123 content (from 100 to 500 nm) and the pore size became more uniform. In agreement with the SEM images in Fig. 3.2, mercury intrusion results provide an indication of the low polydispersity of the particles or domains as well as the pores in macroscopic dimensions.

One unique feature in the processing of glycolated silanes in purely aqueous solution of amphiphilic block copolymers is the formation of periodically arranged mesopores. Thus, a

hierarchical network structure with macropores comprising well-organized pores in the mesoscopic length scale is accessible. Nitrogen sorption, SAXS measurements and TEM observations were performed to determine this mesostructure formation in dependence of the P123 concentration.

Nitrogen sorption measurements show that the surface areas vary from 300–700 m² g⁻¹ and no significant trend is observed. The maximum in the pore size distribution is given by 4.8 nm for the samples with a large amount of P123 (for P123/acid ratios of 26:74 up to 30:70) and 5.5 nm for the other samples. The values for specific surface areas S^{BET}, the maxima of the pore size distributions D^{BJH} and the total pore volumes V^t are given in Table 3.1 together with the SAXS results (the repeating unit distance d_{10} and the corresponding full-width-at-half-maximum (FWHM) of the reflection as well as the pore wall thickness t^{wall}).

Table 3.1 Prepared samples and some structural parameters (sorption/ SAXS)

Sample	Nitrogen sorption			SAXS	
	S^{BET} / m²g⁻¹	V^t/ cm³g⁻¹	D^{BJH} / nm	d_{10} (FWHM) / nm	t^{wall} / nm
5.2/30/70	311	0.54	4.8	9.8 (1.2)	6.5
5.2/29/71	377	0.68	4.8	9.8 (1.2)	6.5
5.2/28/72	478	0.76	4.8	9.9 (1.2)	6.6
5.2/27/73	412	0.98	4.8	9.9 (1.1)	6.6
5.2/26/74	504	1.13	4.8	9.9 (1.1)	6.6
5.2/25/75	446	0.7	5.5	10.0 (1.1)	6.1
5.2/24/76	444	0.56	5.5	10.0 (1.0)	6.1
5.2/23/77	725	1	5.5	10.1 (1.0)	6.2
5.2/22/78	489	0.6	5.5	10.2 (1.1)	6.3
5.2/21/79	404	0.51	5.5	10.3 (1.1)	6.4
5.2/20/80	401	0.5	5.5	10.3 (1.0)	6.4
5.2/19/81	560	1.03	5.5	10.3 (1.3)	6.4
5.2/18/82	611	1.09	5.5	10.4 (1.7	6.5
5.2/17/83	498	0.84	5.5	10.5 (2.0)	6.6
5.2/16/84	512	0.54	5.5	10.8 (2.4)	7.0
5.2/15/85	609	0.58	5.5	10.9 (2.4)	7.1

The isotherms and pore size distributions for the 5.2:30:70, 5.2:25:75, 5.2:20:80 and 5.2:15:85 gels are shown in Fig. 4. One has to be careful with the interpretation of the values

for the pore diameters, since these values represent the maxima of the pore size distributions in the lower nanometer regime and are not average values. Those diameters are slightly larger and will differ more clearly as a sharp look at the curves for the 5.2:20:80 and 5.2:15:85 shows. With a large amount of the polymer the mesostructure is less developed resulting in a broader pore size distribution with a smaller maximum for the pores with a diameter of about 4-5 nm. In addition, the formation of much larger pores is also observed in the hysteresis (Fig. 3.4 a, top two curves) of these samples (5.2:30:85, 5.2:25:85). In all cases the slope of the isotherm can be classified as Type IV (see Fig. 3.4 a), typically for mesoporous materials. Well ordered samples gave a H1 type hysteresis for the adsorption-desorption isotherms (see sample 5.2:20:80) with a steep increase/decrease of the adsorbed volume, indicating a high amount of uniformity of the pore system. By contrast the 5.2:15:85 gel showed a transition to a H2 type hysteresis which is normally observed for pore blocking phenomena[35]. Considering a wormhole-like mesostructure with a more disordered state of the pore system, the occurrence of ink-bottle-type pores or small windows, which will lead to a delayed desorption of the nitrogen within the larger pores would be an appropriate explanation.
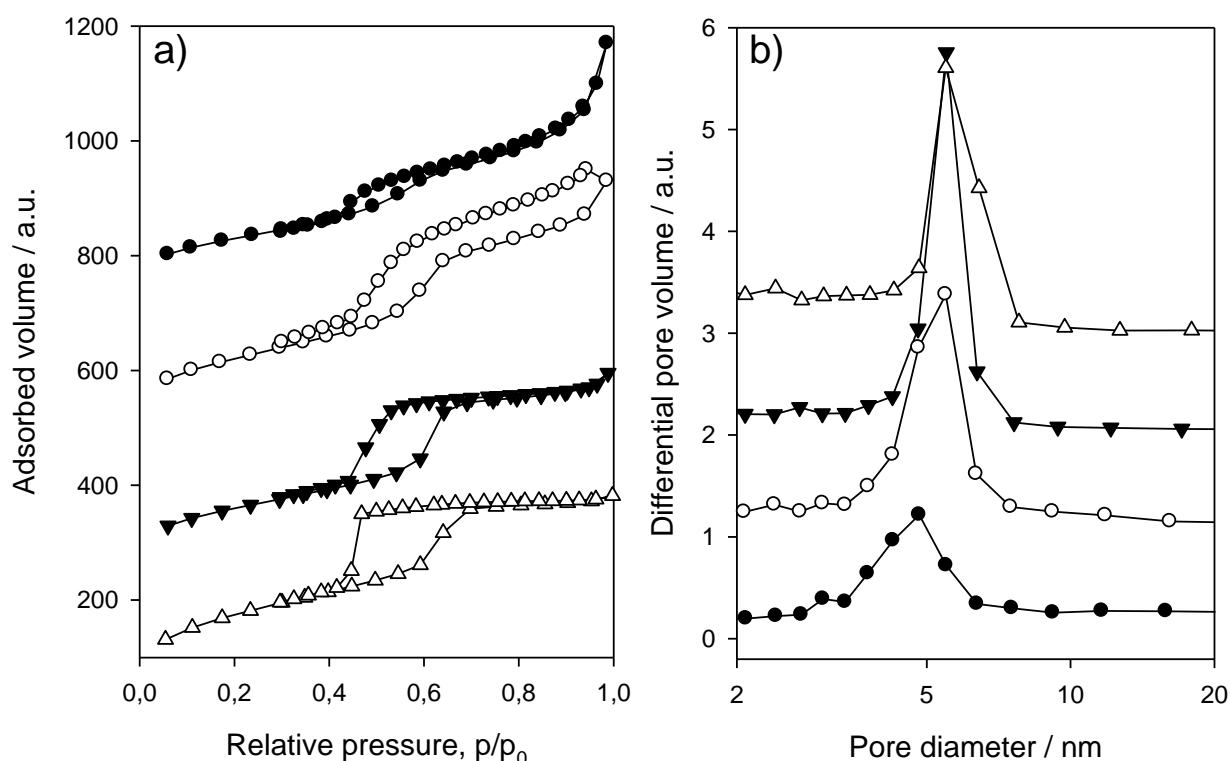
Fig. 3.4. Sol-gel processing of the ethylene glycol-modified ethane-bridged silane

Figure 3.5 shows the small angle X-ray scattering patterns of representative gels. All compositions lead to a periodically arranged mesoporous structure and the highest degree of ordering was observed for the gel composition 5.2:20:80, where the peaks can be indexed from left to right as (10), (20) and (21) reflections of cylindrical pores arranged in a 2D hexagonal lattice. The (11) reflection is not visible due to the overlap with the broad and intense shoulder of the (10) reflection. Concomitantly, the gel composition 5.2/20/80 has the smallest full-width-at-half-maximum (FWHM= 0.99 nm in real space). In comparison to gels obtained from a tetrakis(2-hydroxyethoxy)silane/P123 mixture (with a highly ordered mesostructure for 30/70 P123/solvent), the best order is achieved at lower P123 concentrations for the bridged silane system. The slopes of the scattering patterns at low q are also remarkable and indicate from lower to higher P123/solvent ratio an increasing amount of additional small angle scattering intensity. It is suggested that this is caused by particles building the macroscopic frameworks. This scattering shifts towards larger angles with decreasing particles size. The strong (10) reflections were fit by Gaussian functions, the resulting d-spacings and the corresponding FWHM are listed in Table 3.**1**. With increasing amount of the block copolymer a strong decrease in the dspacing (from 5.2:15:85=10.9 nm to 5.2:30:85=9.8 nm) is observed.
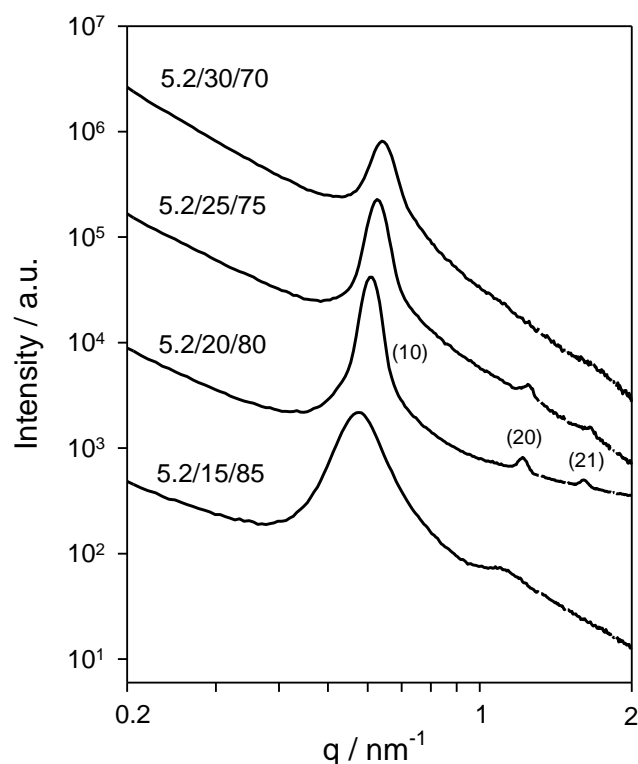
Fig. 3.5. Small angle X-ray scattering patterns of the 5.2:30:70, 5.2:25:75, 5.2:20:80 and the 5.2:15:85 gels. The curves are vertically shifted for clarity

In Fig. 3.6 representative TEM images are shown. For the 5.2:20:80 and the 5.2:25:75 the formation of a 2D hexagonally arranged mesostructure is definitely supported. For the 5.2:30:70 gel there are periodically arranged cylindrical mesopores visible, but also amorphous regions. Reducing the amount of the polymer to a final composition of 5.2:15:85 is leading to the formation of a wormhole-like mesostructure. Somehow reducing the amount of the polymer to this composition seems to favour the formation of such a structure. In addition, TEM images of the 5.2:18:82 gel (not shown here) have proven the coexistence of cylindrical mesopores and wormhole-like structures.
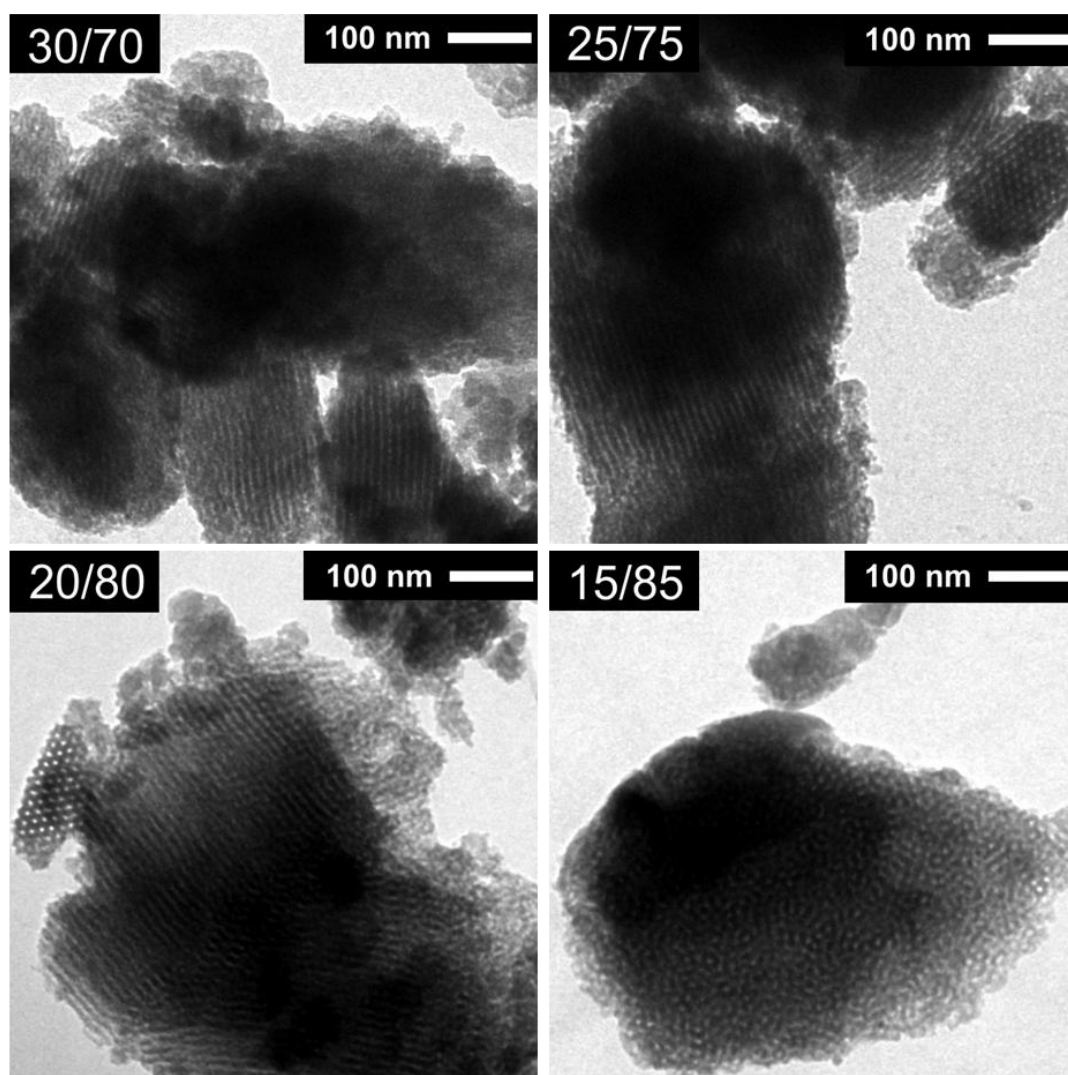
Fig. 3.6. TEM images for the 5.2:30:70, 5.2:25:75, 5.2:20:80 and the 5.2:15:85 gels

In-situ SAXS measurements are a powerful tool to investigate time-dependent processes in the nanometer regime and many publications use this tool to monitor the formation of mesostructures [36–39]. The slow gelation kinetics of our systems allow for an *in-situ* investigation with a time resolution of some minutes applying a laboratory rotating anode generator, whereas the literature usually uses a synchrotron radiation source. As a

representative example, Fig. 3.7 shows time-dependent measurements for a 5.2:20:80 sol mixture: The first scattering pattern was obtained 9 minutes after homogenization of the silica precursor in the P123 solution. Every 5 min a scattering pattern was recorded. Up to about 200 min, weakly correlated micelles are visible from the broad short range order peak between q = 0.3 and q = 0.7 nm^{-1}. This corresponds to the scattering of micelles, which were described by a core-shell structure from experiments with a 20:80 mixture of P123/water **[40]**.
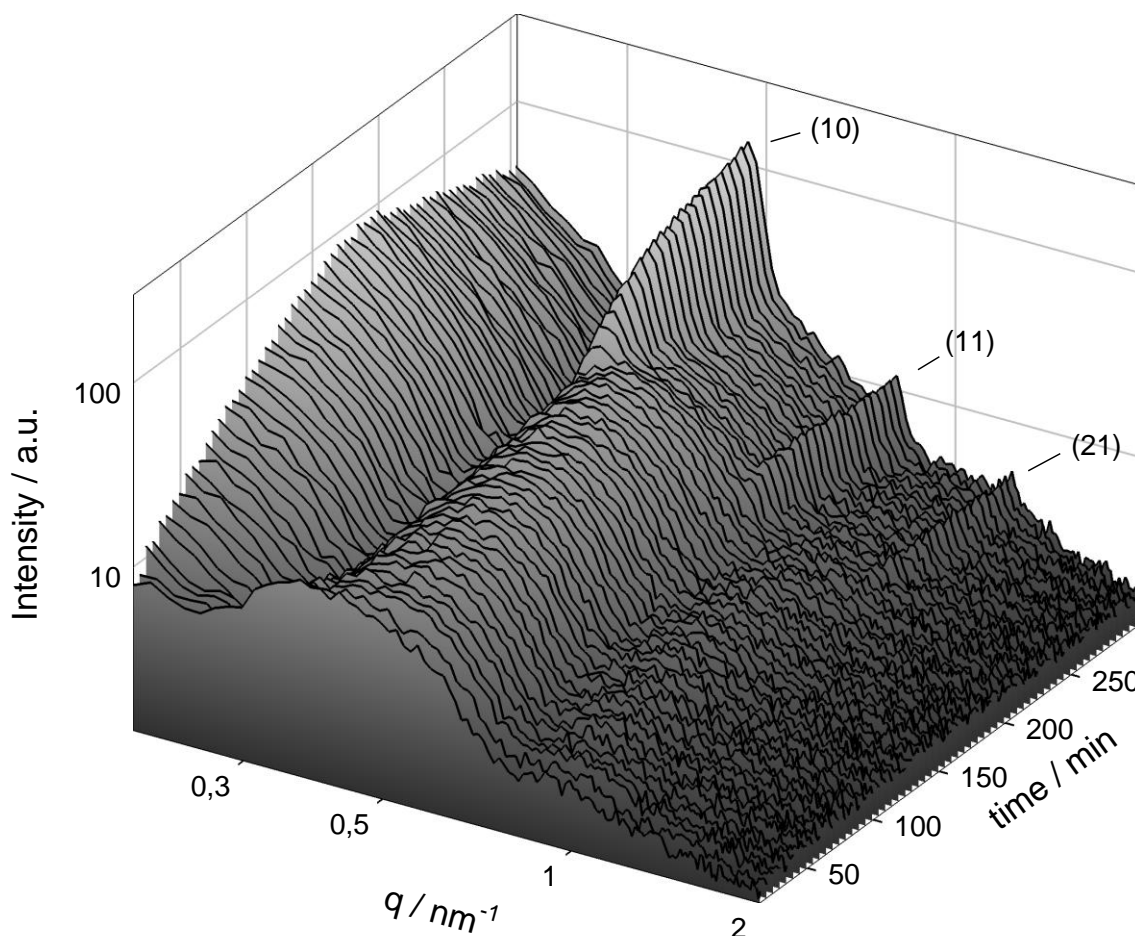
Fig. 3.7. *In-situ* SAXS measurement for a 5.2:20:80 gel composition at 40°C

Directly after mixing, the remaining peak is very broad, indicating that the hydrolyzed silane precursor initially leads to a swelling of the micelles. With time, the FWHM is decreasing and the peak intensity increases. The onset of the macroscopic phase separation is at about 104 min, opaqueness (indicating macroscopic phase separation) of the gel is observed after 114 min. However, the sol was still liquid and gelled only after 174 min. The mesostructure started to develop very rapidly a considerable time after gelation at approximately 200 min. This indicated that even in the gelled state the mobility within the phase separated domains was high. The strong scattering intensity towards low q, which decreases at the same time the mesostructure evolves, is remarkable. This observation is possible evidence for an

intermediate phase, which precedes mesostructure formation. This is supported by results from ultra-small angle X-ray scattering measurements of a similar system by Fritscher et al., where the scattering in the low q region was attributed to a mixture of swelling and growing spherical and/or ellipsoidal hybrid micelles [41].

In a first approach, the system is described as a nucleation and growth of micelles, which build up the grains of the mesostructure [36-39], and the Avrami theory is applied to describe the kinetics as is usual for crystallization and recrystallisation phenomena [42–44]. This has also been reported earlier as a successful way to describe similar mesostructure formation processes [28, 45]. In a system of randomly distributed nuclei, some of them turn to be active growth nuclei and cross the boundary to the metastable region. Such a growth process is frequently described by the Avrami equation:

$$\alpha = 1 - \exp(-kt^m) \tag{3.1}$$

where α is the time-dependent volume fraction of the transformed volume, k is the rate constant for the transition between the two phases, and $m = a + b$ (for linear growth of the particles) with a being a constant that depends on the dimension of the growth (a = 1, 2 or 3 for one-, two- or three-dimensional growth, respectively) and b being the nucleation rate (b = 0 for zero nucleation rate or b = 1 for constant nucleation rate). As the time-dependent growth of the (10) reflection of the 2D-hexagonally arranged cylindrical micelles is direct proof of how much volume has already been transformed, α can be obtained from the fraction of the intensities at a time = $t - t_0$ and $t = \infty$ [46]:

$$\alpha = \frac{I_{t-t_0}}{I_{max}} \tag{3.2}$$

In-situ SAXS measurements were performed in a temperature range from 20°C up to 60°C for a 5.2:20:80 composition at pH = 1. A possible error could arise from the fact that a more wormhole-like mesostructure was observed for lower temperatures of 20 and 30°C. A fit of the evolution of the intensities of the (10) reflections with Gaussian functions allowed the application of the Avrami equation assuming a zero nucleation rate and a one-dimensional growth with an exponent of m = 1 (see Fig. 3.8).

It is obvious that the Avrami equation adequately describes the experimental data: The obtained rate constants show an exponential dependence, so every 10 K the rate of the mesostructure formation increases by a factor of two. Due to the strong temperature dependence of the rate constants, it is possible to describe them by an Arrhenius relationship, where a plot of $ln(k)$ vs. T^{-1} leads to a straight line with slope of $-E_a/R$ (see

Fig. 3.9). Evaluating this fit results in a value of E_a of ~61 kJmol^{-1} representing the activation energy for the growth of the mesoscopic crystallites.

This value for the activation energy of the mesophase growth is comparable to the value obtained by Lindén et al. for a tetraethylorthosilicate/alkyltrimethylammonium bromide system of about 42 kJmol^{-1} by *in-situ* SAXS measurements [28]. Holmes et al. have calculated a value of about 72 kJmol^{-1} by *in-situ* FTIR studies in a similar system [45]. The formation and breaking of siloxane bonds in aqueous solution during silica polymerisation (40– 60 kJmol^{-1}) [47] and the activation energies for zeolite crystal growth (47–65 kJmol^{-1}) [48] are of the same order. Although the Avrami analysis describes our observations fairly well, the fit parameters have to be regarded very carefully. During organosilica polymerisation and expulsion of solvent from the mesophase, the electron density will also increase and lead to an ill-defined end-point of the process. Furthermore, a transition of a wormhole-like structure to perfect cylinders could have an effect, but this is probably less important as the description with one-dimensional growth fits the data very well. Thus, the activation energy of growth seems to be unaffected by small differences in mesostructure formation.
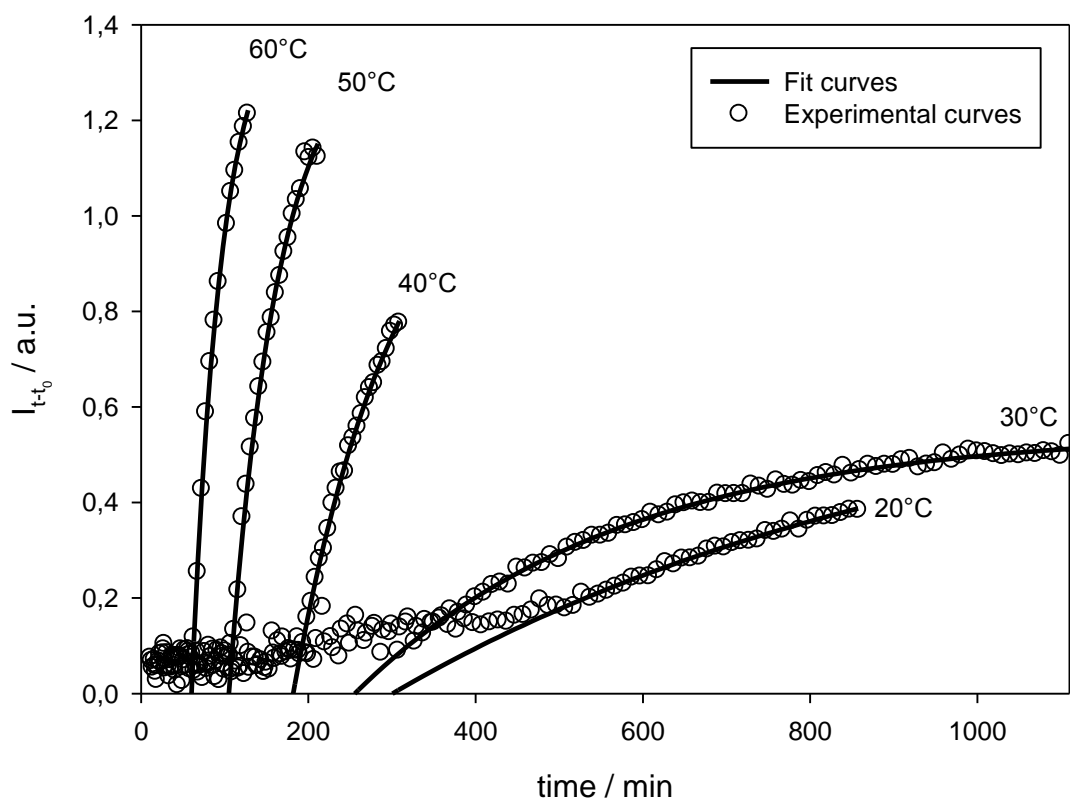
Fig. 3.8. Avrami fits for the investigated temperature range

Several mechanistic models for the formation of a periodic mesostructure from an inorganic precursor/amphiphile solution are discussed **[1, 2, 49, 50]**. On the one hand the true liquid crystal templating mechanism suggests that a precursor species polymerizes around a preformed liquid crystalline template. Therefore, one needs to start with a "true" liquid crystalline phase. This is only observed in very concentrated polymer solutions, for example the 30:70 P123/water mixture. In the present system this preformed liquid crystalline phase is not observed for the concentration of P123 below 30:70. Therefore, a cooperative pathway, in which the structure-directing amphiphile and the organosilica precursor closely interact, is more probable. Considering a preceding macroscopic phase separation event, the whole process becomes even more complicated. With the obtained results, a first step towards a better understanding of the phase separation mechanism on several length scales (meso and macro) is made.
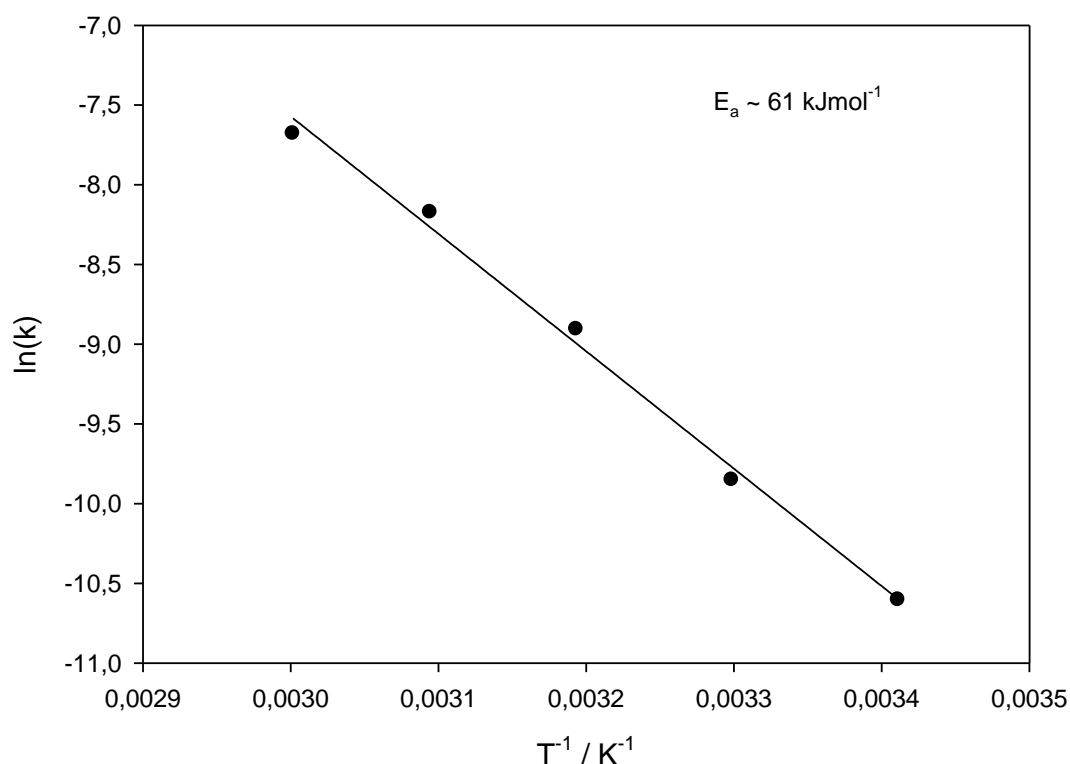
Fig. 3.9. Arrhenius plot based on rate constants obtained from the Avrami fits

3.4 Conclusions

Bis(tris-2-hydroxyethoxysilyl)ethane has proven to be a versatile precursor in the synthesis of hierarchically organized organosilica monoliths with a macroporous network comprising hexagonally arranged mesopores. The resulting framework structure can easily be modified from fine grained particles to a very coarse co-continuous structure by simple variation of the

P123 concentration. *In-situ* SAXS measurements were performed at different temperatures to follow the temporal evolution of the network in the precursor solution. It can clearly be seen, that the formation of the periodic mesostructure is not based on a true liquid crystal templating mechanism. Thus, a cooperative mechanism with the intermediate formation of hybrid organosilica/P123 micelles can be postulated. Considering a nucleation and growth mechanism for the mesostructure formation it is possible to describe the kinetics of the transition by applying the Avrami theory to the time-dependent evolution of the (10) reflection of the mesostructure. From this analysis we deduce (1) a one-dimensional growth for the mesoscopic crystallites, (2) an exponential temperature dependence for the rate constants of the mesostructure formation and (3) an activation energy for the growth of the crystallites of about 61 kJmol^{-1}. This detailed study expands our understanding of the formation processes of this and related sol-gel systems and will be a starting point for the development and the studying of more complex and functional porous organosilica systems in the future.

3.5 Acknowledgements

3.6 References

[1]   C.T. Kresge, M. E. Leonowicz, W.J. Roth, J. C. Vartuli, J. S. Beck, *Nature*, **1992**, 359, 710-712

[2]   J. S. Beck, J. C. Vartuli, W. J. Roth, M. E. Leonowicz, C. T. Kresge, K. D. Schmitt, C. T-W. Chu, D. H. Olson, E. W. Sheppard, S. B. McCullen, J. B. Higgins, J. L. Schlenker, *J. Am. Chem. Soc.*, **1992**, 114, 10834

[3]   S-S. Kim, T. R. Pauly, T. J. Pinnavaia, *Chem. Commun.*, **2000**, 17, 1661

[4]   K. Landskron, G. A. Ozin, *Science*, **2004**, 306, 1529

[5]   K.L. Frindell, J. Tang, J. H. Harreld, G. D. Stucky, *Chem. Mater.* **2004**, 16, 3524 – 3532

[6]   J. M. Wu, M. Antonietti, S. Gross, M. Bauer, B. M. Smarsly, *ChemPhysChem,* **2008**, **9**, 748

[7]   M.J. MacLachlan, N. Coombs, G.A. Ozin, *Nature*, **1999**, 397, 681

[8]   U. Ciesla, S. Schacht, G.D. Stucky, K. K. Unger, F. Schüth, *Angew. Chem.* **1996**, 108, 597

[9]   S. Inagaki, S. Guan, Y. Fukushima, T. Ohsuna, O. Terasaki, *J. Am. Chem. Soc.*, **1999**, 121, 9611

[10]   B.J.Melde, B.T. Holland, C.F. Blanford, A. Stein, *Chem. Mater.* **1999**, 11, 3302

[11] T. Asefa, M. J. McLachlan, N. Coombs, G. A. Ozin, *Nature*, **1999**, 402, 867

[12] F. Hoffmann, M. Cornelius, J. Morell, M. Fröba, *Angew. Chem.* **2006**, 118, 3290

[13] J.E. Martin, M.T. Anderson, J. Odinek, P. Newcomer, *Langmuir,* **1997**, *13*, 4133.

[14] S.A. El-Safty, Y. Kiyozumi, T. Hanaoka, F. Mizukami, *J. Phys. Chem. C* **2008**, 112, 5476.

[15] T. Amatani, K. Nakanishi, K. Hirao, T. Kodaira, *Chem. Mater.* **2005**, 17, 2114

[16] K. Nakanishi, Y. Kobayashi, T. Amatami, K. Hirao, T. Kodaira, *Chem. Mater.* **2004**, 16, 3652

[17] K. Nakanishi, T. Amatani, S. Yano, T. Kodaira, *Chem. Mater.* **2008**, 20, 1108

[18] S. Hartmann, D. Brandhuber, N. Hüsing, *Acc. Chem. Res.*, **2007**, 40, 885

[19] N. Hüsing, D. Brandhuber, P. Kaiser, *J. Sol-Gel Sci. Technol.*, **2006**, 40, 131

[20] M. Weinberger, S. Puchegger, C. Rentenberger, M. Puchberger, N. Hüsing, H. Peterlik, *J. Mater. Chem.*, **2008**, 18, 4783

[21] R. C. Mehrotra, R.P. Narain, *Indian J. Chem.*, **1966**, 5, 444

[22] P. Alexandridis, L. Yang, *Macromolecules,* **2000**, 33, 5574

[23] N. Hüsing, C. Raab, V. Torma, A. Roig, H. Peterlik, *Chem. Mater.* **2003**, 15, 2690

[24] K. Sattler, H. A. Hoffmann, *Prog. Colloid Polym. Sci.*, **1999**, 112, 40

[25] D. Brandhuber, H. Peterlik, N. Hüsing, *Small*, **2006**, 2, 503

[26] D. Y. Zhao, Q. S. Huo, J. L. Feng, B. F. Chmelka, G. D. Stucky, J. Am. Chem. Soc., **1998**, 120, 602

[27] W. Guo, I. Kim, C. –S. Ha, Chem. Commun., **2003**, 21, 2692

[28] I. Beurroies, P. Ågren, G. Büchel, J. B. Rosenholm, H. Amenitsch, R. Denoyel, M. Lindén, *J. Phys. Chem. B*, **2006**, 110, 16254

[29] D. Brandhuber, N. Hüsing, C. K. Raab, V. Torma, H. Peterlik, *J. Mater. Chem.*, **2005**, **15**, 1801

[30] J. Rubio, J.A. Kitchener, *J. Colloid Interface Sci.*,**1976**, 57, 132

[31] K. Nakanishi, H. Komura, R. Takahashi, N, Soga, *Bull. Chem. Soc. Jpn.*, **1994**, **67**, 1327

[32] K. Nakanishi, *J. Porous Mater.*, **1997**, 4, 67

[33] K. Nakanishi, *Bull. Chem. Soc. Jpn.*, **2006**, 79, 673

[34] K. Nakanishi, K. Kanamori, *J. Mater. Chem.*, **2005**, 15, 3776

[35] P. I. Ravikovitch, A. V. Neimark, *Langmuir*, **2002**, 18, 9830

[36] P. Ågren, M. Lindén, J. B. Rosenholm, R. Schwarzenbacher, M. Kriechbaum, H. Amenitsch, P. Laggner, *J. Phys. Chem. B*,**1999**, 103, 5943

[37] P. Ågren, M. Lindén, J. B. Rosenholm, J. Blanchard, F. Schüth, H. Amenitsch, *Langmuir*, **2000**, 16, 8809

[38] K. Flodström, C. V. Teixeira, H. Amenitsch, V. Alfredson, M. Lindén, *Langmuir*, **2004**, 20, 4885

[39] K. Flodström, H. Wennerström, C. V. Teixeira, H. Amenitsch, M. Lindén, V. Alfredsson, *Langmuir*, **2004**, 20, 10311

[40] S.S. Soni, G. Brotons, M. Bellour, T. Narayanan, A. Gibaud, *J. Phys. Chem. B*, **2006**, 110, 15157

[41] C. Fritscher, Self-Assembly, Hierarchical Structure and Mechanical Properties of (Organo-)Silica Monoliths, PhD thesis, Vienna University of Technology, **2008**

[42] M. Avrami, *J. Phys. Chem.*, **1939**, 7, 1103

[43] M. Avrami, *J. Phys. Chem.*, **1940**, 8, 212

[44]   M. Avrami, *J. Phys. Chem.*, **1941**, 9, 177

[45]   S. M. Holmes, V. L. Zholobenko, A. Thursfield, R. J. Plaisted, C. S. Cundy, J. Dwyer, *J. Chem. Soc., Faraday Trans.*, **1998**, 94, 2025

[46]   F. Né, F. Testard, Th. Zemb, I. Grillo, *Langmuir*, **2003**, 19, 8503

[47]   R. K. Iler, *The Chemistry of Silica*, Wiley, New York, **1979**, p. 248

[48]   N. N. Feoktistova, S. P. Zhdanov, W. Lutz, M. Bülow, *Zeolites*, **1989**, 9, 136

[49]   Q. S. Huo, D. T. Margolese, D. G. Demuth, P. Y. Feug, T. E. Gier, P. Sieger, A. Firouzi, B. F. Chmelka, F. Schuth, G. D. Stucky, *Chem. Mater.*, **1994**, 6, 1176

[50]   Q. S. Huo, D. I.   Margolese, U. Ciesla, P. Y. Feng, T. E. Gier, P. Sieger, R. Leon, P. M. Petroff, F. Schüth, G. D. Stucky, *Nature*, **1994**, 368, 317

4. Mesoporous dendrimer silica monoliths studied by small-angle X-ray scattering

Manuel Weinberger [ab], **Stephan Puchegger** [a], **Christian Rentenberger** [a], **Michael Puchberger** [c], **Nicola Hüsing** [b] **and Herwig Peterlik** [a]

[a]*Faculty of Physics, University of Vienna, Strudlhofgasse 4, A-1090, Vienna, Austria.*

[b]*Inorganic Chemistry I, Ulm University, Albert-Einstein Allee 11, D-89081, Ulm, Germany.*

[c]*Institute of Materials Chemistry, Vienna University of Technology, Getreidemarkt 9, A-1060, Vienna, Austria*

Abstract. Monolithic inorganic–organic hybrid materials have been synthesized *via* sol–gel processing of a novel ethylene glycol-modified carbosilane dendrimer precursor in an aqueous solution of the non-ionic block copolymer Pluronic P123. The influences of different precursor concentrations and various pH values on the final gel structure were investigated. The resulting material is built up of nanometer scale building units forming a network of three-dimensionally connected spherical clusters. The structure and chemical composition were characterized by small-angle X-ray scattering, transmission electron microscopy and MAS magnetic resonance spectroscopy. For precise structural information, analytical and numerical *ab initio* fitting of the small-angle X-ray scattering curves was used.

4.1 Introduction

The fabrication of inorganic–organic hybrid materials with periodically ordered porosity in the nanometer range and large specific surface areas has attracted increasing interest in the past years, especially for applications in the areas of adsorption, chromatography, catalysis, gas storage and sensor technologies[1]. In addition, there are several review articles covering all aspects of the synthesis of mesoporous materials from pure silica to other metal oxides[2,3]. In the last years, more and more efforts have been devoted to the incorporation of organic moieties within the inorganic framework to achieve a symbiosis of the properties of both components.

The most important approaches towards hybrid inorganic–organic materials are based on wet chemical processing methods such as sol–gel chemistry, which offers the possibility not only to develop new types of ceramics or glasses, but also to incorporate organic moieties in inorganic networks due to the mild reaction conditions[4]. Together with the improved control

of the mesostructure and the handling of a multicomponent system, the enormous variety in combining the different components allows deliberate tailoring of materials with better or new properties. Modern chemistry enables the control of particle size, shape, surface area, and interfacial properties as well as the mutual arrangement and morphology from completely disordered to completely ordered states of matter in the range between 2 and 500 nm. In the past decade, this has stimulated research in areas that include catalysis and sensors[5], coatings[6], membranes[7], nanoreactors[8], and in electronic applications[9].

Bridged polysilsesquioxanes are a rather new family of hybrid inorganic–organic materials that are prepared *via* sol–gel processing of monomers containing a bridging organic group and two or more trialkoxysilyl groups[10,11]. The use of these bridged precursors, such as $X_3Si-R'-SiX_3$ (R' is an organic spacer, X = Cl, Br, OR) allows the formation of homogeneous molecular hybrid inorganic–organic materials, which have a high degree of local organization. Most of the available bridged precursors can also be condensed in the presence of a structure-directing agent such as a liquid crystalline phase of surfactant molecules or amphiphilic block copolymers necessary for the preparation of periodically arranged mesoporous frameworks. The first synthesis of a periodically arranged mesostructured silsesquioxane material with an organic bridge as an integral part of the network was reported in 1999 independently by three different groups[12-14]. Today these materials are often called periodic mesoporous organosilicas (PMOs) and a variety of examples can be found in the literature[1]. This bridging principle can even be extended to dendrimeric structures in which not only a quarter of all Si-O-Si units are replaced by Si-R-Si units, but in the most extensive case even all four bridges. Sharp *et al.* showed that with sol-gel processing of tetrakis[2-(triethoxysilyl)ethyl]silane bearing twelve condensable alkoxy units it is possible to yield a truly inorganic–organic hybrid gel and Ozin's group introduced this concept of using multisilylated precursors to periodically arranged hybrid networks[15-17].

Most of the above mentioned porous materials were prepared as powders. For many applications it is much more attractive to synthesize bulk materials, *e.g.* as monoliths, with a multimodal pore size distribution. A simple and reproducible method towards such materials is based on sol-gel processing accompanied by phase separation as introduced by the group of Nakanishi. In a sol containing a soluble polymer, phase separation can be induced because of changes in the miscibility and polarity due to the continuous condensation reactions and formation of more hydrophobic siloxane species. At some point during the reaction, the phase-separated structure is just frozen in[18-20]. This approach, also termed polymerization-induced phase separation, has been proven to be a rather successful and variable approach, especially in the synthesis of monolithic inorganic, but also for inorganic–

organic hybrid materials. Nakanishi and coworkers published a series of papers in which they reported the use of water-soluble organic polymers, such as poly(ethylene oxide) (PEO), to control macroscopic phase separation parallel to the sol–gel transition. Lindén *et al.* extended this approach by applying the macroscopic, (PEO) polymer-controlled phase separation of silica particles in combination with an ionic or non-ionic surfactant as structure-directing agent in the nanometer regime[19]. The material they obtained exhibited interconnected porosity on several length scales, for which the macropore diameter is controlled *via* PEO–nanoparticle interactions, and the mesopore diameter by the presence of the surfactant *e.g.* cetyltrimethylammonium bromide or a poly(ethylene oxide)-based polymer. Only recently this approach was extended to bissilylated precursors, *e.g.* bis(triethoxysilyl)ethane, as a precursor for monolithic gels with a bimodal pore size distribution[20].

A different approach to synthesize silica monoliths with a hierarchical build-up of highly ordered mesopores and interconnected, uniform macropores has been recently presented by Hüsing and coworkers[21]. The key of this work was the substitution of ethoxy/methoxy groups of conventional tetraalkoxysilane precursors with short chain glycols as they show much better compatibilities with the self-assembly of silica/surfactant mesophases compared to ethanol or methanol. Furthermore, the glycol-modified silanes, *e.g.* tetrakis(2-hydroxyethyl)orthosilicate (EGMS), are water-soluble and can be hydrolyzed/condensed without addition of an acid or base catalyst under neutral conditions in purely aqueous medium[22-24]. The synthesis process is therefore simplified, as no toxic and/or expensive additives such as swelling agents and co-solvents are required. Substitution of alkoxy to glycoxy units can even be extended to the fabrication of phenylene-bridged silica monoliths with a hierarchical build-up on at least four levels: a) deliberate macroscopic shape, b) uniform macropores, c) highly ordered mesopores (plus micropores), and d) molecular periodicity of the phenylene moieties within the pore walls. The underlying notion of substituting the alkoxy groups of conventional (organo-)alkoxysilane precursors with ethylene glycol can be readily extended to other organic functionalities. This method represents a versatile tool to tailor the chemical functionality of monolithic materials with well-defined, multi-modal pore structures, thus increasing their potential of application significantly.

In this publication, the latter approach—based on modification of silanes with glycoxy groups—is extended to the dendrimeric silane tetrakis[2-(triethoxysilyl)ethyl]silane for the first time. Monolithic porous samples are prepared from the glycol derivative of the carbosilane dendrimer. Detailed structural characterization is performed by transmission electron microscopy, solid state nuclear magnetic resonance spectroscopy (NMR) and in particular by small-angle X-ray scattering (SAXS) with fitting the curves either by analytical methods[25]

or by *ab initio* reconstruction of the scattering data from numerical simulation of 3-dimensional structures**[26]**. The SAXS data allow for showing and discussing the influence of chemical parameters, such as the precursor concentration, the precursor/P123 to water or acid ratio or the pH value, on the morphologies of the resulting structures in detail.

4.2 Materials and Experimental

All reactions were carried out in argon and solvents were dried before use. Tetravinylsilane and Karstedt's catalyst were purchased from ABCR and tetravinylsilane was distilled before use. Trichlorosilane and the block copolymer P123 (Aldrich) were used without further purification.

Precursor synthesis

Tetrakis[2-(triethoxysilyl)ethyl]silane. To a mixture of 12 g (0.088 mol) tetravinylsilane, 3 drops of Karstedt's catalyst and 50 mL tetrahydrofuran were added at 0 °C. Under stirring 40 mL (0.396 mol) trichlorosilane were added over a period of 2.5 h. In the following, the temperature was gradually increased to room temperature and the mixture was stirred for another 24 h. The solvent and excess of trichlorosilane were removed under vacuum. A white solid was obtained. This procedure was repeated until no residual vinyl groups were detectable by NMR spectroscopy. ^{1}H-NMR (400.13 MHz, C_6D_6): 0.72 (m, 2H, SiCH$_2$CH_2SiCl$_3$), 0.31 (m, 2H, SiCH_2CH$_2$SiCl$_3$); ^{13}C-NMR (100.63 MHz, C_6D_6): 16.72 (SiCH_2CH$_2$SiCl$_3$), 1.33 (SiCH$_2$CH$_2$SiCl$_3$); ^{29}Si-NMR (79.49 MHz, C_6D_6): 12.68 (*Si*CH$_2$CH$_2$SiCl$_3$), 11.03 (SiCH$_2$CH$_2$*Si*Cl$_3$).

Tetrakis[2-trichloroethyl]silane was dissolved in 100 mL of heptane and heated to 60 °C. Over a period of 3 h, 70 mL of dry ethanol were added dropwise to the solution with argon bubbling directly through the solution to remove HCl gas. After stirring overnight at room temperature, the volatiles were removed *in vacuo* and the solution filtered, leaving 40.46 g (0.053 mol, 60%) of a yellow liquid. ^{1}H-NMR (400.13 MHz, C_6D_6): 3.83 (q, 6H, Si(OCH_2CH$_3$)$_3$), 1.19 (t, 9H, Si(OCH$_2$CH_3)$_3$), 0.93 (m, 2H, SiCH_2CH$_2$Si(OEt)$_3$), 0.83 (m, 2H, SiCH$_2$CH_2Si(OEt)$_3$); ^{13}C-NMR (100.63 MHz, C_6D_6): 58.55 (Si(OCH$_2$CH$_3$)$_3$), 18.66 (Si(OCH$_2$CH$_3$)$_3$), 3.26 (SiCH$_2$CH$_2$Si(OEt)$_3$), 2.41 (SiCH$_2$CH$_2$Si(OEt)$_3$); ^{29}Si-NMR (79.49 MHz, C_6D_6): 10.35 (*Si*[CH$_2$CH$_2$Si(OEt)$_3$]$_4$), −45.62 (Si[CH$_2$CH$_2$*Si*(OEt)$_3$]$_4$).

Modification with ethylene glycol

The modification of tetrakis[2-trichloroethyl]silane with ethylene glycol was performed by mixing 40.46 g (0.051 mol) of the ethoxide and 34.3 mL (0.613 mol) ethylene glycol in 100

mL of THF. The clear solution was stirred and the volatiles continuously removed by distillation, while the amount of THF in the mixture was kept constant through addition of THF. During distillation a white precipitate formed. The volatiles were completely removed with vacuum distillation leaving a glassy solid. The precursor was characterized by thermogravimetric measurements, showing a silicon content of 13.64% (14.2% for complete substitution of the ethoxy groups).

Gel preparation

Gels were prepared by mixing the glycolated precursor with deionized water or acid solution (10^{-2}, 10^{-3}, 10^{-4} M hydrochloric acid) in the presence or in the absence of the block copolymer P123. Before the gel preparation the polymer was dissolved in water or acid solution. In both cases the mixtures were homogenized under vigorous stirring and kept for gelation and aging over a period of 7 days. The templating polymer was removed *via* solvent extraction with ethanol. All wet gels were dried *via* extraction with supercritical carbon dioxide (T_C = 31,5 °C, p_C = 75 bar) to gain porous monolithic gels following a procedure described elsewhere[22]. The compositions of the starting solutions and the gelation times are summarized in Table 4.1.

Table 4.1 Composition of the starting gels

Identifier	Si content/P123/solvent mixture [mass fractions g]	Gelation conditions
8.1/30/70@pH2	8.1/30/70	4d RT/3d 40 °C
8.1/30/70@pH3	8.1/30/70	4d RT/3d 40 °C
8.1/30/70@pH4	8.1/30/70	1d RT/6d 40 °C
8.1/30/70@pH6	8.1/30/70	1d RT/6d 40 °C
5.4/30/70@pH2	5.4/30/70	2d RT/5d 40 °C
5.4/30/70@pH3	5.4/30/70	1d RT/6d 40 °C
5.4/30/70@pH4	5.4/30/70	2d RT/5d 40 °C
5.4/30/70@pH6	5.4/30/70	2d RT/5d 40 °C
8.1/20/80@pH2	8.1/20/80	1d RT/6d 40 °C
8.1/20/80@pH3	8.1/20/80	1d RT/6d 40 °C
8.1/20/80@pH4	8.1/20/80	1d RT/6d 40 °C
8.1/20/80@pH6	8.1/20/80	1d RT/6d 40 °C
5.4/20/80@pH2	5.4/20/80	1d RT/6d 40 °C
5.4/20/80@pH3	5.4/20/80	1d RT/6d 40 °C
5.4/20/80@pH4	5.4/20/80	1d RT/6d 40 °C
5.4/20/80@pH6	5.4/20/80	1d RT/6d 40 °C
8.1/—/75@pH2	8.1/—/75	1d RT/6d 40 °C
8.1/—/75@pH3	8.1/—/75	1d RT/6d 40 °C
8.1/—/75@pH4	8.1/—/75	1d RT/6d 40 °C
8.1/—/75@pH6	8.1/—/75	1d RT/6d 40 °C
5.4/—/75@pH2	5.4/—/75	1d RT/6d 40 °C
5.4/—/75@pH3	5.4/—/75	1d RT/6d 40 °C
5.4/—/75@pH4	5.4/—/75	1d RT/6d 40 °C
5.4/—/75@pH6	5.4/—/75	1d RT/6d 40 °C

SAXS

SAXS patterns of the dried gels were collected under vacuum using a rotating anode X-ray generator (Nanostar, Bruker AXS) with an X-ray beam monochromatized and collimated from crossed Goebel mirrors and equipped with a 2D position sensitive detector (either Bruker HiStar or Vantec 2000). The samples were prepared as powders and pasted between two Scotch™ tapes. The SAXS patterns were radially averaged to obtain the scattering intensity variation with the scattering vector $q = (4\pi/\lambda)sin(\theta)$, where 2θ is the scattering angle and λ = 0.1542 nm the X-ray wavelength. Measurements were carried out at two different distances (10 cm and 106 cm) to cover a wide q range.

TEM

For the TEM study the samples prepared as powders were put onto a perforated carbon film and imaged with a Philips CM200 microscope operating at 100 kV.

Nuclear magnetic resonance

The products of the precursor synthesis were dissolved in deuterated benzene. The ^{1}H-, ^{29}Si- and ^{13}C-NMR spectra were recorded on a Bruker AVANCE 400 spectrometer at 400.13, 79.49 and 100.63 MHz, respectively.

The solid state NMR spectra were measured using a Bruker AVANCE 300 spectrometer using a 4 mm MAS broadband probe head. The rotor spinning speed for all performed experiments was 6 kHz. The ^{13}C spectra were measured with ramped CP/MAS experiments at a resonance frequency of 75.40 MHz. The [29]Si spectra were measured with ramped CP/MAS experiments at a resonance frequency of 59.57 MHz.

Nitrogen sorption measurements

Surface areas and pore size distributions were determined by sorption measurements which were performed at 77 K on a Quantachrome NOVA4000e. The specific surface areas were determined by 5 point analysis from the lower relative pressure range (p/p_0 = 0.05–0.15).

Thermogravimetric analysis

Information on the silicon content of the precursor was obtained by heating the precursor in a NETZSCH STA 449 C cell to 1000 °C.

4.3 Theory

The scattering intensity from a network structure with a certain cluster size ξ, built up from particles with a size r, is usually described by[25]

$$I(q) = I_0 S(q) P(q) \tag{4.1}$$

where q is the absolute value of the scattering vector, $S(q)$ the structure factor and $P(q)$ the form factor of the units. I_0 contains experimental parameters such as the beam intensity, the phase contrast, the number and volume of the particles and additional variables due to the setup of the experiment. Usually, a background from parasitic scattering from residual air or the pinhole has to be added to eqn (1).

For spherical particles with a wide size distribution, the Debye approximation can be used for the form factor

$$P(q) = \left(1 + \frac{\sqrt{2}}{3} q^2 r^2\right)^{-2} \tag{4.2}$$

whereas for narrow particle distributions, a numerical approach with a Gaussian distribution is more appropriate,

$$P(q) \propto \int dR \Theta^2(r) \exp\left(-\frac{0.5(R-r)^2}{\sigma^2}\right) \tag{4.3}$$

with $\Theta(r)$, the Fourier transform of the sphere,

$$\Theta(r) = 3 \frac{\sin(qr) - qr\cos(qr)}{(qr)^3} \tag{4.4}$$

The structure factor for individual spheres, which build up a network with a fractal dimension D and a correlation length , was derived by Freltoft *et al.*,[27]

$$S(q) = 1 + \frac{C\Gamma(D-1)\xi^D}{q\xi}(1 + q^2\xi^2)^{(1-D)/2}\sin((D-1)\arctan(q\xi)) \tag{4.5}$$

for which the correlation length ξ is correlated to the radius of gyration of the clusters:[28]

$$R_{Cl} = \xi\left(\frac{D(D+1)}{2}\right)^{0.5} \tag{4.6}$$

The fractal dimension characterizes the density and arrangement of the single particles to aggregates or clusters and allows information on the aggregation process to be obtained[29].

To obtain more precise information about the structure, numerical evaluation methods were used. *Ab initio* analysis fits one-dimensional scattering curves[30] by varying the density and arrangement of small scattering units to recover the three-dimensional structure. For the numerical simulation of the structure, the software programs DAMMIN**[26]** and GNOM**[31]** were used.

4.4 Results and Discussion

Monolithic white hybrid gels were produced by sol–gel processing of an ethylene glycol substituted carbosilane under aqueous conditions in the presence and in the absence of a structure-directing agent (see Fig. 4.1).
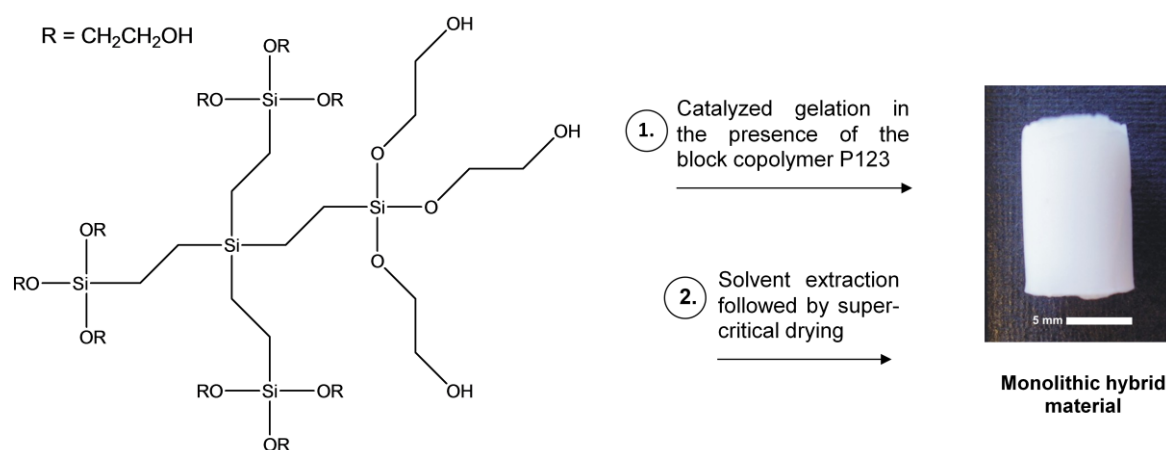
Fig. 4.1. Scheme of the sol–gel processing, which results in a hybrid "dendri-gel".

Structural characterization of the gels

SAXS was used to characterize the influence of the variation of the precursor concentration, the pH value and the ratio precursor/P123 to water or acid solution on the resulting structures. Fig.4.2 shows typical SAXS patterns.: In Fig. 4.2 a, the scattering curves for different amounts of precursor concentrations and precursor/P123 to water or acid ratios in the solution are depicted, and Fig. 4.2 b shows the comparison of the scattering patterns for gels synthesized in the presence and in the absence of the block copolymer. The curves are vertically shifted for better visibility.

All scattering curves indicate scattering from particles or aggregates in the nanometer range. In the case of block copolymer containing systems a characteristic shoulder at low q values and a peak at approximately $q = 7$ nm^{-1} is always obtained. However, the shoulder at low q

values is not obtained in systems which were synthesized in the absence of the block copolymer.
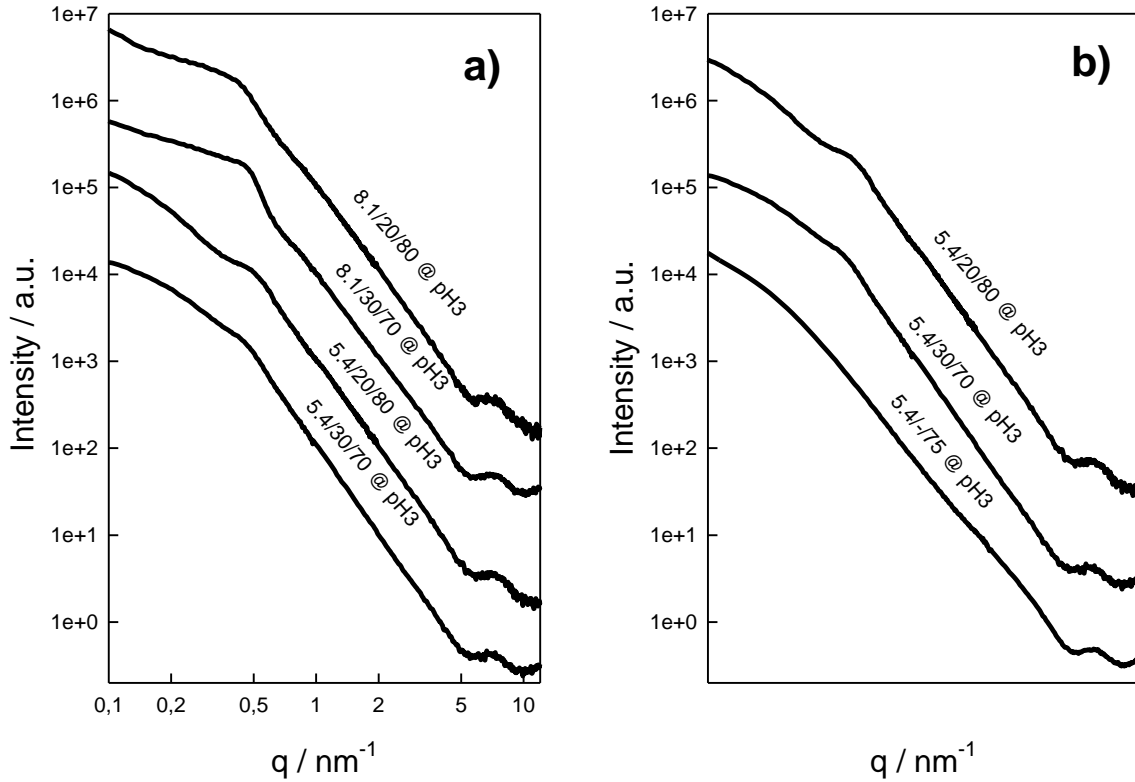
Fig. 4.2. Scattering intensities for a) different precursor concentrations and precursor/P123 to water or acid ratio, b) for different contents of block copolymer. The curves are shifted for better visibility.

In a first step, the scattering curves are interpreted as a system consisting of small interconnected scattering units, which form spherical clusters. It is suggested that the small peak at approximately $q = 0.4$ nm^{-1} is attributed to a short range order of pores, which were templated into the material by micelles formed by the polymer. This model is supported by the absence of such a short range order peak for systems that were prepared without the block copolymer (Fig. 2b). The second peak at $q = 7$ nm^{-1} can be assigned to a short range order of the basic scattering units. By interpolating the shoulders on both sides of the short range order peak with a Bézier curve, it is possible to separate the scattering contributions from the small units building up the clusters and the short range order of the templated pores. (Fig. 4.3 a) shows an example for the interpolating curve, which gives information on the cluster size ξ and the density of the network (fractal dimension D). After subtraction of the interpolated curve, Fig. 4.3 b visualizes the distance distribution of the templated pores. Though the distance distribution is asymmetric, a measure for the distance in real space is obtained from the intensity maximum in reciprocal space by $D_{pore} = 2\pi/q_{max}$. It should be

noted that one has to be careful with interpreting the precise numerical values, as the peak maximum q_{max} can shift considerably for a wide size distribution of particles[32].
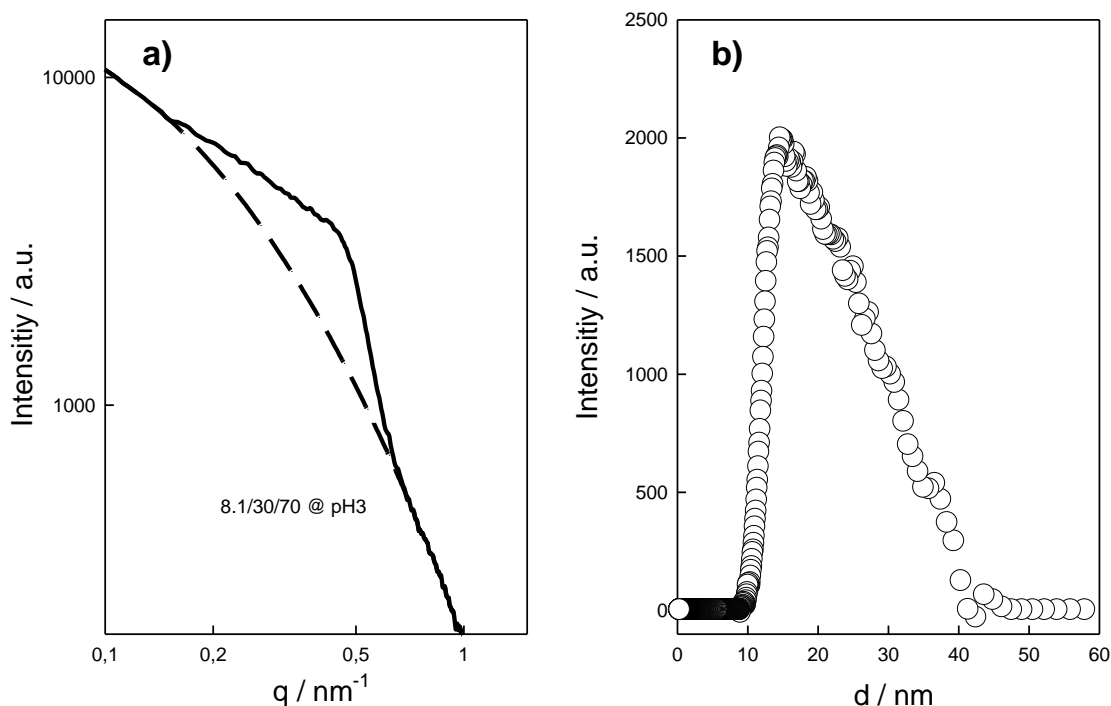
Fig. 4.3. a) Scattering intensity and interpolated curve without short range order peak. b) Distance distribution of pores D_{pore} in real space, obtained from subtraction of the interpolated curve from the measured intensities (experimental curve).
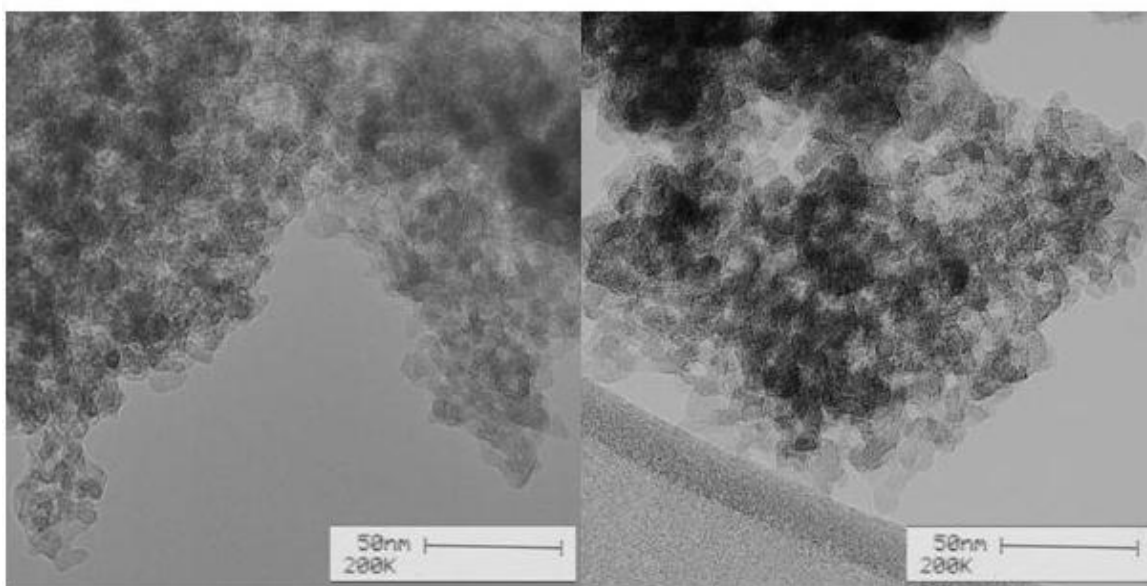
Fig. 4.4. TEM images of the gels 5.4/30/70@pH3 (left image) and 8.1/30/70 @ pH3 (right image).

The interpretation that spherical clusters/particles form an interconnected three-dimensional network is supported by TEM images (Fig. 4.4). The shape of the clusters is not perfectly

spherical, but more irregular and ellipsoidal or elongated, which makes numerical evaluation difficult. The mean size of the particles as visible in the TEM image is approximately 9 ± 3 nm with a typical separation of about 20 nm. It is also visible that 8.1/30/70@pH3 (Fig. 4.4 b) seems to have a more open network than 5.4/30/70@pH3 (Fig. 4.4 a). This coincides with the numerical data obtained by SAXS, which are precisely discussed in Fig. 4.6.

The flexibility and polyfunctionality of the precursor molecule lead to a wide range of possible network architectures. To prove that the short range order peak of the templated pores does not originate from remaining block copolymer from an incomplete washing procedure or partial degradation of the precursor molecule (Si-C bond cleavage resulting in SiO_4 units), solid state NMR measurements were carried out. The different gels showed quite similar spectra and are discussed together in the following. No peak for Q units is observed in the ^{29}Si CP-MAS spectrum (Fig. 4.5, left), indicating that the tetrakis[2-(trishydroxyethoxysilyl)ethyl]silane can be condensed without Si–C bond cleavage. The materials showed four peaks at 4.05, −53.73, −62.46 and −71.42 ppm corresponding to the silicon building the core of the dendrimer and the T^1, T^2, T^3 units (T^1 $SiC(OSi)(OH)_2$ (−53.8 ppm), T^2 $SiC(OSi)_2(OH)$ (−61.9 ppm) and T^3 $SiC(OSi)_3$ (−71.2 ppm)), respectively. No signal from residual P123 was observed in the ^{13}C spectra (Fig. 5, right), thus the block copolymer was completely removed by extraction with ethanol. However, signals at 50.29 ppm and 10.12 ppm occur, which are assigned to ethoxy groups arising from transalkoxylation reactions of the extraction solvent ethanol with free silanol groups. The signal at about −6.22 ppm is typical for an ethane bridge between two silicon atoms.
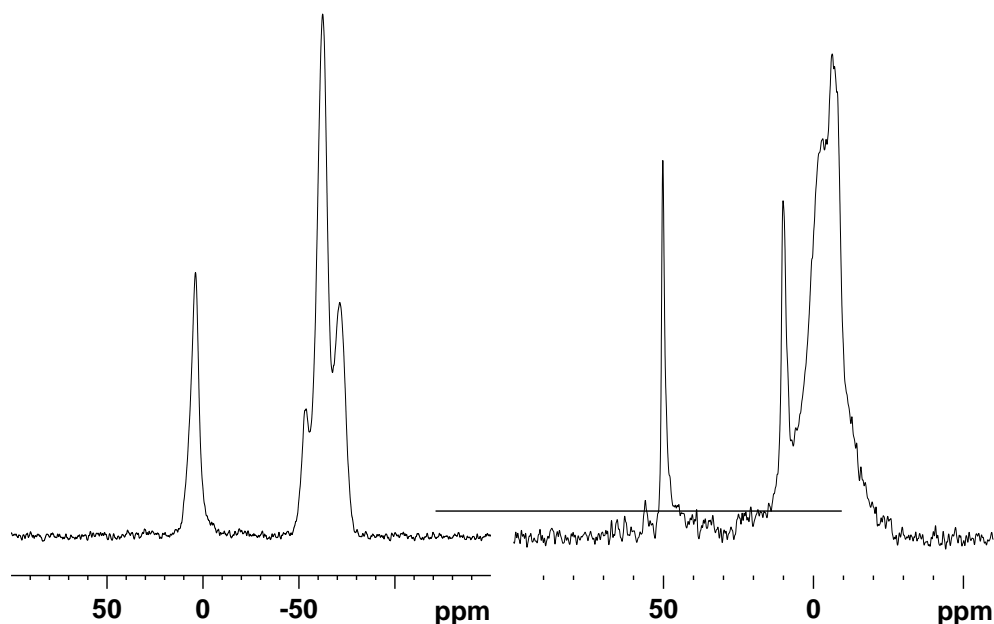
Fig. 4.5. Solid state ^{29}Si (left) and ^{13}C (right) CP-MAS NMR measurements of the 8.1/30/70@pH2 gel.

The correlation between the structural parameters obtained from the SAXS measurements for the different materials is summarized in Fig. 4.6. There is no clearly visible dependence of the cluster size ξ as obtained from eqn (4.5), Fig. 4.6 a, on the parameters under investigation, *i.e.* the pH value, the precursor concentration or the precursor/P123 to water or acid ratio. Differently, the mean pore distance D_{pore}, Fig. 4.6 b, is not affected by the precursor/P123 to water or acid ratio, but increases strongly with increasing precursor concentration (higher precursor concentration 8.1, grey symbols, lower precursor concentration 5.4, open symbols). The fractal dimension, Fig. 4.6 c, depends on both the precursor concentration and the precursor/P123 to water or acid ratio. The fractal dimension describes the density of the network: the denser the network, the higher the fractal dimension. A lower precursor concentration leads to a higher network density. The same effect is obtained by a higher precursor/P123 to water or acid ratio, which also leads to a denser network.

For the gels prepared without block copolymer, the cluster size ξ and the fractal dimension D were constant and no dependence on the acidity of the solution was observed. Additionally, the fractal dimension was between 2.4 and 2.5 for all samples; however, a slightly higher value for the cluster size (6 nm compared to 5 nm) for the gels with the higher precursor concentration could be found.

The separation of the basic scattering units obtained from the short range order peak at large q values (Fig. 4.2) has a value of approximately 0.8 nm and was constant within the measurement error for all gels.

To gain deeper insight into the fine structure of the material, we have chosen a numerical approach. The software programs DAMMIN[26] and GNOM[31] vary the three-dimensional distribution of small basic units to determine the structure, which leads to the experimentally observed one-dimensional scattering curves. As the measured q range in our experiments is too wide for a numerical simulation, we used only the scattering curve in the q range from 0.8 to 12.5 nm^{-1} to describe the arrangement of the basic scattering units within the clusters. Fig. 4.7 shows the experimental values (gray circles), the numerical fit (solid line) and the analytical fit (dashed lines) in this q range. The analytical fit was separated into two parts: the interpolated curve according to eqn. (4.1) and the short range order peak (after subtraction of the interpolating curve). The results from the numerical fit are visible in Fig. 4.8.
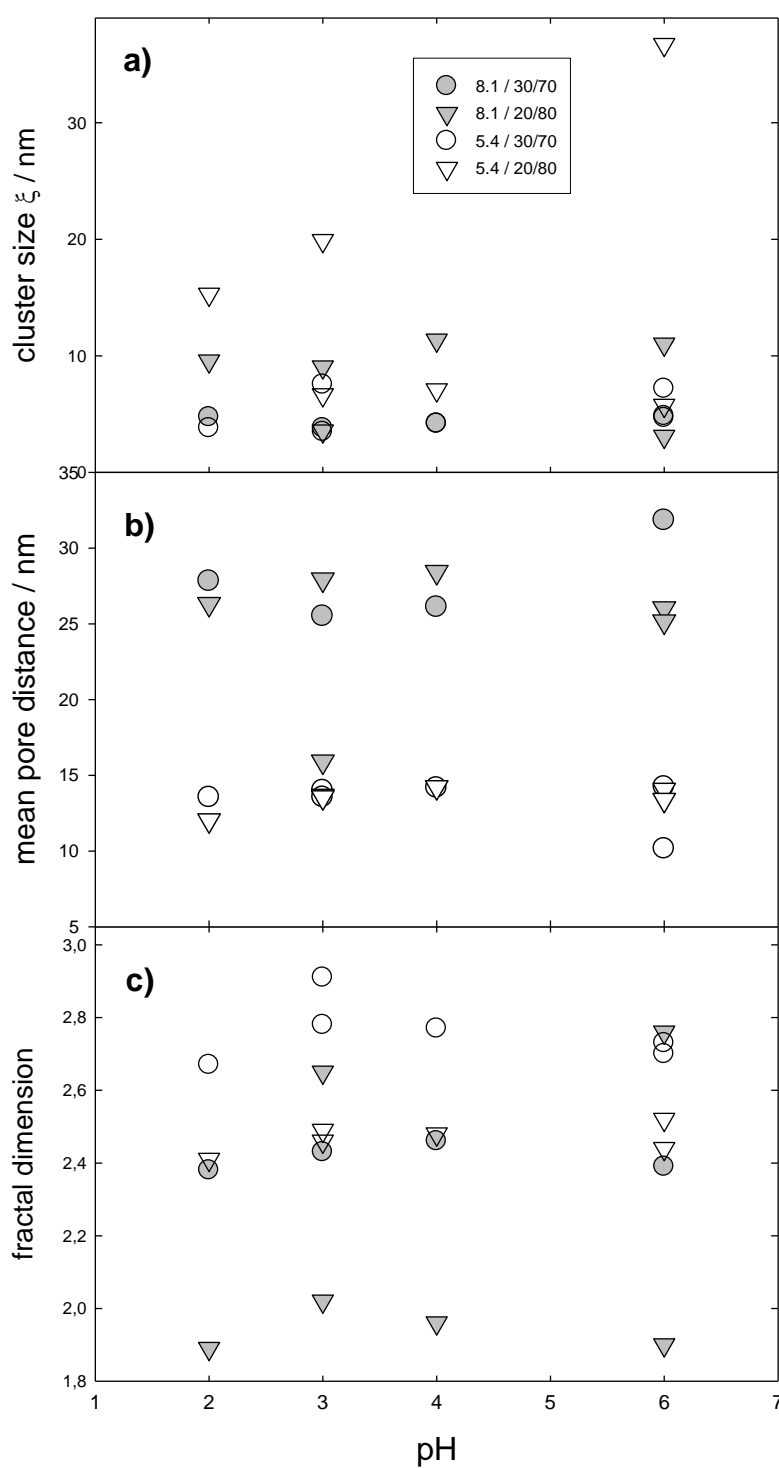
Fig. 4.6. Dependence of structural parameters (a) cluster size ξ, b) mean pore distance Dpore and c) fractal dimension D on the precursor concentration, the precursor/P123 to water or acid ratio and the pH value.

In the center of Fig. 4.8, the arrangement of the basic scattering units within the cluster obtained from the numerical calculation is found, which resembles a quite dense, but not completely filled network. The left part of Fig. 4.8 describes the arrangement of different clusters in a short range order as suggested from the analytical models (different runs of the

numerical fit and different perspectives), the right part the composition of the probable basic scattering unit, the dendrimer.
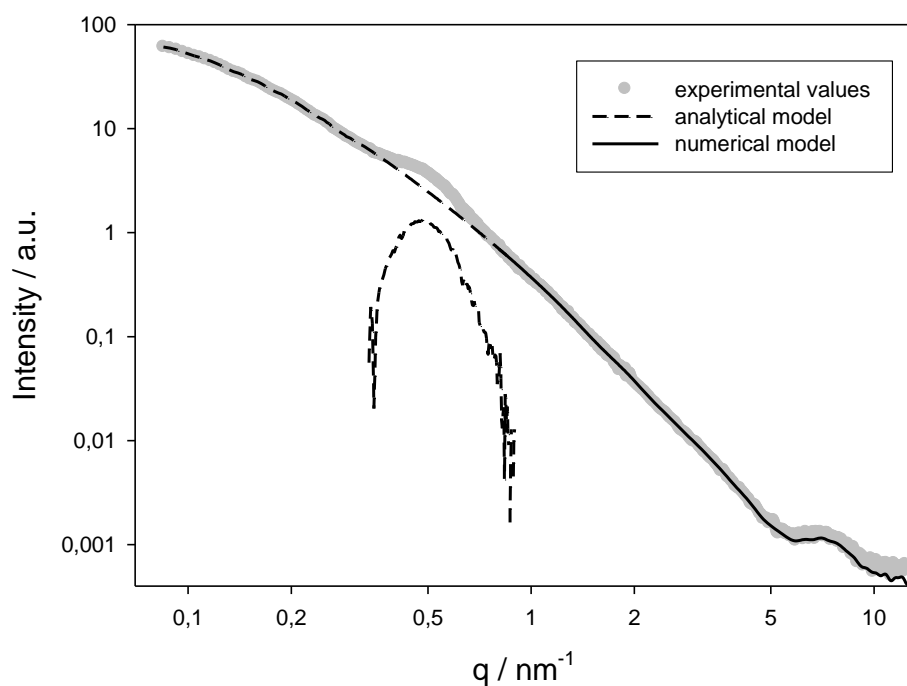
Fig. 4.7. Experimental scattering curve (gray circles) together with the numerical fit (solid line) in the q range from 0.8 to 12.5 nm^{-1}, the short range order curve and the analytical model according to eqn (1) (dashed lines).
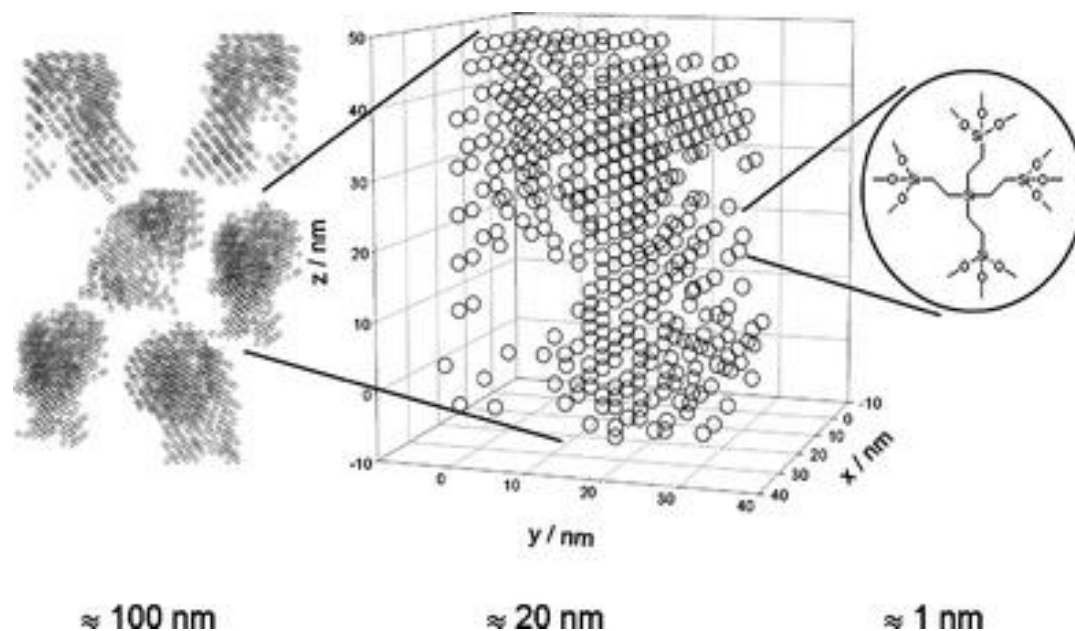
Fig. 4.8. Structural model from the numerical fit. In the centre, the arrangement of the basic scattering units within the cluster is shown; left: arrangement of clusters as suggested from analytical results; right: probable composition of basic scattering units (condensation product of tetrakis[2-(trishydroxyethoxysilyl)ethyl]silane).

Sorption measurements from all samples prepared at pH 3 (8.1/20/80@pH3, 8.1/30/70@pH3, 8.1/—/75@pH3, 5.4/20/80@pH3, 5.4/30/70@pH3, 5.4/—/75@pH3) have shown typical type IV isotherms indicating mesoporous materials (Fig. 9). The surface areas are rather high (600–800 m^2 g^{-1}). With 730 m^2 g^{-1} for sample 5.4/30/70@pH3, and 745 m^2 g^{-1} for 5.4/—/75@pH3 being prepared without template, no significant influence of the block copolymer on the specific surface area was observed. The size of the mesopores using Barrett–Joyner–Halenda (BJH) analysis is within the range 2 to 50 nm, with a maximum between 10 and 20 nm. An evaluation according to the Frenkel-Halsey-Hill (FHH) equation as performed in ref. [33] to compare the fractal dimension from SAXS and nitrogen sorption gave values between 2.4 and 2.8. However, a comparison of SAXS and nitrogen sorption is not applicable in our case, as SAXS measures the fractal dimension of a mass fractal (the arrangement of the particles with a fractal size distribution within a cluster), whereas nitrogen sorption is sensitive only to the surface (the fractal dimension due to the fractal surface of pores and/or particles).
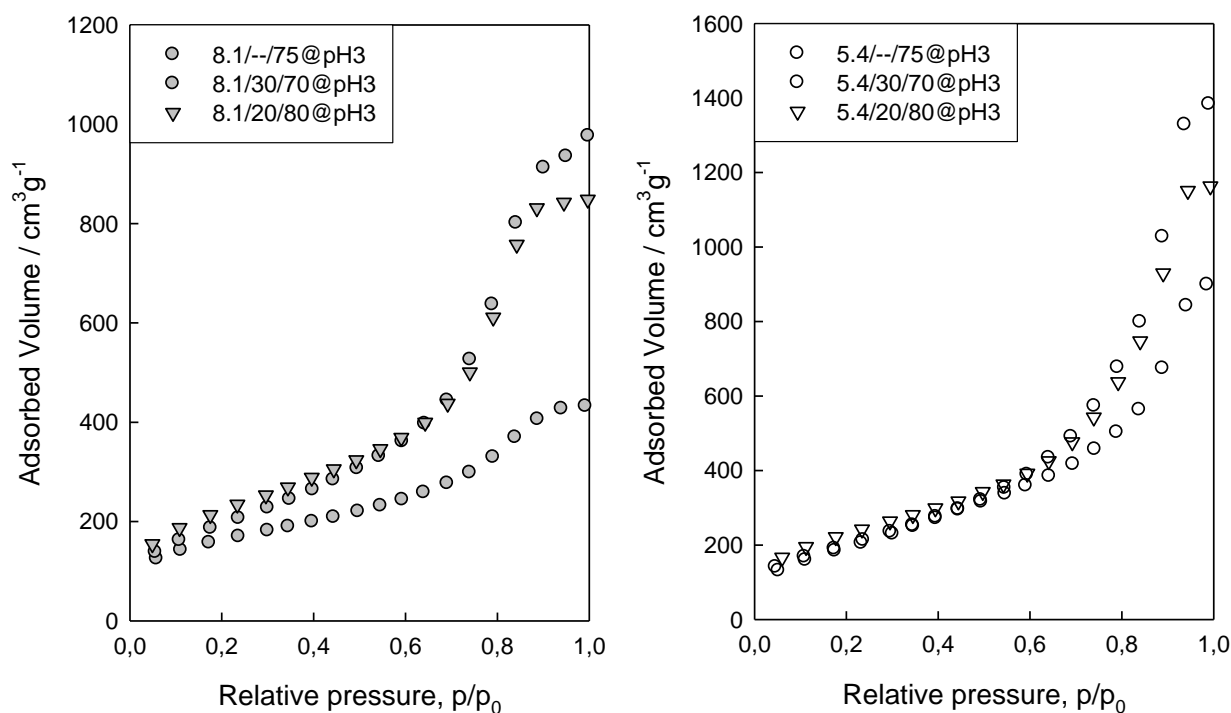
Fig. 4.9. Typical type IV nitrogen sorption isotherms for gels which were prepared at pH 3.

In previously published reports, mesoporous structures from dendrimers were obtained by using alkoxide based carbosilanes.[17,34-36] In this work, the ethoxy/methoxy groups of conventional tetraalkoxysilane precursors were substituted with short chain glycols as they show much better compatibilities with the self-assembly of silica/surfactant mesophases

compared to ethanol or methanol. Whereas in ref. **[17, 34-36]** the main focus was laid on the synthesis and characterization by nitrogen adsorption, electron microscopy, solid state NMR and mechanical properties, we investigated the mesoporous structure by SAXS. With this method, it is possible to obtain quantitative information on the size and the arrangement of the basic structural units as well as the clusters and to concisely investigate the influence of different processing parameters such as the pH value, the precursor concentration or the precursor/P123 ratio.

Recently, periodic mesoporous monolithic materials have been synthesized successfully by substitution of alkoxy groups with short chain glycols. Best known examples are the conversion of modified TEOS or phenylene-bridged silane. With these precursors nanostructured monoliths with a high degree of periodic ordering can be prepared from sols containing a block copolymer templating agent such as P123. Interestingly, the same templating mechanism cannot be investigated for the "dendri-silane". Here, the gel structure shows some regularity in the pore to pore distances, probably due to templating of a micellar block copolymer structure, however, true liquid crystal templating of a lyotropic surfactant phase is not observed. Different reasons can be discussed for this phenomenon. On one hand the systems reacts very sensitively to changes in the polarity of the reaction mixture, often leading to macroscopic demixing. On the other, the reaction rates of hydrolysis and condensation reactions are very high for the "dendri-silane"—perhaps resulting in such a fast polycondensation reaction that no time for the rearrangement of the micellar or LC phase is left. The high density of functional groups on the "dendri-silane" monomer surface makes the latter point highly probable, resulting in a disturbance of the interaction of block copolymer template and network forming species, thereby suppressing cooperative self-assembly or phase separation.

4.5 Conclusion

Monolithic inorganic–organic hybrid materials have been synthesized *via* sol–gel processing of a novel ethylene glycol modified carbosilane dendrimer precursor in aqueous solution with and without the block copolymer Pluronic P123. The resulting material is built up of small units, which form a network of three-dimensionally connected clusters. The clusters themselves consist of a quite dense but not completely filled network of the dendrimers. Its density is described by the fractal dimension and increases with increasing precursor/P123 to water or acid ratio and decreasing precursor concentration. The cluster size is independent of the investigated parameters, *i.e.* precursor/P123 to water or acid ratio, precursor concentration and pH value, whereas the mean pore distance of the templated pores increases with increasing precursor concentration. If the material is prepared without

block copolymer, the morphology does not show any significant dependence on precursor concentration or on the pH value.

4.6 Acknowledgements

4.7 References

[1]   F. Hoffmann, M. Cornelius, J. Morell, M. Fröba, *Angew. Chem., Int. Ed.*, 2006, **45**, 3216

[2]   A. Stein, *Adv. Mater.*, 2003, **15**, 763

[3]   G. J. de AA Soler-Illia, C. Sanchez, B. Lebeau, J. Patarin, *Chem. Rev.*, 2002, **102**, 4093

[4]   U. Schubert, N. Hüsing, A. Lorenz, *Chem. Mater.*, 1995, **7**, 2010

[5]   Y. Lu, R. Ganguli, C. A. Drewien, M. T. Anderson, C. J. Brinker, W. L. Gong, Y. X. Guo, H. Soyez, B. Dunn, M. H. Huang, J. I. Zink, *Nature*, 1997, **389**, 364

[6]   R. A. Caruso, M. Antonietti, *Chem. Mater.*, 2001, **13**, 3272

[7]   C. Liu, C. R. Martin, *Nature*, 1991, **325**, 50

[8]   A. Stein, B. J. Melde, R. C. Schroden, *Adv. Mater.*, 2002, **12**, 1403

[9]   J. H. Fendler, *Chem. Mater.*, 2001, **13**, 3196

[10]   D. A. Loy and K. J. Shea, *Chem. Rev.*, 1995, **95**, 1431; K. J. Shea, D. A. Loy, *Chem. Mater.*, 2001, **13**, 3306

[11]   R. J. P. Corriu, D. Leclercq, *Angew. Chem., Int. Ed. Engl.*, 1996, **35**, 1421

[12]   S. Inagaki, S. Guan, Y. Fukushima, T. Ohsuna, O. Terasaki, *J. Am. Chem. Soc.*, 1999, **121**, 9611

[13]   B. J. Melde, B. T. Holland, C. F. Blanford, A. Stein, *Chem. Mater.*, 1999, **11**, 3302

[14]   T. Asefa, M. J. MacLachlan, N. Coombs, G. A. Ozin, *Nature*, 1999, **402**, 867

[15]   K. G. Sharp, *J. Mater. Chem.*, 2005, **15**, 3812

[16]   K. Landskron, G. A. Ozin, *Science*, 2004, **306**, 1529; K. Landskron, B. D. Hatton, D. D. Perovic, G. A. Ozin, *Science*, 2003, **302**, 266; W. J. Hunks, G. A. Ozin, *Adv. Funct. Mater.*, 2005, **15**, 259

[17]   B. Boury, R. J. P. Corriu, R. Nuñez, *Chem. Mater.*, 1998, **10**, 1795

[18]   K. Nakanishi, *J. Porous Mater.*, 1997, **4**, 67; K. Nakanishi, *Bull. Chem. Soc. Jpn.*, 2006, **79**, 673; K. Nakanishi, K. Kanamori, *J. Mater. Chem.*, 2005, **15**, 3776

[19]   J. H. Smått, S. Schunk, M. Lindén, *Chem. Mater.*, 2003, **15**, 2354

[20]   K. Nakanishi, Y. Kobayashi, T. Amatani, K. Hirao, T. Kodaira, *Chem. Mater.*, 2004, **16**, 3652

[21]   D. Brandhuber, H. Peterlik, N. Hüsing, *Small*, 2006, **2**, 503

[22]   D. Brandhuber, V. Torma, C. Raab, H. Peterlik, A. Kulak, N. Hüsing, *Chem. Mater.*, 2005, **17**, 4262

[23]   D. Brandhuber, H. Peterlik, N. Hüsing, *J. Mater. Chem.*, 2005, **15**, 3896; D. Brandhuber, N. Hüsing, C. K. Raab, V. Torma, H. Peterlik, *J. Mater. Chem.*, 2005, **15**, 1801

[24]   S. Hartmann, D. Brandhuber, N. Hüsing, *Acc. Chem. Res.*, 2007, **40**, 885

[25]   A. Emmerling, R. Petricevic, A. Beck, P. Wang, H. Scheller, J. Fricke, *J. Non-Cryst. Solids*, 1995, **185**, 240

[26]   D. J. Svergun, *Biophys. J.*, 1999, **76**, 2879

[27]   T. Freltoft, J. K. Kjems, S. K. Sinha, *Phys. Rev. B*, 1986, **33**, 269

[28]   J. Teixera, *J. Appl. Crystallogr.*, 1998, **21**, 781

[29]   P. Meakin, *J. Sol–Gel Sci. Technol.*, 1999, **15**, 97

[30]   V. V. Volkov, D. I. Svergun, *J. Appl. Crystallogr.*, 2003, **36**, 860

[31]   D. I. Svergun, *J. Appl. Crystallogr.*, 1992, **25**, 495

[32]   H. Peterlik, P. Fratzl, *Monatsh. Chem.*, 2006, **137**, 529

[33]   P. G. Weidler, G. Degovics, P. Laggner, *J. Colloid Interface Sci.*, 1998, **197**, 1

[34]   K. G. Sharp, *J. Mater. Chem.*, 2005, **15**, 3812

[35]   K. G. Sharp, M. J. Michalczyk, *J. Sol–Gel Sci. Technol.*, 1997, **8**, 541

[36]   K. Landskron, G. A. Ozin, *Science*, 2004, **306**, 1529

5. Sol-gel processing of a glycolated cyclic organosilane and its pyrolysis to silicon oxycarbide monoliths with multiscale porosity and large surface areas

Manuel Weinberger [ab], **Stephan Puchegger** [a], **Thomas Fröschl** [b], **Florence Babonneau** [c], **Herwig Peterlik** [a] **and Nicola Hüsing** [b]

[a]*Faculty of Physics, University of Vienna, Strudlhofgasse 4, A-1090, Vienna, Austria.*

[b]*Inorganic Chemistry I, Ulm University, Albert-Einstein Allee 11, D-89081, Ulm, Germany.*

[c]*Laboratoire de Chimie de la Matière Condensée de Paris, Université Pierre et Marie Curie, Collège de France and CNRS, UMR 7574, F-75005, Paris, France*

Abstract. This study is related to the preparation silicon oxycarbide monoliths comprising a hierarchical network built-up from the pyrolysis of monolithic organosilica gels. A novel glycol-modified 1,3,5-trisilacyclohexane-carbosilane "$[Si(OCH_2CH_2OH)_2CH_2]_3$" was processed via a polymerisation-induced phase separation process in hydrochloric acid solution containing the Pluronic P123 block copolymer and potassium chloride. Highly porous organosilica monoliths with interconnected macropores and a large amount of uniformly sized polymer-templated mesopores within the macroscopic framework domains were obtained after supercritical fluid extraction. The monoliths were pyrolyzed in argon atmosphere at 1000 °C to yield silicon oxycarbide monoliths by maintaining the hierarchical porosity of the organosilica gel. Both, the organosilica gels and the silicon oxycarbide monoliths were thoroughly investigated with standard characterisation techniques. If no salt was used for the preparation of organosilica gels, no distinct macroporous structures were obtained. Instead the gels show the characteristics of typical aerogels with surface areas of 600 – 900 m^2g^{-1} and mesopores with pore sizes > 10 nm. A different behaviour was observed if potassium chloride was added to the sols. Then, the system showed the tendency for a polymerisation-induced phase separation leading to gels exhibiting multiscale porosity. The onset of the phase separation as well as the macropore/domain size thereby strongly depends on the concentration of KCl. These gels with a surface area of about 1071 m^2g^{-1} and pore diameters of about 11.6 nm were subjected to pyrolysis at 1000 °C under inert gas atmosphere. Although volume shrinkages of 54 % were observed, the monoliths maintained their shape and structural features. The surface areas remained rather high with 531 m^2g^{-1} and the diameter of the mesopores dropped to 9.1 nm. From solid state NMR measurements and elemental analysis of the pyrolyzed sample the formation of true silicon oxycarbide monoliths with multiscale porosity and a composition of $SiC_{0.23}O_{1.53} + 0.58 C_{free}$ were proven. From resonant ultrasound spectroscopy measurements the Youngs modulus of 1.42 GPa was obtained.

5.1 Introduction

Silicon oxycarbide (SiCO) materials offer several advantages compared to (organo) silica. The partial substitution of oxygen by carbidic carbon species inside an amorphous silicon dioxide phase improves the materials thermal[1], chemical[2] and mechanical properties[3, 4]. Thus, these materials may be regarded as a modification of amorphous silica, which is suitable for application at extreme conditions. For example, the material overcomes the limited use of silica at high temperatures due the high devitrification tendency, low viscosity together with high creep rates of the latter one. There are several routes for the preparation of SiCO materials. The most common approaches use the pyrolytic conversion of polyorganosiloxanes or polycarbosilanes at temperatures > 800 °C[5-11]. The molecular composition of the ceramic precursor has a direct influence on the final composition of the SiCO material. It was shown that the amount of carbidic carbon within the SiCO seems to be inversely related to the O/Si – ratio of the preceramic species[6, 10] and it is also well known that terminal alkyl groups, such as $Si-CH_3$ give a poor carbidic carbon content[6]. It is thus reasonable to use a carbosilane with low oxygen content and mainly methylene groups, such as 1,1,3,3-tetraethoxy-1,3-disilacyclobutane, $[Si(OEt)_2CH_2]_2$ or its ring-opening polymerization products[7,8]. Indeed, the carbidic carbon content in SiCO obtained from the pyrolysis of the polycondensation products of these precursors is rather high. However, the formation of an additional free carbon phase, which has only a minor influence on many properties of the SiCO and acts more or less as an inert secondary phase[2], is a usual byproduct of the pyrolysis of organosilicas. Detailed studies have shown that carbon is formed during the pyrolysis at 500 – 600 °C via cracking and cyclisation of aliphatic hydrocarbons[12, 13]. The formation of this phase could be inhibited by incorporation of Si-H groups into the material. These groups will, for example, react with terminal methyl groups, which are in the initial material or formed *in-situ*, to give H_2 and a bridging methylene group[14-16].

Due to the drastic pyrolysis conditions it is still a challenging task to maintain the porosity of a SiCO precursor powder or gel. Only recently, some publications demonstrated the successful pyrolysis of mesostructured organosilica powders to SiCO ceramics by maintaining the mesoporous system and thus a large surface area[17, 18]. Interestingly, whether or not a mesostructured SiCO is obtained seems to depend on the type of mesostructure itself. Detailed studies have shown that cubic mesostructures can be maintained very well, while the 2D hexagonally arranged mesopores will not lead to an SiCO but to phase separated SiO_2 and free carbon[18-20]. Until now, the reaction mechanism still remains unclear.

Most of SiCO materials are available only in form of powders or dense glasses. But for several applications, for example in catalysis, monoliths with multiscale porosity would be

much more attractive. In recent years, great efforts were devoted to independently design structural features of materials on several length scales. This goal has already been achieved for silica and organosilica-based materials, for which monolithic materials (of several centimetres in size) comprising a macroporous network and disordered or even periodically ordered mesopores have successfully been prepared by utilizing phase separation phenomena of polymer mixtures, from which the macroscopic morphologies may be frozen by the concomitantly occurring sol-gel transition[21-25, 27-29, 30-34]. Inside the pore walls of the mesopores one also may find micropores smaller than 2 nm. Such materials with multiscale porosity offer an excellent mass transfer through the material due to the macropores combined with large specific surface areas (from the mesopores) and therewith a lot of room for functionalisation making these materials promising candidates for applications in chromatography or catalysis.

In 2003, two groups independently reported the preparation of silica monoliths with macropores and uniformly sized, periodically arranged mesopores within the framework domains. Hüsing et el. were applying tetrakis(2-hydroxyethoxy)silane in a sol-gel process containing the surfactant Pluronic P123[30]. As was shown by SAXS studies[26], the glycol released upon hydrolysis showed a better compatibility with surfactant mesophases from poly(alkylene oxide)-based surfactants than conventional alkoxides and therewith mesostructure formation and phase separation were facilitated. A unique, cellular macroscopic framework was obtained, with highly ordered 2D hexagonally arranged mesopores[27]. In another approach, Lindén et al. demonstrated the preparation of silica monoliths with multimodal hierarchical porosity via a double templating route using poly(ethylene oxide) as well as alkylammonium surfactants[28]. However, the templated mesopores showed a lower degree of periodicity than in P123 systems. A year later Nakanishi et al. prepared the first organic-inorganic hybrid monoliths with a 2D hexagonal mesostructure from 1,2-bis(triethoxysilyl)ethane[29]. Since then various inorganic-organic hybrid materials[30-34] and even transition metal oxides with multiscale porosity became accessible[35, 36].

The application of lyotropic phases as templates as well as the polymerization-induced phase separation process in the synthesis of multiscale materials rely to a large extent on a well-balanced polarity of the sol-gel system. With increasing complexity of e.g. bridged organosilanes this balance is disturbed and the controlled formation of pores on several length scales becomes more difficult.

To our knowledge few publications report the preparation of hierarchically structured ceramic materials. Smarsly and co-workers reported the successful preparation of hierarchically organized silicon carbide monoliths using the nanocasting approach with impregnation of

hierarchically structured silica monoliths with mesophase pitch or furfuryl alcohol and subsequent carbothermal reduction[37]. Another interesting approach was presented by Schwieger et al.[38] They infiltrated Rattan with liquid silicon. The obtained silicon/silicon carbide composite was then coated with zeolites to finally generate a silicon/silicon carbide/zeolite composite ceramic with multiscale porosity[38].

The present contribution demonstrates a new and original route for the preparation of hierarchically structured silicon oxycarbide monoliths and expands the availability of highly porous, thermally stable porous materials. We were able to prepare hierarchically structured organosilica monoliths from a modified 1,3,5-trisilacyclohexane carbosilane precursor. This precursor was chosen due to its low O/Si – ratio and its potential as a sol-gel precursor for mesostructured materials[39]. The monoliths obtained from this precursor were subjected to pyrolysis at elevated temperature under inert gas atmosphere. The monolithic shape together with the structural features of the inorganic-organic hybrid monoliths in macroscopic and mesoscopic dimensions are still retained after the pyrolysis procedure. Solid-state MAS-NMR measurements, elemental analysis and Raman spectroscopy prove the formation of a true silicon oxycarbide ceramic together with a free carbon phase. Additionally, the mechanical properties of the material were determined using the Resonant Ultrasound Spectroscopy.

5.2 Material and Experimental

Chemicals

Chloromethyltrimethoxysilane was received from Wacker AG. Magnesium turnings (> 99%) were purchased from Merck, Pluronic P123 ($Mn = 5800$ $gmol^{-1}$) from Aldrich and potassium chloride (> 99.5%) from Fluka. These chemicals were used without further purification. Ethylene glycol (> 99.5%) was purchased from Merck and dried with sodium. The solvents tetrahydrofuran (THF) and pentane were distilled over sodium hydride dispersion.

Precursor synthesis

All reactions were carried out with dried glassware in argon atmosphere using Schlenck techniques.

Synthesis of 1,3,5-tris[dimethoxysila]cyclohexane [$(MeO)_2SiCH_2]_3$. 45 g (1.85 mol) of magnesium turnings were given into 300 mL of THF. The solution was heated to 50°C. To activate the magnesium a spatula tip of iodine was added. The solution was stirred for 10 min then a solution of 31.5 mL (0.21 mol) of chloromethyltrimethoxysilane in 300 mL of THF

was added slowly via a dropping funnel. The mixture was kept at this temperature for 6 hours and then cooled to room temperature and stirred overnight. The volatiles were removed by distillation and the residues were extracted with 200 mL of pentane and filtered. The pentane was then evaporated to yield 14.49 g of a colorless liquid consisting of a mixture of several silanes[40]. Via distillation 5.01 g (16 mmol) of the desired product were obtained (65-67 °C at 0.1 mbar) in 23 % yield.

^{1}H NMR (400.13 MHz, d_6-benzene, δ): 0.19 (s, 6H, -Si-CH_2-Si-), 3.40 (s, 18H, -Si-O-CH_3); ^{13}C NMR (100.62 MHz, d_6-benzene, δ): -1.68 (-Si-CH$_2$-Si-), 50.23 (-Si-O-CH$_3$); ^{29}Si NMR (79.49 MHz, d_6-benzene, δ): -4.91 ([(MeO$_2$)SiCH$_2$]$_3$)

Transesterification with ethylene glycol. 5.01 g (16 mmol) of 1,3,5-tris(dimethoxysila)cyclohexane were mixed with 16.1 mL (0.29 mol) of ethylene glycol. The mixture was heated to 140 °C under vigorous stirring. Most of the methanol was removed via distillation. Subsequently, remaining methanol and excess of ethylene glycol were removed by vacuum distillation yielding almost quantitatively 7.76 g of a glassy solid (theoretical yield for complete conversion: 7.88 g). The silicon content of the precursor was determined by thermogravimetric analysis to be 16.96 %. This is in accordance with the theoretically expected value for a 1:2 ratio of silicon to glycol of 17.1 %.

Preparation of organosilica monoliths

Pluronic P123 was mixed with 0.1 M aqueous hydrochloric acid solution in mass fractions of 10:90, 15:85, 20:80 and 30:70. In a typical gel synthesis, 0.3 g of potassium chloride was added to 3.26 g of a 20:80 polymer solution (1.5 molL^{-1} KCl referred to the amount of HCl solution). 1g of the glassy precursor was pulverized and given to the solution at ambient conditions under vigorous stirring. The amount of silicon in grams contained within the employed amount of precursor to the amount of Pluronic P123 and HCl solution in grams gives a ratio of 5.2 g / 20 g / 80 g. This results in the identifier 5.2:20:80 if the gel was prepared in the absence of KCl. If the HCl solution is 1.5 M in KCl, the identifier changes to 5.2:20:80@1.5M. The sols were kept in sealed cylindrical sample tubes for gelation and ageing at 40 °C. Opaqueness indicating phase separation occurred within the first hour followed by gelation several minutes thereafter. Gels which were prepared without salt showed no phase separation prior to gelation. For the 5.2:20:80@1.5M composition, wet gels were washed two times with 0.1 M aqueous hydrochloric acid and three times with ethanol within 48 hours to remove most of the salt and polymer. The other samples, whether they were prepared with different amounts of salt or without salt, were washed 5 times with ethanol within 48 hours. All gels were dried via supercritical solvent extraction with CO$_2$ to yield opaque and crack-free monoliths (in the abscence of salt or after washing with

hydrochloric acid solution). Cracks occurred during extraction of Pluronic P123, if ethanol was used as extraction solvent, probably due to osmotic pressure or crystallization of KCl.

Pyrolysis of organosilica monoliths

The 5.2:20:80@1.5M monoliths were put inside a corundum tube which was placed in a tubular furnace. In a flow of argon (50 mLmin^{-1}) the samples were heated within 2.5 hours to 120 °C and kept there for 0.5 h. Within 3 hours the system was heated to 1000 °C. The temperature was kept there for another 2 hours, followed by cooling under argon flow to room temperature. The resulting materials can be described as crack-free and dark brown to black colored monoliths. The ceramic yield is about 83 %.

Characterisation

Nuclear Magnetic Resonance (NMR) spectra of the precursor were acquired on a Bruker Avance DRX 400. Dried deuterated d$_6$-benzene was used as solvent.

The solid state NMR spectroscopy was performed on a Bruker AVANCE 500 spectrometer (11.75 T), except the ^{29}Si single pulse MAS spectrum on the organosilica sample, which was recorded on a Bruker AVANCE 300 spectrometer (7.05 T). 7 mm double resonance MAS probe heads were used with 5 kHz spinning rate. Long recycle delays were used for the ^{29}Si single pulse MAS spectra to account for long T$_1$ relaxation times, and allow for quantitative analysis of the spectra (100 s and 45° pulse for the organosilica sample and 150 s and 90° pulse for the SiCO sample). Contact times of 3 ms and 1 ms were used for ^{29}Si and ^{13}C CP-MAS spectra, respectively. Simulations of the spectra were obtained using the dmfit software**[41]**.

Small angle X-ray scattering measurements of the dried organosilica as well as of the pyrolyzed samples were performed in vacuum using a rotating anode X-ray generator (Nanostar, Bruker AXS) with an X-ray beam monochromatized and collimated from crossed Goebel mirrors. The scattering was collected with a 2D position sensitive detector (Vantec 2000). The samples were prepared as powders and pasted between two Scotch^{TM} tapes. The resulting SAXS patterns were radially averaged to obtain the intensity in dependence of the scattering vector $q = (4\pi/\lambda)sin(\theta)$. 2θ is the scattering angle and λ = 0.1542 nm is the X-ray wavelength. Measurements were carried out at two different distances (11 cm and 107 cm) to cover a wide q range from 0.07 to 15 nm^{-1}.

The morphology of the materials was investigated by scanning electron microscopy (SEM) with a Zeiss DSM 692 operating at 15 kV on gel pieces sputtered with AuPd. The lower

nanometer regime was investigated by transmission electron microscopy (TEM) using a Philips 400T operating at 80 kV.

Nitrogen sorption measurements were performed at 77 K on a Quadrasorb SI (Quantachrome). The samples were outgassed in vacuum at 100°C prior to the measurement. The specific surface areas were determined by application of the Brunauer/Emmett/Teller (BET) equation in the lower relative pressure range (p/p_0 = 0.05 − 0.15), where the isotherm behaves in a linear fashion. The pore size distributions were obtained by Barett/Joyner/Halenda (BJH) analysis of the adsorption branch of the isotherm.

Thermogravimetric measurements were performed on a Netzsch STA 449 C Jupiter. In both cases a heating rate of 10 Kmin^{-1} was used. Raman spectra were recorded on a Labram spectrometer from Horiba Jobin Yvon GmbH with a laser wavelength of 632.82 nm. Elemental analysis was performed on a 2400 CHN Elemental Analyzer from Perkin Elmer. The elastic moduli were determined using a self-developed dynamical measuring equipment based on resonance vibrations (Elastotron 2000) and complete numerical data evaluation (resonant ultrasound spectroscopy)[42].

5.3 Results and Discussion

Highly porous silicon oxycarbide monoliths with multiscale porosity were obtained from pyrolysis of organosilica monoliths which were prepared via sol-gel processing of a glycol-modified trisilacyclohexane-carbosilane in aqueous hydrochloric acid solution in the presence of the surfactant Pluronic P123 and potassium chloride (figure 5.1).
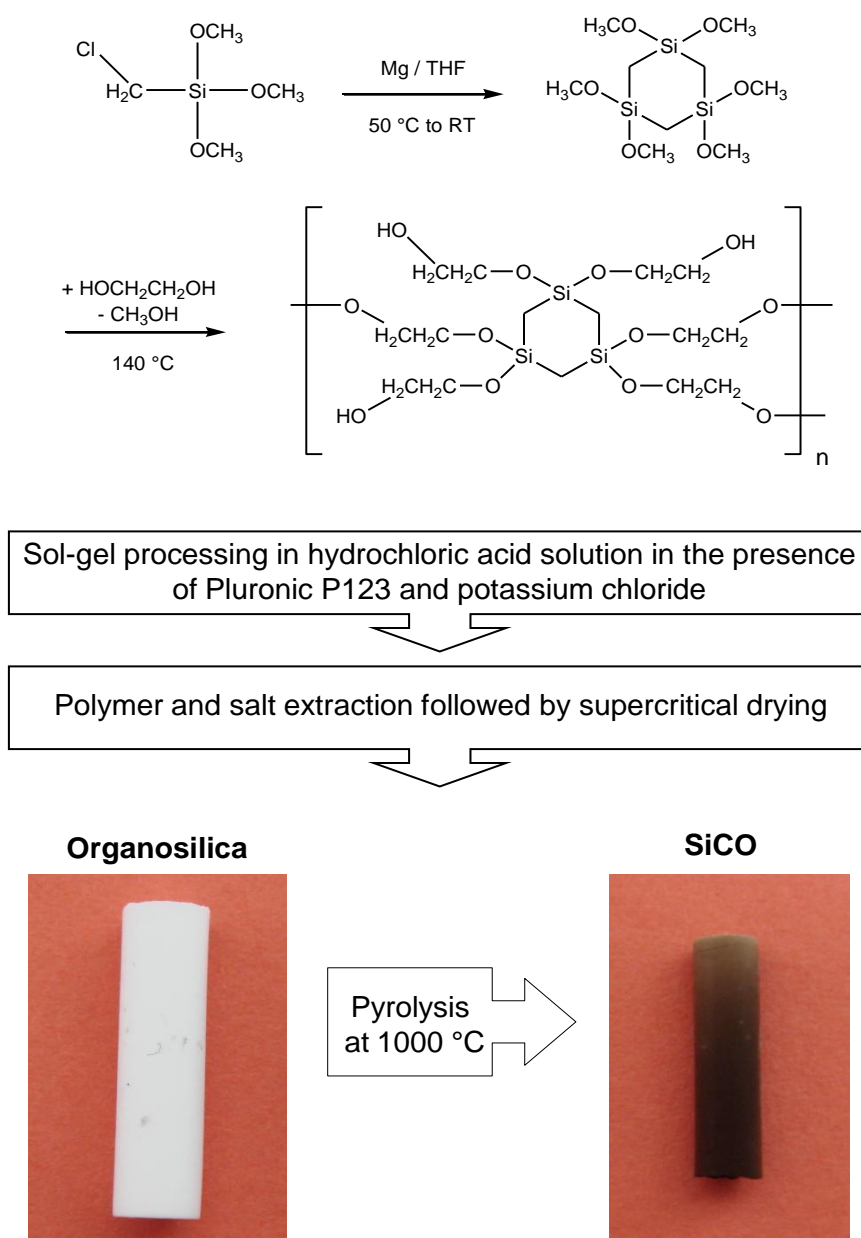
Fig. 5.1. Preparation scheme of silicon oxycarbide monoliths (diameter of the organosilica monolith ca. 5 mm)

Preparation of the organosilica gels

The successful preparation of hierarchically organized silsesquioxane monoliths from a glycol-modified bis-silylated ethane has been shown by our group in previous work**[34]**. Such hierarchically structured materials were obtained for a wide range of synthesis parameters. The morphology of the gel skeleton and the size of the macroscopic framework domains comprising periodically arranged mesopores can be influenced by the P123 / acid ratio. In contrast to these results, increasing the size of the organosilane precursor from a simple ethane-bridged derivative to a dendrimeric structure (4,4,10,10-tetraethoxy-7,7-bis[2-(triethoxysilyl)ethyl]-3,11-dioxa-4,7,10-trisilatridecane) always resulted in highly porous materials consisting of 3-dimensionally connected particles with average diameters of about 10 – 20 nm**[43]** exhibiting no hierarchical built-up of the network. In that case no macroscopic phase separation was observed for the applied wide variation of the synthesis parameters indicating a pronounced difference in the polarity of the mixture, and thus a disturbed tendency for phase separation in addition to a different hydrolysis and condensation kinetics. If one considers the increased surface density of condensable groups of the dendrimer (12 compared to 6), a fast branching of the units could lead to a kinetically frozen state.

First sol-gel experiments with the glycol-modified 1,3,5-tris[dimethoxysila]cyclohexane indicated a chemical behaviour similar to that of the dendrimer. We varied the mass fractions of Pluronic P123 to 0.1 M aqueous hydrochloric acid solution from 10/90 up to 30/70 by keeping the precursor concentration constant. Within this region macroscopic phase separation is easily observed for the glycol-modified bis-silylated ethane precursor. But for the cyclic derivative only translucent wet gels were formed indicating the absence of larger framework domains.

Investigations of the macroscopic morphology by electron microscopy were performed on different gels prepared using a fixed amount of precursor and a variation of the P123 / 0.1 M hydrochloric acid ratio. No significant influence of the sol composition on the final gel structure is observed. Figure 5.2 shows TEM and SEM images for the 5.3:20:80 gel, which are representative images for all these gels. In the nanometer regime, the system consists of 3-dimensionally interconnected particles with a size of about 10 nm (figure 5.2 a). As expected from the translucent appearance of the gels, there is no significant macroscopic porosity seen in the SEM images (figure 5.2 b). Similar gels were obtained even in the absence of the surfactant (gel 4.9:0:80) indicating a sol-gel behaviour similar to the one seen for the carbosilane dendrimer resulting in nanoporous gels.
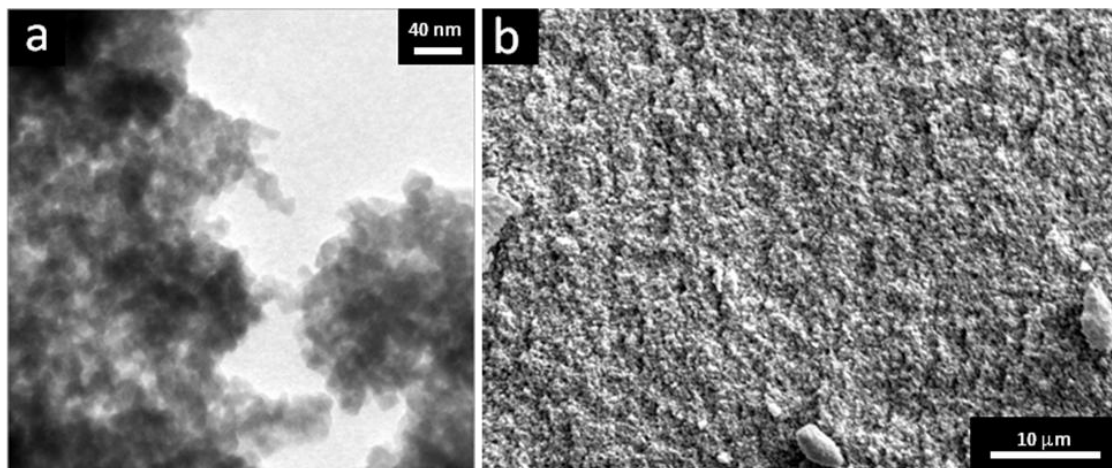
Fig. 5.2. Electron microscopy images of the sample 5.2:20:80; a: TEM; b: SEM
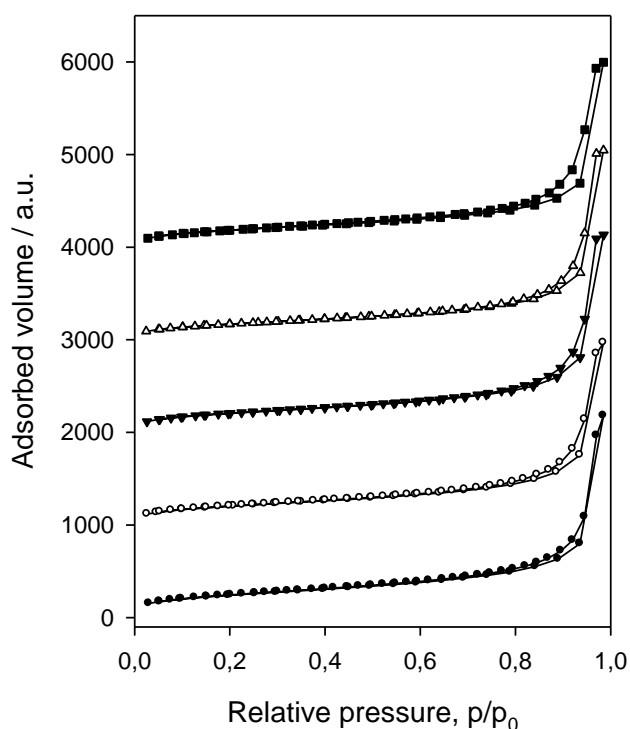
Fig. 5.3. Sorption measurements for nanoporous aerogels; filled circles: 4.9:0:80; open circles: 5.2:10:90; filled triangles: 5.2:15:85; open triangles: 5.2:20:80; filled squares: 5.2:30:70

From nitrogen sorption measurements (see figure 5.3) typical type IV isotherms were obtained with a very late and steep increase of the adsorbed volume indicating large mesopores. BJH analysis of the desorption branch confirms the presence of pores of about 10 nm in diameter with a broad size distribution typical for silica aerogels. A significant microporosity was not observed and the specific surface areas are in the range of 600 – 900 m^2g^{-1}. The exact values are given in table 5.1.

Table 5.1 Structural parameters for the nanoporous aerogels derived from the cyclic glycolated silane

Sample	Nitrogen sorption		SAXS	
	S^{BET} / m^{2}g^{-1}	V^t / cm^{3}g^{-1}	D	ξ / nm
4.9:0:80	868	3.37	2.76	10
5.2:10:90	738	3.04	2.74	7.8
5.2:15:85	750	3.3	2.8	7.06
5.2:20:80	626	3.16	2.82	6.65
5.2:30:70	676	3.09	2.84	6.27

SAXS has proven to be an excellent tool to analyze the nanostructure of such gels in detail. In figure 5.4, the SAXS patterns for various gels obtained from the cyclic silane in the presence of different surfactant concentrations are shown. The formation of a periodic mesostructure with a long range order was not observed, however, a short range order peak at about 10 nm^{-1} is visible. This peak can be assigned to molecular building blocks with a diameter d in real space of approximately 0.6 nm. Towards low q-values, the curves display the typical scattering of silica aerogels[43].

To gain structural information, the SAXS intensities were fitted with a model based on spherical molecular building blocks with the specific diameter obtained from the short-range order peak and building up a network with correlation length ξ and a fractal dimension D as previously successfully used to describe the scattering for gels derived from the carbosilane dendrimer. The correlation length is directly related to the cluster size[44], which is also qualitatively accessible from TEM images. The results are given in table 5.1. The fractal dimension of about D =2.8 and the correlation length of about 10 nm lead to the conclusion that the molecular building blocks build up a three-dimensional network, which is relatively dense on the cluster scale of ten to thirty nanometers. As seen in table 5.1, there is a trend that the size of the clusters decreases with an increasing P123 / hydrochloric acid ratio, similar as in the case of dendrimer-derived organosilicas. A possible explanation is that the polymer blocks the free silanol groups and therewith suppresses further condensation reactions, from which a larger particle size is obtained.
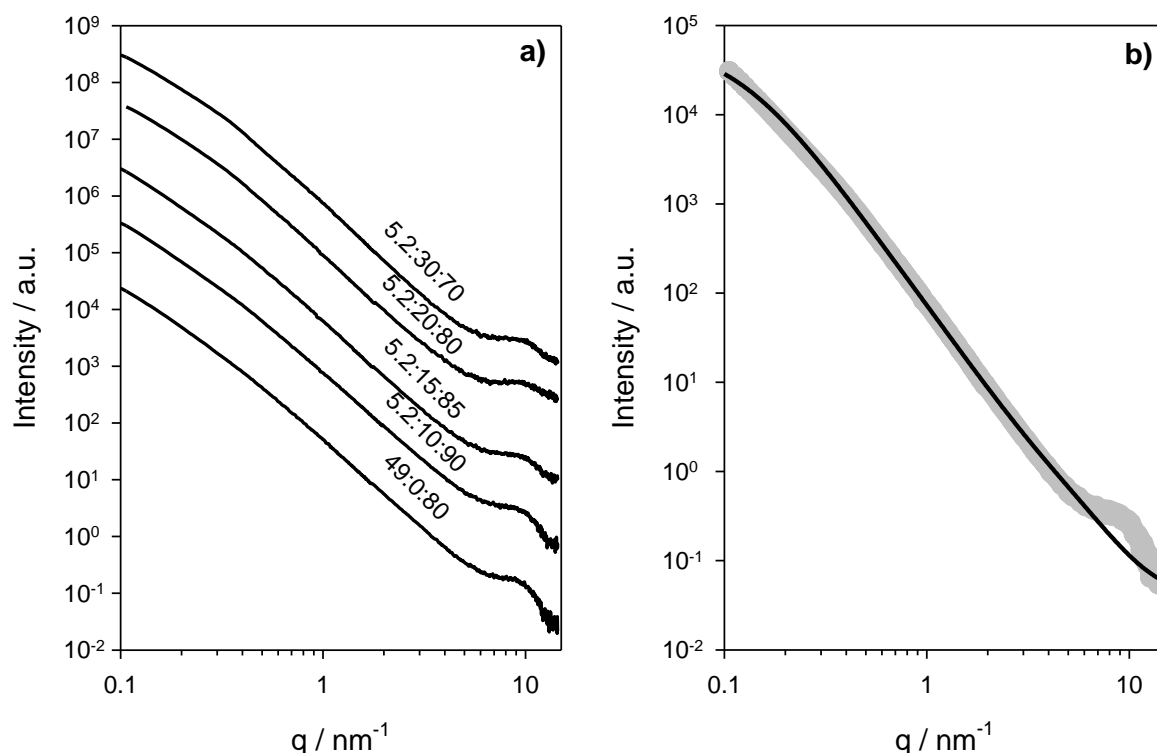
Fig. 5.4. SAXS measurements of the organosilica aerogels (a); exemplary fit of the 5.2:10:90 gel (b)

As can be seen from the above results, it was not possible to induce macroscopic phase separation under the given synthesis parameters by simply processing the glycolated cyclic silane in surfactant/water solutions. This might be due to the change in polarity, but also due to the change in the sol-gel reaction kinetics compared to other glycolated silanes such as the ethylene-bridged derivative or tetrakis(2-hydroxyethyl)orthosilicate. It is known from literature that inorganic salts have a strong influence on phase separation phenomena[45, 46]. The colloidal particles or hybrid micelles formed during the precursor polymerisation will be stabilized due to the positive surface charge given under acidic conditions, however agglomeration of these species is then hindered. Thus, larger aggregates may not be obtained and the tendency for phase separation is decreased. Addition of a salt, such as potassium chloride, will increase the ionic strength and therewith the surface charge may be better shielded. By this, the potential barrier between the colloidal species is decreased and agglomeration is facilitated. In addition, the agglomeration of more hydrophobic organosilica oligomers with surfactant micelles should also be facilitated due to the dehydration of the poly(ethylene oxide) moieties of the outer shell of the micelles by the Cl$^-$ anions[47]. If these assumptions are correct, it should be possible to control the phase separation and with it the macroscopic morphology of the final gel network as well as the formation of mesostructures by addition of different amounts of potassium chloride (0 M up to

2 M aqueous solutions) to the 5.2:20:80 sol. A first promising indication of a phase separation was observed as all gels turned opaque prior to gelation. The onset of the change in transparency of the gel depends strongly on the concentration of KCl with larger amounts resulting in faster change. Up to a concentration of 1.5 M aqueous KCl, homogeneous wet gels are formed, a concentration of 2 M will lead to precipitation, most probably due to the formation of very large aggregates. After gelation and ageing, the gels were washed with ethanol and finally dried supercritically. The powder was also washed with ethanol, but dried at ambient conditions.
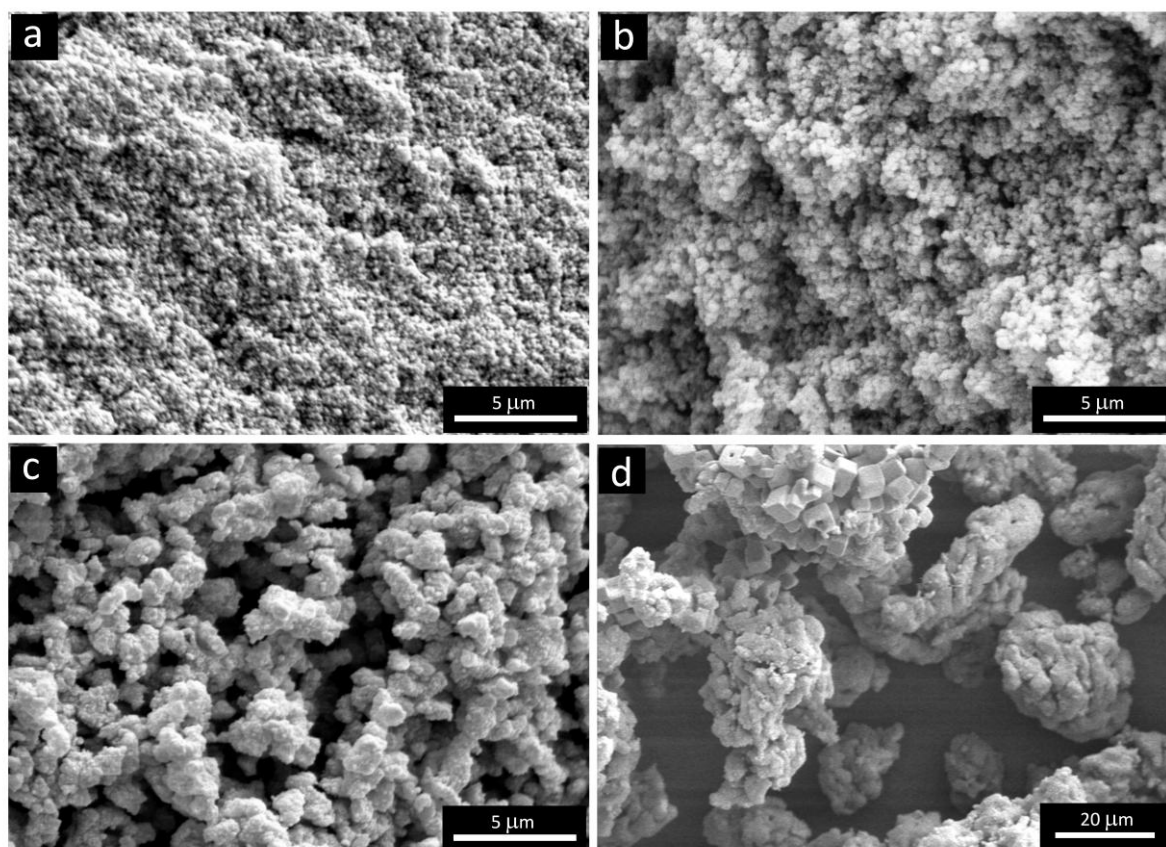
Fig. 5.5. SEM images for gels which were prepared with different amounts of salt: a) 0 M; b) 1.25 M; c) 1.5 M; d) 2M; note the different scalebar of 20 μm and the cubic KCl crystals for d) after washing with ethanol

Since KCl is not soluble in ethanol, an osmotic pressure or the crystallization of KCl will lead to a cracking of the monoliths. Washing with water or hydrochloric acid solution allows to maintain the monolithic shape. In figure 5.5, SEM images of the macroscopic frameworks are shown. The increase of the domain size with increasing amount of salt is clearly seen. From 0 M up to 1.25 M the differences are rather small (about 250 nm), but with larger amounts of KCl the size of the particles increases drastically to about 900 nm. This can be explained by a coarsening during the intermediate stage of the spinodal decomposition**[23]**. The sooner the phase separation occurs compared to the gelation of the system, the larger the domains

may grow. For 1.5 M we obtained a gel showing the co-continuous characteristics of a spinodally phase separated system. Remaining KCl crystals are clearly visible in figure 5.5 d), however, all samples still contain a significant amount of the salt.

Figure 5.6 a) shows a sample washed with hydrochloric acid prior to the drying process, thus allowing for a direct comparison with the gels from washing with ethanol (figure 5.5 c)). The gels display a similar framework domain size, but the gel washed with ethanol shows a coarser structure probably due to remaining KCl. In the following we will concentrate the discussion for the pyrolyzed samples on the structural and chemical characterisation of gels prepared with 1.5 M KCl and subsequently washed with aqueous hydrochloric acid, since here KCl was removed completely as was shown by XRD and XPS measurements of the pyrolyzed samples.
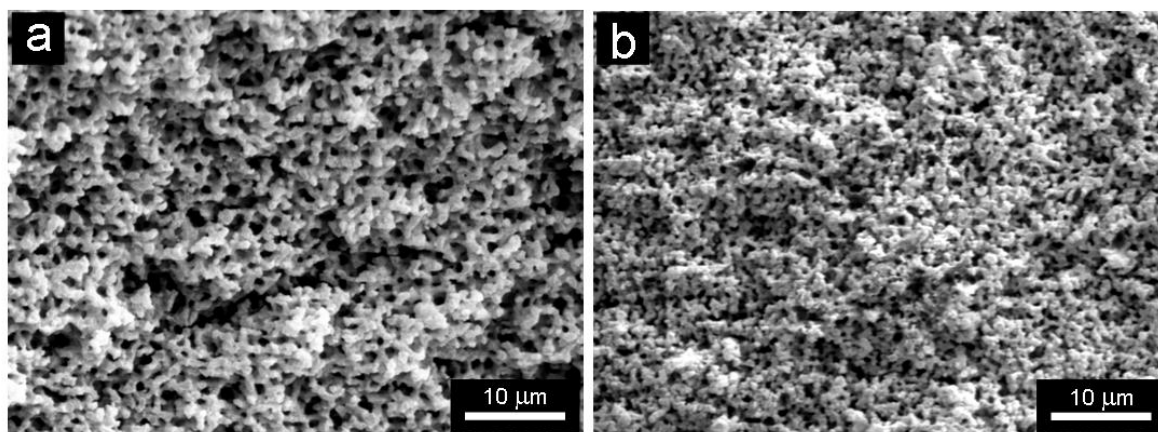
Fig. 5.6. Comparison of SEM images for a) organosilica 5.2:20:80@1.5M and b) corresponding silicon oxycarbide

With similar sol-gel-processing conditions we have previously demonstrated that the surfactant Pluronic P123 is not only able to induce a macroscopic phase separation but also acts as a structure directing agent to give highly ordered mesostructures. Template removal then gives access to the corresponding mesopores. It was shown that the mesostructure formation is directly connected to the phase separation and the mechanism of this process may be understood as a nucleation of hybrid micelles and the growth of the nucleation sites by consumption of other hybrid micelles, for example to 2D hexagonally arranged mesopores[34]. In the case of the glycolated cyclic silane, TEM investigations of the salt effect on the mesostructure have shown that no distinct periodic mesostructures are obtained for salt concentrations lower than 1 M, but for larger salt concentrations we observed the formation of weakly ordered MSU-like mesostructures[48]. In the TEM images micelle templated mesopores are clearly seen (figure 5.7 a).
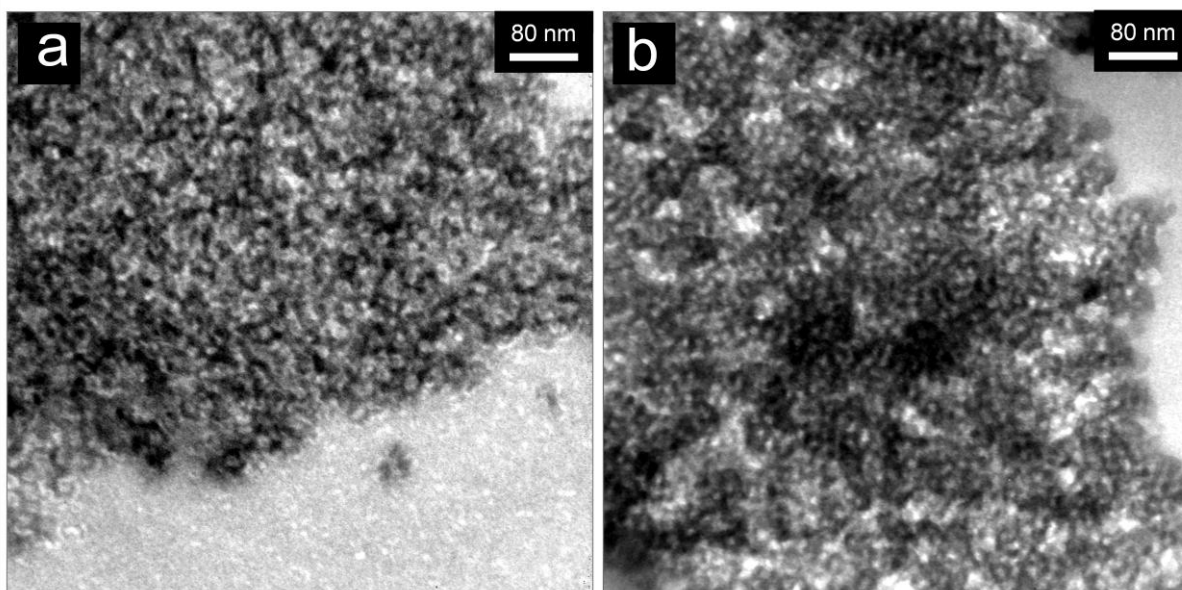
Fig. 5.7. Comparison of TEM images for a) organosilica 5.2:20:80@1.5M and b) corresponding silicon oxycarbide
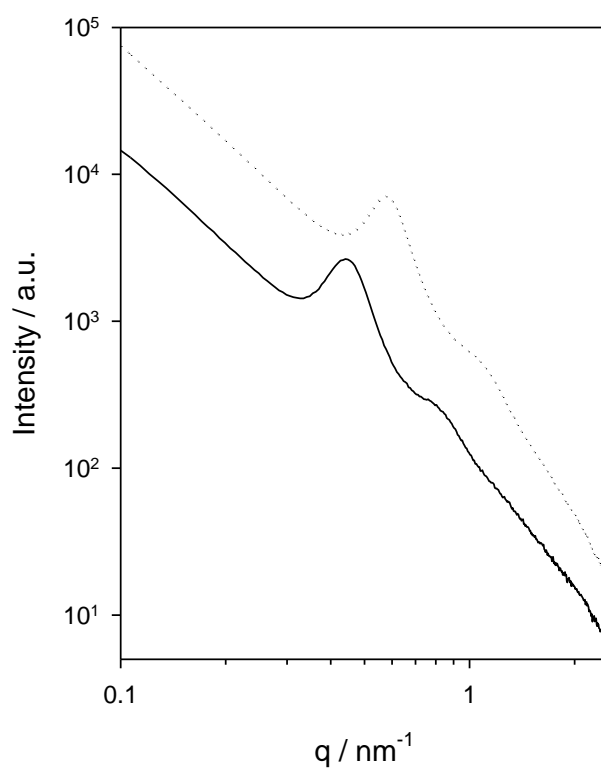
Fig. 5.8. SAXS measurements for the organosilica 5.2:20:80@1.5M (continuous line) and SiCO (dotted line) material

SAXS measurements (continuous line in figure 5.8) show an intense but broad peak at low q = 0.44 nm^{-1} (corresponding d-spacing d_{max} = 14.3 nm) and a shoulder at larger q = 0.6 nm^{-1} (corresponding d-spacing = 10.5 nm). Such scattering patterns are usually obtained for wormhole-like mesostructures[49], thus confirming the results from electron microscopy. Although the hybrid micelles give weakly ordered nanostructures we assume a mechanism for the mesostructure formation that is induced by a preceding phase separation leading to a metastable state and thus favouring nucleation and growth routes. A reason for the absence of nanostructures with a mesoscopic ordering in the case of the gels prepared with lower salt concentrations could be the late onset of the macroscopic phase separation. Thereby the sol-gel transition may proceed, leading to highly branched species showing a lower flexibility and thus no tendency for nucleation and growth.

Nitrogen sorption measurements for the organosilica gel show type IV isotherms with a H2 type hysteresis loop typical for periodic mesoporous materials (see curve with filled circles in figure 5.9 on the left). The BET surface area is rather large S^{BET} = 1071 m^{2}g^{-1}. There is as well a significant amount of micropores present as is seen from the lower relative pressure range. Moreover, desorption seems not to be greatly delayed indicating an open mesoporous system. The material exhibits an extraordinarily large total pore volume of 2 cm^{3}g^{-1}. Compared to the gels obtained from the glycol-modified ethane-bridged silane system[34] with pore diameters of 4.8 nm to 5.5 nm, the mesopores are very large (maximum in pore size distribution: D^{BJH} = 11.6 nm) as is seen from the late and steep increase of the adsorption branch (capillary condensation) and the corresponding BJH analysis (see curve with filled circles in figure 5.9 on the right). The salt seems to have a significant influence on the pore size. The chloride anions could lead to a dehydration of the outer shell of the micelles, thus the hydrophilicity of the poly(ethylene oxide) moieties is decreased and the outer shell is less accessible to species such as the oligomeric silane precursor molecules. This could probably lead to a thinner hydrophobic shell and therewith to an enlarged hydrophobic core and thus to larger mesopores. Regarding the phase separation another explanation is that the newly formed phase rich in hybrid micelles could favour larger micelle radii due its polarity. However, more detailed studies in the future have to be applied for a better understanding of this pore expanding phenomenon.
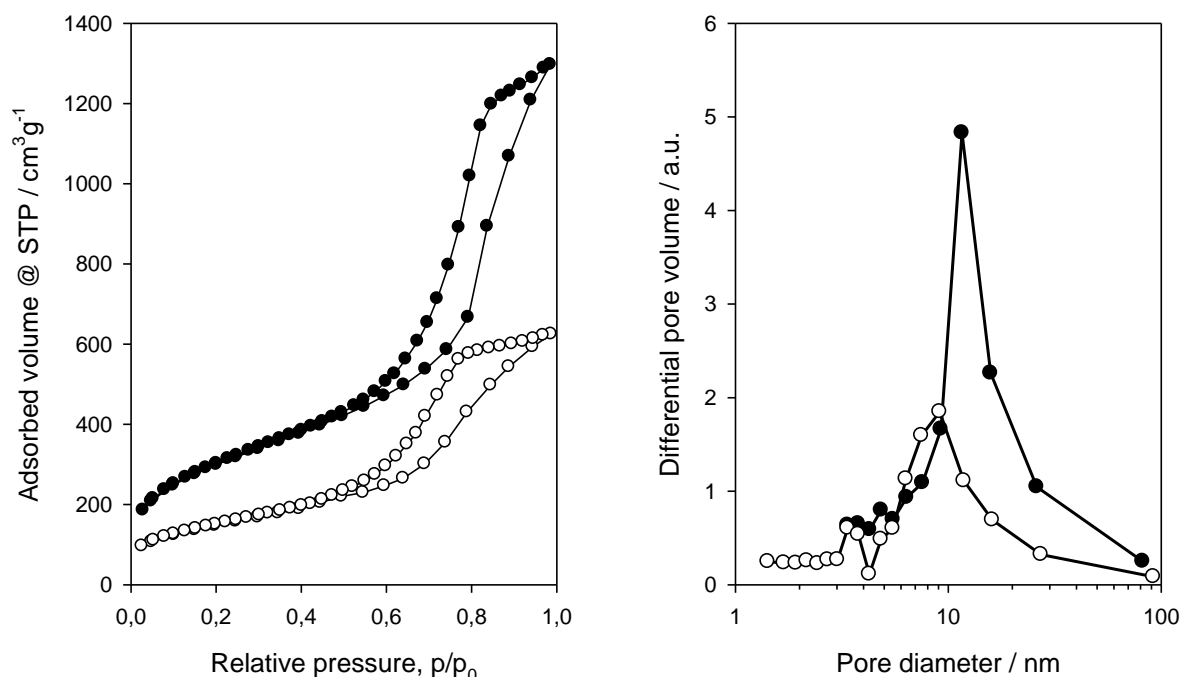
Fig. 5.9. Comparison of nitrogen sorption data: Sorption isotherms (left) and pore size distributions (right); filled circles: organosilica; open circles SiCO

To get information on the chemical composition of the materials solid state ^{29}Si and ^{13}C MAS-NMR measurements were performed (figure 5.10). Interrante and co-workers published an investigation of the polycondensation products of the 1,3-bis[dimethoxysila]cyclobutane carbosilane by NMR measurements[7]. The silane was condensed at ambient conditions and then either vacuum-dried at 50 °C or dried at ambient pressure at 160 °C. The vacuum-dried product showed a D-unit peak as expected for the four membered ring, but the other material contained a significant amount of cleaved Si-C-bonds leading to the formation of T-units. Although the six-membered ring should show a minimum of ring tension, it is of interest if such phenomena are also observable in the present case since the precursor was transalkoxylated at around 140 °C. In figure 5.10 b) the ^{29}Si NMR spectrum of the polymer, salt extracted and dried organosilica material is shown. There are three peaks at -8.15 (weak shoulder), -17.04 and -23.60 ppm, which can be assigned to the D-units D_0 $(CH_2)_2Si(OH)_2$, D_1 $(CH_2)_2Si(OSi)(OH)$ and D_2 $(CH_2)_2Si(OSi)_2$ with the following relative intensities of 7%, 48% and 45%, respectively[39]. In the ^{13}C NMR spectrum in figure 5.8 a) we observed a peak at 7.40 ppm which is characteristic for bridging methylene groups[39]. However, two peaks at 16.3 and 57.8 ppm indicate the presence of ethoxy groups, probably formed during the washing procedure with ethanol and some smaller signals can be assigned to residual P123 block copolymer (70.74 ppm; -OCH_2CH_2O-), to the methyl groups of residual methoxy groups (47.49 ppm) and most probably to residual glycol groups (63.42 ppm). Both measurements

indicate that the molecular structure of the precursor is maintained upon transesterification with ethylene glycol and the subsequent acid-catalyzed condensation reaction.
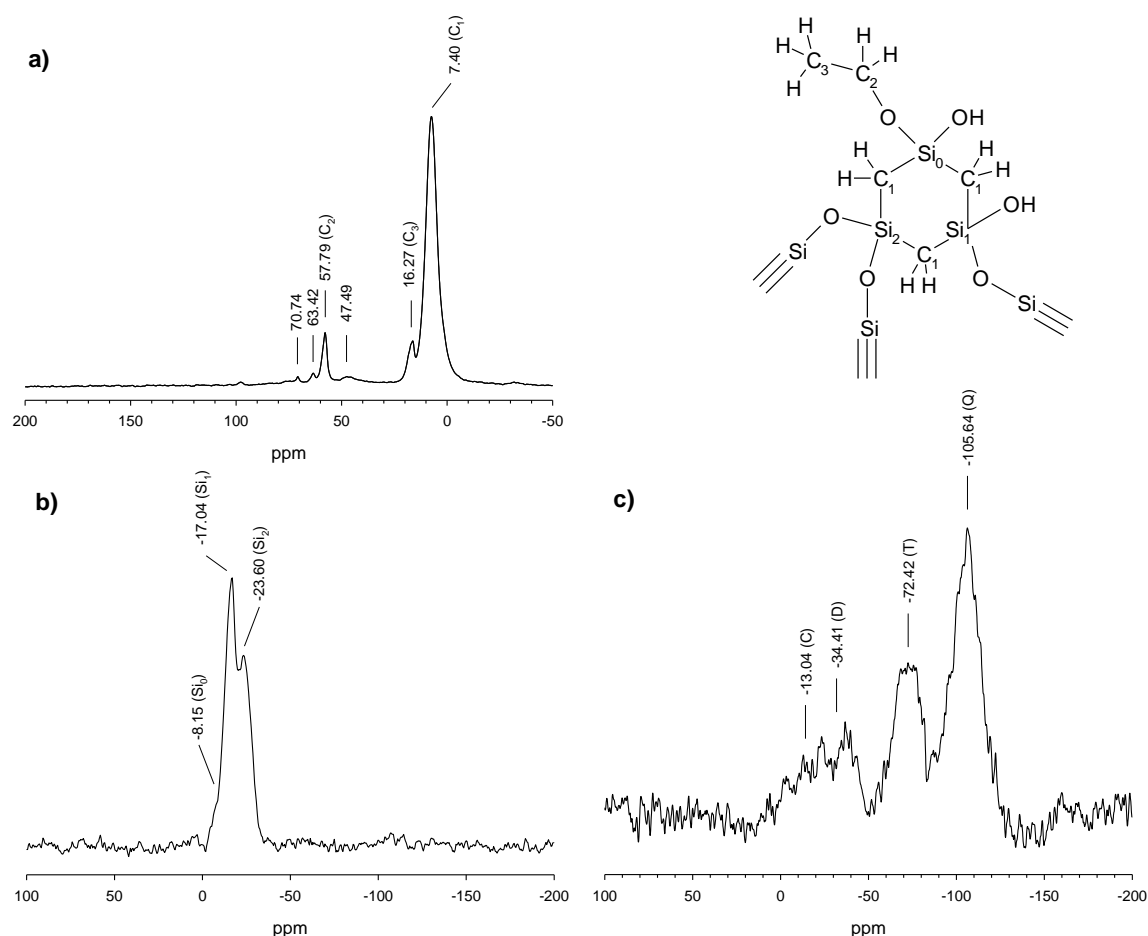
Fig. 5.10. a) ^{13}C-NMR spectra of Organosilica and comparison of ^{29}Si-NMR spectra for b) organosilica and c) corresponding silicon oxycarbide

We could show that it is possible to prepare hierarchically organized inorganic-organic hybrid monoliths comprising a macrocellular network and uniform mesopores as well as a large micropore volume from a glycolated cyclic silane by the addition of salt to the silane/water/ surfactant precursor mixture. Such co-continuous network structures combined with a large meso/micropore volume and high specific surface areas are desirable for many applications. To improve the thermal and mechanical strength of these hybrid materials the monoliths obtained from 1.5 M KCl solution were pyrolyzed to yield silicon oxycarbide ceramic materials.

Pyrolysis of organosilicas

The thermal treatment of the porous organosilica monoliths was investigated in detail via thermogravimetric analysis from room temperature up to 1400 °C in nitrogen atmosphere (figure 5.11). In the temperature range from RT up to 200 °C, a weight loss of about 7.2 % is observed, which can be assigned to the desorption of water. The following weight losses up to 600 °C of about 5.9 % occur most probably due to the thermal decomposition of remaining P123, further condensation reactions releasing water and ethanol and minor decomposition reactions of the framework. The rearrangement of the Si-O and Si-C bonds starts at temperatures higher than 600 °C with a final weight loss of 4 %. The sum of the weight losses is 17.2 %, resulting in a ceramic yield of 82,8 %, which is in good agreement with the ceramic yield of the pyrolyzed monoliths. The residue of the thermally treated material was black probably due to the formation of a free carbon phase. Wide angle XRD measurement showed no SiC peaks indicating that no carbothermal reduction occurred.
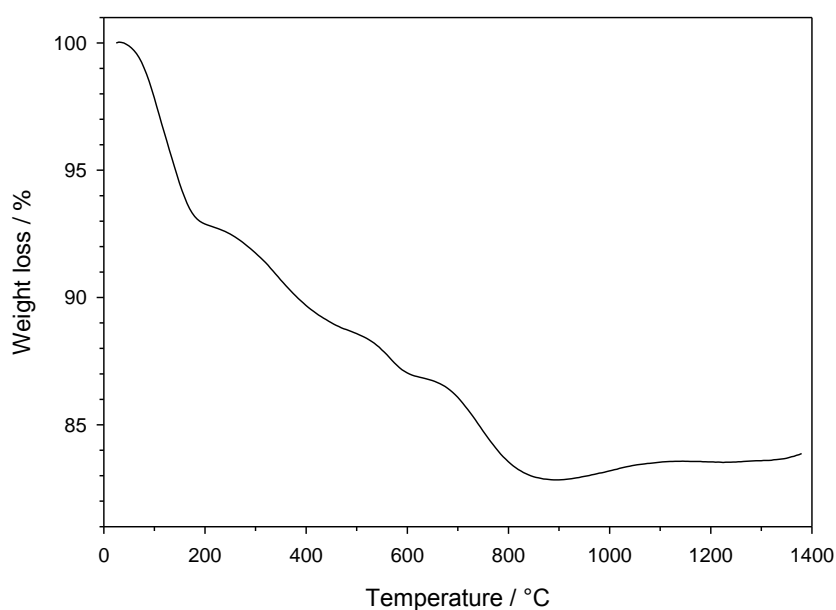
Fig. 5.11. Thermogravimetric measurement of the pyrolysis of the organosilica

Due to the stability of the material at temperatures above 1000 °C as seen from thermogravimetric measurements, the material should also withstand a longer thermal treatment of 2 h. This is necessary for a complete conversion of the organosilica monoliths into SiCO and for a further stabilization of the network. Indeed, the monolithic shape could be maintained (see figure 5.1) but an average volume-shrinkage of about 54 % is observed. However, from a structural point of view a quite unique behaviour is observed with a very homogeneous shrinkage of the whole network. SEM and TEM images in figures 5.6 b and 5.7 b show that the domain sizes as well as the macropores shrink by approximately 50 %

but the filigree interconnected pore structure is maintained. The bicontinuous framework obviously has the capability to withstand the stress occurring during the decomposition and reorganisation of the molecular moieties of the organosilica material. In addition, the mesostructure within the macroscopic framework domains has shrunk, but maintained, as can be clearly seen in the TEM images as well as in the SAXS investigations (see dotted line in figure 5.8). The d-spacing for the intense peak at low q is shifted to larger q = 0.57 nm^{-1} (corresponding d-spacing = 11 nm). From sorption measurements (see curve with open circles in fig. 5.6 on the left) we observe a drop of the surface area from 1071 m^{2}g^{-1} for the initial organosilica to 531 m^{2}g^{-1} for the SiCO what would still be rather high if a true silicon oxycarbide was obtained. There is still a huge mesopore volume present (approximately 50 %) what is seen from capillary condensation at large relative pressures and the corresponding total pore volume was estimated to be 0.97 cm^{3}g^{-1}. The hysteresis indicates that the mesopore system is still well accessible. The maximum in the pore diameter distribution is shifted to smaller values (from 11.6 nm to 9.1 nm) and due to the drastic reaction conditions the micropores are lost. The comparison of the structural parameters of the 5.2:20:80@1.5M gel and the pyrolyzed sample is given in table 5.2.

Table 5.2 Structural parameters for the 5.2:20:80@1.5M gel and the SiCO

Sample	Nitrogen sorption			SAXS
	S^{BET} / m^{2}g^{-1}	V^t / cm^{3}g^{-1}	D^{BJH} / nm	d_{max} / nm
5.2:20:80@1.5M	1071	2	11.6	14.3
SiCO	531	0.97	9.1	11

A silicon oxycarbide is a silicon dioxide matrix in which divalent oxygen is partly substituted by tetravalent carbidic carbon. ^{29}Si MAS-NMR measurements are the most straightforward method to deduce if a true silicon oxycarbide material was formed and to describe the composition of the material quantitatively. In the ^{29}Si MAS-NMR spectrum we should see a distribution of SiC$_x$O$_{4-x}$-units with x = 0 (Q-units), x = 1 (T-units), x = 2 (D-units), x = 3 (M-units) and x = 4 (C-units). And indeed, the pyrolysis procedure applied is leading to a rearrangement and redistribution of the carbon and silicon species and we observe several peaks in the NMR spectrum (figure 5.10 c), which can be attributed to the above mentioned species. In our case we obtained 4 peaks at -105.64 (Q-units, 48.3 %), -72.42 (T-units, 29 %), -34.41 (D-units, 13.4 %) and -13.04 (C-units, 9.3 %). Since the formation of the SiCO is accompanied by the formation of a free carbon phase, as indicated by the occurrence of Q-units in the ^{29}Si NMR spectrum and the black colour of the monoliths, quantitative information of the amount of this free carbon phase is necessary in order to give a complete quantitative description. With Raman spectroscopy the formation of the free carbon phase could be evidenced by the occurrence of two bands, one at 1334.1 cm^{-1} characteristic for disordered

carbons such as glassy carbon and one band at 1597.2 cm^{-1} which is probably observed due to the occurrence of tiny graphene layers with many edge carbons[50]. C/H/N elemental analysis was performed to estimate the whole amount of carbon within the pyrolyzed sample. Therewith it was possible to estimate the following formula, $SiC_{0.23}O_{1.53}$ + 0.58 C_{free} from which we may conclude the formation of a material rather rich in carbidic carbon if we compare our results to the mesostructured SiCOs of Pauletti et al. ($SiC_{0.17}O_{1.66}$ + 0.45 C_{free})[17] or Toury et al. ($SiC_{0.11}O_{1.78}$ + 0.66 C_{free})[18].

The elastic properties of the hierarchically organized SiCO cylinders were determined in a dynamical resonance system. The cylindrical sample is clamped carefully between two piezoelectric transducers, one to excite the sample and the other to detect the answer (i.e. the resonance frequencies). Both transducers are connected to a network analyzer, which is able to sweep a wide frequency range with an extremely high signal to noise ratio. Nevertheless, the damping of the organosilica monoliths was so high that no resonance frequencies could be determined, whereas from the SiCO cylinder, clear resonances were obtained. The material with a density of about 0.4 gcm^{-3} has a Youngs modulus of 1.42 GPa and a shear modulus of 0.54 GPa. This is significantly higher than the value of silica monoliths (70 MPa) with a similar hierarchical structure and a density of 0.21 gcm^{-3} or the value of 100 MPa of silica aerogels with a comparable density[51]. Though the density of the SiCO is slightly higher, the Youngs modulus exceeds the one of comparable silica materials by more than one order of magnitude. This is attributed to the higher binding energy of SiC bonds in comparison to silica bonds and is of the same size than the ratio of dense SiC ceramics in relation to dense silica glasses. More detailed studies of the influence of processing parameters and the amount of incorporated carbidic carbon on the elastic properties will be subject for future research.

There are only a few publications which investigate and discuss the possibility of the pyrolytic conversion of mesostructured organosilicas into the corresponding silicon oxycarbides by maintaining the mesostructural features. Toury et al. and Pauletti et al. have demonstrated the successful SiCO preparation from ethylene-bridged and mesostructured silsesquioxanes obtained from sol-gel processing of the corresponding bis-silylated alkoxysilane[17, 18]. However, the amount of carbidic carbon within these powder materials is low compared to many other SiCO materials. There is also a restriction to cubic mesostructures since it seems not possible to obtain SiCO from 2D hexagonally arranged cylindrical mesopores. The approach presented here to prepare (organo)silica monoliths with multiscale porosity from a cyclic carbosilane with bridging methylene-groups and thus to reduce the O/Si – ratio, resulting in a material richer in carbidic carbon, was a quite challenging task. However, the preparation of the desired material was successfully achieved and the pyrolytic conversion

gave a material much richer in carbidic carbon and even the structural features could be maintained at all length scales. Thus, a first step towards the preparation of a new class of monolithic materials with multiscale porosity and improved thermal and mechanical properties is made.

5.4 Conclusions

The carbosilane 1,3,5-tris[dimethoxysila]cyclohexane was synthesized by a Grignard reaction of chloromethyltrimethoxysilane. The obtained cyclic precursor was successfully modified with ethylene glycol without Si-C-bond cleavage to yield a highly water-soluble sol-gel precursor. Organosilica gels were prepared via sol-gel processing in hydrochloric acid solution in the presence of the block copolymer Pluronic P123. After polymer extraction and supercritical drying highly porous organosilica monoliths were obtained. Within a wide range of synthesis parameters no distinct phase separation phenomena and mesostructure formation were observed. However, upon addition of potassium chloride macroscopic phase separation was successfully induced. Depending on the amount of KCl the onset of the phase separation and the morphology of the macroscopic framework domains could be deliberately controlled. If the concentration of KCl was chosen to be 1.5 M a co-continuous framework structure was achived with a huge amount of wormhole-like mesopores as well as micropores within the framework domains and thus this material shows a huge surface area of 1071 m^2g^{-1}. Both ^{13}C and ^{29}Si MAS solid state NMR measurements showed that the gel truly consists of the polycondensed cyclic precursor species and no Si-C-bond cleavage occurred during precursor and gel synthesis.

This organosilica material was subsequently pyrolyzed at 1000 °C under inert gas atmosphere. The appearance changed from white to black and volume shrinkages of 54 % were observed, but the monolithic shape could be maintained. Detailed electron microscopy investigations revealed that the framework and macropores as well as the mesopores shrunk homogeneously as well. The surface area decreased to 531 m^2g^{-1}. From Raman spectroscopy the formation of a free carbon phase was observed. To elucidate if a true silicon oxycarbide material was formed, quantitative ^{29}Si MAS solid state NMR measurements were performed. The best fit of the spectra with Gaussian functions gave 4 peaks which can be assigned to a distribution of Q-, T-, D- and C-units of a silicon oxycarbide. Together with the determination of the whole carbon content by elemental analysis the following formula can be estimated to be $SiC_{0.23}O_{1.53}$ + 0.58 C_{free}. First Resonant Ultrasound Spectroscopy measurements revealed a Youngs modulus of 1.42 GPa which is significantly higher than that of similar silica systems.

5.5 Acknowledgements

5.6 References

[1]   T. Rouxel, G. Massouras, G-D. Sorarù, *J. Sol-Gel Sci. Tech.*, **1999**, 14, 87

[2]   G-D. Sorarù, E. Dallapiccola, G. D'Andrea, *J. Am. Ceram. Soc.*, **1996**, 79, 2074

[3]   G-D. Sorarù, S. Modena, E. Guadagnino, P. Colombo, J. Egan, C. Pantano, *J. Am. Ceram. Soc.*, **2002**, 85, 1529

[4]   C. Moysan, R. Riedel, R. Harshe, T. Rouxel, F. Augereau, *J. Eur. Ceram. Soc.*, **2002**, 22, 2389

[5]   F. Babonneau, K. Thorne, J.D. Mackenzie, *Chem. Mater.*, **1989**, 1, 554

[6]   F. Babonneau, L. Bois, C-Y. Yang, L.V. Interrante, *Chem. Mater.*, **1994**, 6, 51

[7]   Q. Liu, W. Shi, F. Babonneau, L.V. Interrante, *Chem. Mater.*,**1997**, 9, 2434

[8]   G.D. Sorarù, Q. Liu, L.V. Interrante, T. Apple, *Chem. Mater.*, **1998**, 10, 4047

[9]   R. J. P. Corriu, D. Leclercq, P. H. Mutin, A. Vioux, *J. Sol-Gel Sci. Techn.*, **1997**, 8, 327

[10]   R.J.P. Corriu, D. Leclerq, P.H. Mutin, A. Vioux., *J. Mater. Sci.*, **1995**, 30, 2313

[11]   E. Kockrick, R. Frind, M. Rose, U. Petasch, W. Böhlmann, D. Geiger, M. Herrmann, S. Kaskel, *J. Mater. Chem.,* **2009**, 19, 1543

[12]   S. Trassl, G. Motz, E. Rössler, G. Ziegler, *J. Am. Ceram. Soc.*, **2002**, 85, 239

[13]   S. Trassl, H.-J. Kleebe, H. Störmer, G. Motz, E. Rössler, G. Ziegler, *J. Am. Ceram. Soc.*, **2002**, 85, 1268

[14]   F. Babonneau, G.D. Sorarù, G. D'Andrea, S. Dirè, L. Bois, *Mater. Res. Soc. Symp. Proc.*, **1992**, 271, 789

[15]   G.D. Sorarù, G. D'Andrea, R. Campostrini, F. Babonneau, G. Mariotto, *J. Am. Ceram. Soc.*, **1995**, 78, 379

[16]   A. K. Singh, C. G. Pantano, Mater. Res. Soc. Symp. Proc., 1992, 271, 795

[17]   A. Pauletti, S. Handjani, C. Fernandez-Martin, C. Gervais, F. Babonneau, *J. Ceram. Soc. Jpn.*, **2008**, 116, 449

[18]   B. Toury, R. Blum, V. Goletto, F. Babonneau, *J. Sol-Gel Sci. Techn.*, **2005**, 33, 99

[19]   B. Toury, F. Babonneau, *J. Eur. Ceram. Soc.*, **2005**, 25, 265

[20]   S. Masse, G. Laurent, F. Babonneau, *J. Non-Cryst. Sol.*, **2007**, 353, 1109

[21]   K. Nakanishi, N. Soga, *J. Am. Ceram. Soc.*, **1991**, 74, 2518

[22]   K. Nakanishi, H. Komura, R. Takahashi, N, Soga, *Bull. Chem. Soc. Jpn.*, 1994, **67**, 1327

[23]   K. Nakanishi, *J. Porous Mater.*, **1997**, 4, 67

[24]   K. Nakanishi, K. Kanamori, *J. Mater. Chem.*, **2005**, 15, 3776

[25]   K. Nakanishi, *Bull. Chem. Soc. Jpn.*, **2006**, 79, 673

[26]   R. Ivanova, B. Lindman, P. Alexandridis, Langmuir, 2000, 16, 3660

[27]   N. Hüsing, C. Raab, V. Torma, A. Roig, H. Peterlik, *Chem. Mater.* **2003**, 15, 2690

[28]   J-H. Smått, S. Schunk, M. Lindén, *Chem. Mater.*, **2003**, 15, 2354

[29]   K. Nakanishi, Y. Kobayashi, T. Amatani, K. Hirao, T. Kodaira, *Chem. Mater.*, **2004**, 16, 3652

[30]   D. Brandhuber, V. Torma, C. Raab, H. Peterlik, A. Kulak, N. Hüsing, *Chem. Mater.*, **2005**, 17, 4262

[31]   D. Brandhuber, H. Peterlik, N. Hüsing, *Small*, **2006**, 2, 503

[32]   S. Hartmann, D. Brandhuber, N. Hüsing, *Acc. Chem. Res.*, **2007**, 40, 885

[33]   K. Nakanishi, T. Amatani, S. Yano, T. Kodaira, Chem. Mater., **2008**, 20, 1108

[34]   M. Weinberger, T. Fröschl, S. Puchegger, H. Peterlik, N. Hüsing, Silicon, **2009**, 1, 19

[35]   J. Konishi, K. Fujita, K. Nakanishi, K. Hirao, Chem. Mater., **2006**, 18, 864

[36]   J. Konishi, K. Fujita, S. Oiwa, K. Nakanishi, K. Hirao, Chem. Mater., **2008**, 20, 2165

[37]   K. Sonnenburg, P. Adelhelm, M. Antonietti, B. Smarsly, R. Nöske, P. Strauch, *PCCP*, **2006**, 8, 3561

[38]   A. Zampieri, S. Kullmann, T. Selvam, J. Bauer, W. Schwieger, H. Sieber, T. Fey, P. Greil, *Microp. Mesop. Mater.,* **2006**, 90, 162

[39]   K. Landskron, B.D. Hatton, D.D. Perovic, G.A. Ozin, *Science*, **2003**, 302, 266

[40]   D. J. Brondani, R.J.P. Corriu, S. El Ayoubi, J.J.E Moreau, M. Wong Chi Man, *Tetrahedron Lett.*, **1993**, 34, 2111

[41]   D. Massiot, F. Fayon, M. Capron, I. King, S. Le Calvé, B. Alonso, J-O. Durand, B. Bujoll, Z. Gan, G. Hoatson, *Magn. Reson. Chem.*, **2002**, *40*, 70

[42]   A. Migliori, J.L. Sarrao, Resonant Ultrasound Spectroscopy, John Wiley & Sons, Inc., New York, 1997

[43]   M. Weinberger, S. Puchegger, C. Rentenberger, M. Puchberger, N. Hüsing, H. Peterlik, *J. Mater. Chem.*, **2008**, 18, 4783

[44]   J. Teixeira, *J. Appl. Cryst.*, **1988**, 21, 781

[45]   H. Zhong, J. Liu, P. Wang, J. Yang, Q. Yang, *Microp. Mesop. Mater.*, **2009**, 123, 63

[46]   C. Yu, J. Fan, B. Tian, D. Zhao, *Chem. Mater.*, **2004**, 16, 889

[47]   W. Guo, J-Y. Park, M-O. Oh, H-W. Jeong, W-J. Cho, I. Kim, C-S. Ha, *Chem. Mater.*, **2003**, 15, 2295

[48]   S.A. Bagshaw, E. Prouzet, T.J. Pinnavaia, *Science*, **1995**, 269, 1242

[49]   E. Prouzet, F. Cot, G. Nabias, A. Larbot, P. Kooyman, T.J. Pinnavaia, *Chem. Mater.*, **1999**, 11, 1498

[50]   M. Fukushima, E. Yasuda, Y. Teranishi, K. Nakamura, Y. Tanabe, *J. Ceram. Soc. Jpn.*, **2004**, 112, 612

[51]   S. Puchegger, D. Brandhuber, N. Hüsing, H. Peterlik, *J. Non-Cryst. Solids*, **2006**, 352, 5251

6. Conclusion and outlook

The aim of this thesis was to broaden our understanding of the formation of organosilca monoliths with pores in the nanometer as well as in the micrometer range. The main research topics can be summarized as follows:

- Investigations related to the different sol-gel processing behavior of glycol-modified silanes with different structural complexity.

- Investigations related to the mechanism and the kinetics of the formation of organosilica monoliths with multiscale porosity via *in-situ* SAXS measurements.

- Investigations concerning the potential of organosilica monoliths for the pyrolytic conversion to highly porous silicon oxycarbide monoliths.

As already mentioned in the introduction, these materials are expected to be promising candidates for important applications, such as catalysis and chromatography. If these materials are not prepared as powders, but as highly functionalized monoliths with multiscale porosity, the field of applications is increased significantly. Post-synthetic treatments, such as the surface silylation with functional silanes, to give the material certain functionality, are in some cases possible, but they do not necessarily yield a high density of functional groups on the pore surface. Because of that, scientists tried extensively to obtain such hierarchically porous monoliths directly from the sol-gel processing of complex and functionalized organosilane precursors. But up to now no breakthrough in this field was reported. It is thus essential to perform studies to increase our understanding of the factors, which influence the formation of these materials.

If one considers the rather complex polymerization-induced phase separation processes, it is obvious that the phase separation is very sensitive regarding the interactions between the precursor species, the solvent and the polymeric additive. The latter plays a keyrole to induce a phase separation, from which macroscopic structures could be frozen by the concomitantly occurring sol-gel transition. The modification of organosilanes with ethylene glycol is a versatile approach to prepare precursors, from which phase separation phenomena are easily obtained. Ethanol or methanol are expected to disturb the formation of larger surfactant/(organo)silica aggregates, which are formed via hydrogen bonds, due to their amphiphilic nature. The glycol in contrast comprises two hydroxy functions leading to a much higher polarity, which supports the formation of the surfactant/(organo)silica complex and thus facilitates the phase separation. In addition, the glycol shows a much better compatibility with surfactant mesophases, which as well should support the formation of

mesostructures. However, until now, there are no detailed studies about the interplay of the two processes. Thereby it is of interest, if there even is a polymerisation-induced phase separation, as the formation of the macroscopic framework domains could probably also be obtained by the growth of the mesoscopic crystallites induced by the aggregation of hybrid micelles. On the other hand, if there is a preceding phase separation, how is it connected to the mesostructure formation? The profound understanding of the interplay between structure and reaction mechanism is of great importance towards a rational materials design and the aim of this thesis was to contribute essential aspects to this point.

Organosilica monoliths with multiscale porosity: detailed investigation of the influence of the surfactant on structure formation

In the first paper which is presented within this thesis *in-situ* small angle X-ray scattering studies were applied to shed light on the mechanism of the gel formation of the glycol-modified bis-silylated ethane. Within this study it was shown that gels with multiscale porosity are obtained from sol-gel processing of the precursor in hydrochloric acid solution in the presence of the surfactant Pluronic P123. For the *in-situ* SAXS measurements, a specific gel composition (5.2:20:80), which leads to the formation of a framework consisting of particles with an average size of about 750 nm, was chosen. These particles comprised 2D hexagonally arranged mesopores. From the measurements it was shown that at the beginning of the reactions, directly after mixing, weakly correlated micelles are visible for quite a long time (approx. 200 min at 40 °C). The mesostructure starts to evolve very rapidly. This is an indication for a process, which precedes the "crystallization". Observations of the gel parallel to the SAXS measurement showed that opaqueness occurred after about 114 minutes. This is a proof that phase separation is preceeding the mesostructure growth. The formation of a new phase (a metastable one), where the concentrations and the polarity differ from the original not phase separated system seems to be essential for the mesostructure formation. This leads to the conclusion that from this newly formed metastable phase the nucleation of some micelles starts, which grow into the 2D hexagonally arranged aggregates by consumption of other micelles. This reminds to a typical crystallization szenario and the Avrami kinetics should be able to describe this phenomenon. The data from in-situ SAXS measurements in dependence of the temperature were successfully fitted using the Avrami equation and it was shown that the growth of the mesoscopic crystallites is one-dimensional. In addition, the activation energy of this process was determined to be 61 kJmol^{-1}, which is in accordance with similar results of other mesoscopic systems[1, 2].

Within the same paper it was also shown that hierarchically structured organosilica gels could be obtained within a wide variation of the synthesis parameters. The

domain/macropore size could be controlled by varying the P123/solvent ratio. With a decrease of this ratio the particles or domains grow larger and the mesostructure showed a transition from 2D hexagonal to wormhole-like. The results indicate that for this precursor the interaction with the Pluronic P123 is strong enough to form a stable P123/precursor complex, from which phase separation occurs after a certain time depending on the amount of precursor and the acidity of the solution. The onset of phase separation thereby determines the size of the particles/domains. In the case of a phase separation after only a short time, the coarsening will lead to large particles/domains and vice versa. This phase separation is then always accompanied by mesostructure formation. The question, if these results are also observed for a more complex carbosilane dendrimer, is answered in the following publication.

Mesoporous dendrimer silica monoliths studied by small-angle X-ray scattering

In this work the synthesis of macro/mesoporous gels from a more complex glycol-modifed carbosilane dendrimer (4,4,10,10-tetraethoxy-7,7-bis[2-(triethoxysilyl)ethyl]-3,11-dioxa-4,7,10-trisilatridecane) was investigated. Similar sol-gel processing parameters as in the previous case were chosen. However, in this system it was not possible to obtain a macroscopic phase separation within the investigated parameter range. SAXS measurements indicated the formation of a short-range, but no long-range order concluded from two broad peaks in the scattering intensities at low and large values of the scattering vector q. The peak at low q is easily understood as a short range order of the basic structural units, the dendrimers. TEM images of these gels revealed a network of three-dimensionally connected randomly shaped particles with sizes of about 10-20 nm. By interpolating the scattering curve and thus extracting a distance distribution, originating from the polymer templated mesopores (mean pore distance), it was possible to apply a fit according to the theory usually used for aerogels, which describes scattering from fractal organosilica clusters. From these fits it was possible to draw conclusions of the cluster density (by the fractal dimension ξ) and the cluster size in dependence of the processing parameters. In addition, we applied a numerical ab-initio procedure to visualize the three-dimensional structure from one-dimensional scattering curves, which was developed to describe the structure of proteins[3]. From this simulation, an averaged organosilica cluster was derived, which showed a size in accordance with the data from the analytical fits and the observations from TEM.

It is assumed from these data that the interaction of the surfactant Pluronic P123 with the polymerizing dendrimers is much weaker than in the case of the glycol-modfied bis-silylated ethane. This leads to the idea of a system, where polycondensation of the dendrimers occurs

independently from the surfactant to finally form a gel, with a typical gel network similar to one obtained from a simple sol-gel processing under acidic conditions in the abscence of a surfactant. The surfactant has just the role of a placeholder. Though micelles are present in the solution, they do not form a stable complex with the dendrimers, but they are only incorporated into the particulate network. There are two possible explanations for the different behaviour of this system compared to the bis-silylated ethane-bridged one. On the one hand, the organic content of this precursor is increased. The surface of the P123 micelles, however, has an affinity to more polar molecules, thus the formation tendency of a stable complex is decreased and thereby, phase separation and mesostructure formation are not possible. On the other hand the carbosilane dendrimer shows a huge surface density of functional groups. This could probably lead to a very quick cross-linking of the basic structural units and thus the units are fixed by chemical bonds and a kinetically frozen state is reached, from which as well phase separation phenomena cannot occur. In the third work performed within the frame of this thesis, efforts were thus taken to overcome these problems.

Sol-gel processing of a glycolated cyclic organosilane and its pyrolysis to silicon oxycarbide monoliths with multiscale porosity and large surface areas

The polycondensation products of cyclic methylene-bridged alkoxysilanes, like 1,3-bis[dimethoxysila]cyclobutane, have proven to be valuable ceramic precursors. In addition, such alkoxysilanes were also used to successfully synthesize mesostructured powders or films. Recently, first studies concerning the pyrolytic conversion of mesostructured ethane-bridged or methane-bridged polysilsequioxanes to mesostructured silicon oxycarbide powders were presented[4, 5]. Due to the beneficial properties of silicon oxycarbide materials, the preparation of monoliths with multiscale porosity would be of particular interest. For this purpose the glycol-modified 1,3,5-tris[dimethoxysila]cyclohexane was prepared from the cyclisation of the Grignard reagent obtained from chloromethyltrimethoxysilane and subsequent transesterification with ethylene glycol. First sol-gel processing experiments revealed a similar reaction behaviour in the presence of structure-directing agents as the dendrimeric silane discussed in the second publication. Only nanoporous aerogels were obtained showing similar scattering patterns as the dendrimer gels. Thus, the same aerogel fit could be applied to obtain structural parameters like the organosilica cluster size or the fractal dimension.

If the agglomeration tendency of this system is decreased due to the hydrophobic organic content, the addition of inorganic salts could probably facilitate this process. On the one hand an increase of the ionic strength will lower the potential barrier for colloid agglomeration. On

the other hand the anions could probably dehydrate the poly(ethylene oxide) shells of Pluronic P123 micelles. Consequently, the shell gets more hydrophobic and the formation of hybrid micelles would be possible. The addition of potassium chloride indeed has a significant influence and phase separation can successfully be induced to generate macroscopic framework domains and pores. The higher the concentration of the salt, the earlier the onset of phase separation is observed. A self-similar coarsening, which usually follows a spinodal decomposition process, will then lead to a significant size difference of the phase separated domains. For the 5.2:20:80@1.5M gels were obtained, which show true co-continuous framework domains comprising a huge amount of micelle templated wormhole-like mesopores. The BET surface area of this gel was determined to be 1071 m^2g^{-1} and the mesopore diameter from BJH analysis was 11.6 nm. From ^{13}C and ^{29}Si MAS NMR measurements it was proven that the carbosilane cycles are maintained during the gel synthesis. With these results it was shown for the first time that with the aid of inorganic salts it is indeed possible to prepare hierarchically structured organosilicas with huge surface areas.

The salt assisted sol-gel process which was introduced here, could most probably also be applied in the case of other more complex and functional organosilanes. If one considers the two advanced precursor concepts, which were already introduced in chapter 2.1, the modification with ethylene-glycol could most probably lead to precursors showing a much better solubility under aqueous conditions and better compatibility with surfactant mesophases. Aggregation is then facilitated by the addition of inorganic salt and thus hierarchically structured and highly functional organosilica monoliths may be obtained. However, the preparation of these precursor compounds is rather difficult and involves many steps. In addition, the transesterification in the case of the boron-containing compounds could be problematic due to their usually observed thermal instability. The precursor compounds from Polarz et al. are partly solids, which is disadvantageous for transesterification reactions. But if one is able to overcome these issues, novel exciting materials for chromatography or catalysis could be accessible from these systems. Another interesting aspect for post-functionalisation is the microporosity. The gels, which were obtained in the presence of potassium chloride, show an extraordinarily large microporosity. Thus, the functional groups could be well accessible for further post-functionalization. It is known from literature that the methylene protons from the cycles are rather acidic[6]. With the use of butyl lithium one could post-synthetically generate carbon nucleophiles, which could be reacted with various electrophiles, for example alkyl or acyl halides. Microporosity could as well be interesting in the case of polysilsesquioxanes obtained from the bis-silylated ethene, where various functional groups could be added to the double bond.

Another interesting possibility is given by the pyrolytic conversion of these organosilica monoliths. Gels with the 5.2:20:80@1.5M were subjected to pyrolysis at 1000 °C under argon atmosphere. The monolithic structure was maintained even after this high temperature treatment and the color of the material changed from white to black due to the formation of a free carbon phase. In addition, volume shrinkage of approximately 50 % occurred. SEM and TEM as well as SAXS measurements of the resulting material revealed the maintenance of the materials' structural features on all length scales, except for the micropores, which vanished. The BET surface area decreased to 531 m^2g^{-1} and BHJ pore diameter to 9.1 nm. ^{29}Si MAS NMR measurements showed a distribution of SiC_xO_{4-x} units. Together with elemental analysis the composition of the material was determined to be $SiC_{0.23}O_{1.53}$ + 0.58 C_{free}. By this, the successful preparation of silicon oxycarbide monoliths with multiscale porosity was demonstrated for the first time. These materials could have an impact for applications at severe conditions, i. e. as a support for highly exothermic catalytic reactions.

Summary

In summary, this work deals with intensive investigations concerning the formation of hierarchically porous organosilica monoliths and their pyrolytic conversion into silicon oxycarbide monoliths.

The first publication, which was presented, deals with the sol-gel processing of the glycol-modifed ethane-bridged silane in the presence of the structure directing Plunronic P123. This work provides the theoretical background about the mechanistic details concerning the phase separation and the mesostructure formation on the one hand by a variation of the synthesis parameters and on the other hand with *in-situ* SAXS measurements.

In the second publication nanoporous organosilica aerogels were prepared from a more complex carbosilane dendrimer. In contrast to the ethane-bridged silane phase separation and mesostructure formation were not observed, what is explained by a weaker interaction with the structure directing agent or higher sol-gel reactivity. Advanced SAXS evaluation with analytical and numerical approaches led to a detailed understanding of the structural built-up of the monoliths.

Since complex carbosilanes show weak tendency for phase separation, a salt assisted sol-gel processing route was chosen in the case of a glycol-modified cyclic carbosilane. Organosilica monoliths with multiscale porosity were successfully prepared and could even be used as precursors for hierarchically porous silicon oxycarbide monoliths.

All these novel materials may become interesting candidates for chromatographic or catalytic applications and a pyrolytic conversion to silicon oxycarbide monoliths may even improve the materials properties and thus expand their application spectrum, for example for high temperature applications. Anyway, the acquired fundamental results will most certainly give direction to the preparation of highly functionalized monolithic organosilica and ceramic systems in the future.

6.1 References

[1]   S. M. Holmes, V. L. Zholobenko, A. Thursfield, R. J. Plaisted, C. S. Cundy, J. Dwyer, *J. Chem. Soc., Faraday Trans.*, **1998**, 94, 2025

[2]   I. Beurroies, P. Ågren, G. Büchel, J. B. Rosenholm, H. Amenitsch, R. Denoyel, M. Lindén, *J. Phys. Chem. B*, **2006**, 110, 16254

[3]   D. J. Svergun, *Biophys. J.*, 1999, **76**, 2879

[4]   A. Pauletti, S. Handjani, C. Fernandez-Martin, C. Gervais, F. Babonneau, *J. Ceram. Soc. Jpn.*, **2008**, 116, 449

[5]   B. Toury, R. Blum, V. Goletto, F. Babonneau, *J. Sol-Gel Sci. Techn.*, **2005**, 33, 99

[6]   K. Landskron, G.A. Ozin, *Angew. Chem. Int. Ed.*, **2005**, 44, 2107

List of figures

List of tables

Curriculum Vitae

Manuel Weinberger

Nationality:	german
Place of birth:	Heilbronn, Germany
Date of birth:	21st August 1981
Family status:	unmarried

School education

Sept. 1988 - Jul. 1992	Albert-Einstein-Schule in Geislingen; Elementary school
Sept. 1992 - Jul. 1998	Schubart-Realschule in Geislingen; O-levels
Sept. 1998 - Jul. 2001	Wirtschaftsgymnasium Geislingen; A-levels

University education

Oct. 2001 - Dec. 2006 **Studies of chemistry at Ulm University** with a concentration in inorganic chemistry and elective studies of polymer chemistry.

Topic of the diploma thesis: "Synthesis of mesoporous Dendrisilica monoliths". The work was elaborated under the guidance of Prof. Dr. Nicola Hüsing.

Since Jan. 2007 **PhD studies at the University of Vienna** within the Initiative College "Experimental Materials Science – Nanostructured Materials".

Under the guidance of Prof. Dr. Nicola Hüsing and Prof. Dr. Herwig Peterlik novel porous materials will be prepared and characterized with standard methods of materials science, in particular with (*in-situ*) small angle X-ray scattering.

Other activities

2000 - 2006 Member of the „Technisches Hilfswerk" (a disaster protection organization of the state) in Geislingen an der Steige, Germany.

Professional experience

Jan. 2007 to date	Scientific coworker at the University at Vienna in Austria .
During 2007 to date	Several research stays at the Institute of Inorganic Chemistry I of Ulm University in Germany were conducted.
Dec. 2007	Research stay at the Synchrotron Bessy in Berlin, Germany.

Publications

Diploma thesis

- M. Weinberger, Synthesis of mesoporous dendrisilica monoliths, Diploma thesis, Ulm University, Germany, **2006**

Peer-reviewed journal articles to date

- M. Weinberger, S. Puchegger, T. Fröschl, F. Babonneau, H. Peterlik, N. Hüsing, Sol-gel processing of a glycolated cyclic organosilane and its pyrolysis to silicon oxycarbide with multiscale porosity and large surface areas, *Chem. Mater*., submitted

- M. Weinberger, T. Fröschl, S. Puchegger, H. Peterlik, N. Hüsing, Organosilica monoliths with multiscale porosity: detailed investigation of the influence of the surfactant on structure formation, *Silicon*, **2009**, 1, 19 - 28

- M. Weinberger, S. Puchegger, C. Rentenberger, M. Puchberger, N. Hüsing, H. Peterlik, Mesoporous dendrimer silica monoliths studied by small-angle X-ray scattering, *J. Mater. Chem*., **2008**, 18, 4783 - 4789 **(Journal cover page)**

Posters

- M. Weinberger, H. Peterlik, N. Hüsing, *Glycol-modified organosilanes: versatile sol-gel-precursors for the preparation of hierarchically organized hybrid materials*; 5th European Silicon Days Conference, Vienna, Austria; 20.09.2009 - 22.09.2009

- S. Pabisch, M. Weinberger, N. Hüsing, H. Peterlik, *Orientation of mesoporous structures*; 5th European Silicon Days Conference, Vienna, Austria; 20.09.2009 - 22.09.2009

- M. Weinberger, S. Puchegger, H. Peterlik, N. Hüsing, *Temperature dependence of the gel formation of the glycolated ethane-bridged silane in the presence of Pluronic P123*; First International Conference on Multifunctional, Hybrid and Nanomaterials, Tours, France; 15.04.2009 - 19.04.2009

- S. Pabisch, M. Weinberger, N. Hüsing, H. Peterlik, *Orientation of mesoporous structures*; 58. Annual Conference of the Austrian Physical Society, Leoben, Austria; 22.09.2008 - 26.09.2008

- M. Weinberger, T. Fröschl, M. Weidelener, H. Peterlik, N. Hüsing, *Synthesis of periodic mesoporous organosilica monoliths and examination of the dynamics and kinetics of the gelation process*; VI International Mesostructured Materials Symposium, Namur, Belgium; 08.09.2008 - 11.09.2008

- M. Weinberger, H. Peterlik, N. Hüsing, *Synthesis of mesoporous dendrisilica monoliths*; XIV International Sol-Gel Conference, Montpellier, France; 02.09.2007 - 07.09.2007

Talks

- M. Weinberger, *Organosilica monoliths with multiscale porosity prepared from glycol-modified organosilanes*; Young chemists' workshop of the CERC3: Solution chemical processing of advanced materials; Stockholm, Sweden, 10.05.09 - 13.05.09

Acknowledgements